Dynamic Characterization of Thin Deformable PVDF Mirror

THESIS

Eric M. Trad, Second Lieutenant, USAF

AFIT/GAE/ENY/05-M24

DEPARTMENT OF THE AIR FORCE
AIR UNIVERSITY

AIR FORCE INSTITUTE OF TECHNOLOGY

Wright-Patterson Air Force Base, Ohio

AFIT/GAE/ENY/05-M24

Dynamic Characterization of Thin Deformable PVDF Mirror

THESIS

Presented to the Faculty

Department of Aeronautical and Astronautical Engineering

Graduate School of Engineering and Management

Air Force Institute of Technology

Air University

Air Education and Training Command

In Partial Fulfillment of the Requirements for the

Degree of Master of Science in Aeronautical Engineering

Eric M. Trad, B.S.E.

Second Lieutenant, USAF

March 2005

AFIT/GAE/ENY/05-M24

Dynamic Characterization of Thin Deformable PVDF Mirror

Eric M. Trad, B.S.E.
Second Lieutenant, USAF

Approved:

/signed/	21 Mar 2005
Dr. Richard G. Cobb Chairman	date
/signed/	21 Mar 2005
Dr. Anthony N. Palazotto Member	date
/signed/	21 Mar 2005
Dr. Donald L. Kunz Member	date

Abstract

An increased need for higher resolution space-based optics creates requirements for enlarged apertures on the primary optical surface. Traditional space-based optical systems are limited in aperture size by weight and the payload capacity of current launch vehicles. Membrane-like optical structures which could be rolled for space-lift and deployed in orbit have the potential to greatly reduce weight and increase the aperture size of next generation mirrors in space. However, thin, deformable membrane-like structures require active control for stabilization and shaping of the optical surface. The primary goal of this research is to obtain a methodology for the characterization of piezo-actuated, thin, deformable optical structures. The response of this membrane-like structure to dynamic disturbances is given particular focus. Modal analysis and active wavefront measurements were carried out for a five inch membrane-like optical structure and the results are compared to theoretical analysis. Control patches etched into the piezoelectric polymer material are used to characterize the optical surface response subject to static and sinusoidal forcing functions. Various fabrication techniques are also investigated for a polyvinylidene fluoride (PVDF) membrane-like structure with a silicone substrate surface coating.

Acknowledgements

At times, the pursuit of an education can seem terribly selfish. I have not always been able to achieve a perfect balance between the energy I have put into my studies and that which I had left to spend on those I love. If it were not for the patience, support and understanding of those closest to me, I would have certainly strayed from the course long ago.

I would like to give a special thanks to Dr. Cobb (AFIT/ENY), Dr. Mollenhauer (AFRL/ML), Dr. Johnson (AFRL/ML), Dr. Palazotto (AFIT/ENY), Dr. Kunz (AFIT/ENY), Maj. Shepherd (AFIT/ENY), Jay Anderson, Wilber Lacy, Andy Pitts, Randy Miller and Dwight Gehring. I would also like to acknowledge the contribution of Herb DeSilva at AOA, without his tcl script, this work would have been a much larger challenge.

This project has the great fortune of continued financial support from the Air Force Office of Scientific Research. I would like to extend a special thanks to Lt. Col. Sharon Heise at AFOSR for her work on the financial aspects of this project.

Eric M. Trad

Table of Contents

Page

Page

List of Figures

List of Tables

List of Symbols

Symbol		Page
λ	Wavelength, nm	1
d	Diameter, m	1
θ_R	Minimum Angular Separation, rad	1
L	Minimum Separation Distance, m	1
h	Height or altitude, m	1
ρ_{areal}	Areal density, $\frac{kg}{m}$	6
m	Mass, kg	6
V	Volume, m^3	6
L	Length, m	15
d_{31}	Piezoelectric coefficient	15
v	Applied voltage, v	15
h	Thickness, m	15
w	Width, m	16
d_{32}	Piezoelectric coefficient	16
d_{33}	Piezoelectric coefficient	16
r	Radius, m	24
A	Area, m^2	24
θ	Angle coordinate on membrane, rad	26
$W(r,\theta)$	Surface deformation, μm	27
ω	Natural frequency of membrane, Hz	27
c	Membrane wave speed	27
J_m	Bessel function of the first kind with order m	28
β_{mn}	Zeros of the Bessel function	29
$\eta(t)$	Generalized temporal coordinates	32
T	Tension per unit length, $\frac{N}{m}$	33
$N(t)$	Generalized forces	33

Dynamic Characterization of Thin Deformable PVDF Mirror

I. Introduction

1.1 Overview

Satellite imaging systems are critical to the information gathering needs of the U.S. Department of Defense. The aperture size of the primary optical surface determines the detail level and distance at which the system is able to gather useful data. An increase in aperture size translates to an increase in observed detail, referred to as resolution. An increase in aperture size also allows the optical system to take quality images from a larger distance, which equates to a larger coverage area on the surface of the earth, reducing the need for large satellite constellations in low earth orbit.

An estimate of the resolution of an optical system is given by Equation 1. This is known as Rayleigh's resolution criterion [12].

$$\theta_R = 1.22\frac{\lambda}{d} \tag{1}$$

The variables λ and d are the wavelength and aperture diameter of the primary mirror, respectively. θ_R represents the minimum angular separation that two point sources can be resolved as separate entities. Notice that d is inversely proportional to θ_R, which means increasing the diameter of a mirror will enable a smaller angular separation between two given objects to be resolved.

Figure 1 shows a typical scenario for satellite observation. From these dimensions, Equation 2 can be used to calculate the minimum distance that two objects on earth can be discerned as separate entities.

$$L = 2h * tan\left(\frac{\theta}{2}\right) \tag{2}$$

Let L be the minimum resolvable separation distance from an assumed geosynchronous orbit of h= 35,800 km. Since the minimum angular separation increases as wavelength is increased, an approximation for the largest wavelength in the visible spectrum is used, λ = 700 nm. This will give a 'worst case' estimate for the entire visible spectrum. Table 1 provides a summary of these calculations.

These calculations clearly illustrate the fact that the larger the lens, the finer the details that can be collected. There are numerous reasons that space-based optical systems created to date have not incorporated the large aperture sizes needed for a very high level of resolution.

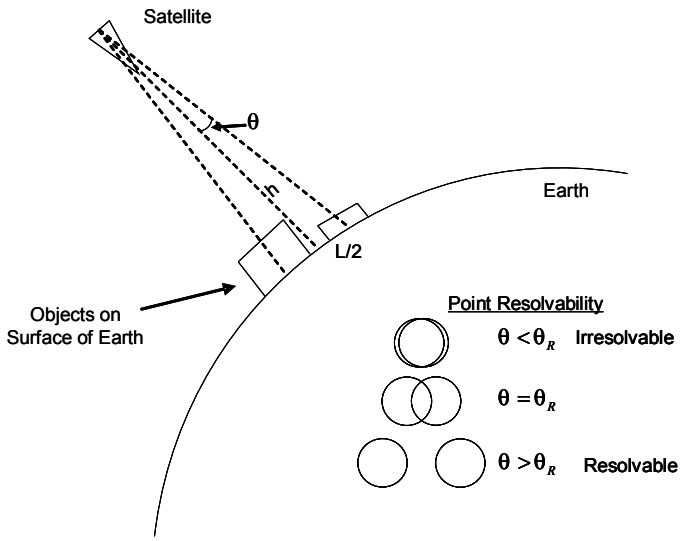

Figure 1: Typical scenario for satellite observation

Table 1: Calculated Separation Distances

Diameter of Primary Mirror (m)	θ_R (rad)	L (m)
3	2.85e-7	10.2
10	8.54e-8	3.06
100	8.54e-9	0.31

Traditional space-based optical systems are constructed of highly polished monolithic glass. These mirrors are expensive to produce in large sizes and the polishing that is required over the entire surface is very time consuming. Additionally, the weight of traditional mirrors makes them costly to lift into space with the launch craft that are presently available. Another major limitation is that glass mirrors cannot be stored in any compact configuration for launch, therefore the maximum diameter is limited to what will fit in the cargo bay of a launch vehicle, presently about 3 meters.

One obvious solution is a change of material. If a lightweight material could be substituted for the heavy glass of traditional optical systems, the weight problem could be eliminated. A further advancement may involve the use of a thin, deformable, lightweight material. Such a material would allow lightweight, compact storage of the mirror for the space-lift phase. The mirror could then be deployed to its final size once positioned in its predetermined orbit. Of course, such a flexible material would most likely need active control to create the desired surface shape and maintain a high quality optical surface.

An optical quality surface must have a surface flatness below the order of magnitude of the light one hopes to reflect. Visible light has a spectrum of 400 nm - 700 nm. With advances in compensated optical systems and adaptive optics, this requirement can be reduced by one order of

magnitude. Therefore, high optical quality is defined to be on the order of 0.5 μm and compensated optical quality (or simply optical quality) is assumed to be approximately 5 μm.

The solutions described here require advancements in a diverse range of engineering disciplines. Materials and manufacturing researchers are finding new and innovative ways to use lightweight materials as a replacement for traditional mirrors. Electrical and control systems engineers are researching the necessary stabilization and surface shaping methods which will be incorporated into this new class of mirrors. Optical engineers are attempting to tie all of these advancements together to create a working optical system which will have unprecedented imaging properties.

1.2 Scope

Lightweight, thin deformable optical structures are the key to achieving the goal of large aperture imaging systems in space. One of the largest hurdles preventing this advancement is the problem of stabilization and control of the membrane surface. Previous efforts at the Air Force Institute of Technology (AFIT) have demonstrated the validity of the use of piezo-actuated control patches etched onto the under-surface of the mirror [21]. This research involved testing the static deformation pattern of a 5 inch silicone coated PVDF mirror. Up to seven control patches were etched into the PVDF layer as actuators. The scope of the present research seeks to extend the previous effort by developing a data acquisition system capable of sampling the optical wavefront at rates as high as 30 Hz and using it to characterize static and dynamic actuation of the mirror surface. The scope of the project is also expanded to include the development of a methodology for a calculation of membrane tension, verification of previously developed static actuation results and improvement in membrane fabrication methodology.

A data acquisition system was developed to work with existing wavefront measurement equipment. This acquisition system was necessary in order to establish a link between the motion of the optical surface, the acquisition equipment and the analysis and control equipment. This new system enabled detailed measurement of the optical surface subject to a sinusoidal forcing function. The improved acquisition system is also capable of quickly taking data, which is used for statistical analysis of static deflection results.

A scanning laser vibrometer was used to characterize the membrane-like optical structures over a full range of frequencies. This data was instrumental in a prediction of the tension in the PVDF membrane layer.

The methodology of fabrication was also improved to decrease the areal density of the membrane-like optical structures, this lower weight is a result of a decreased thickness of the silicone surface

coating. A decrease in thickness creates a more membrane-like structure, which allows standard membrane theory to better predict the dynamics.

1.3 Problem

The primary concern with previous work involves the data acquisition system. Data could be taken only in single frames, and had to be post-processed for an accurate description of the surface. An active control system requires that the data acquisition system be able to grab data and provide feedback for the controller in a timely manner, typically many times a second. Therefore the primary focus of this research is to create a data acquisition system which can be used with Matlab®. This will enable future researchers to use Simulink® and dSpace® control hardware to develop wavefront control algorithms for the optical surface.

At present, the data acquisition system is used to investigate the behavior of the optical surface subject to static and dynamic loading. Multiple data samples on a statically loaded membrane could provide statistical information about the mean and variance of the optical surface. Additionally, the optical surface could be observed in 'real' time, subject to sinusoidal forcing functions.

A secondary concern involves the tension on the membrane. An accurate tension is essential to the development of a finite element model for this optical system. Currently, the tensioning of the membrane is done on a tensioning apparatus where the load is applied via uncalibrated mechanical torsion. Modal analysis methods were utilized to estimate the tension of the membrane, which provides critical information for use by the numerical modeling researchers.

Taking only one measurement at a time will give a general idea of the results that can be obtained, but a proper statistical analysis of the system requires that data be collected quickly. This will enable a mean and standard deviation calculation and this information clearly gives a more accurate description of the system. The newly developed data acquisition system was also used to perform this detailed analysis.

1.4 Summary of Thesis

The first chapter is devoted to a general introduction to the subject of this research and an outline of the problems that were approached here in. In the second chapter, a review of the relevant literature is provided. This chapter is intended to further develop an understanding of the problem and quantify some of the research efforts that have been made regarding this issue. As this is a very active, multidisciplinary area of research, this review is by no means exhaustive. Simply the most

relevant information to this project is provided and the reader is encouraged to investigate other references at his leisure.

The third chapter describes the design and fabrication of the membrane-like optical structures. This summarizes the iterative process that was used to produce the optical test subjects.

Chapter four provides a complete description of the modal analysis of the test articles, which was performed with the scanning laser vibrometer. Included in this chapter is a detailed outline of the theory of vibrating circular membranes, an analysis and prediction of the membrane tension and an analysis and comparison of the primary modes of the membrane test subjects.

The fifth chapter includes a complete description of the wavefront imaging system. The optical test setup and data acquisition system are described and test results for the static and dynamic loading of the 5 inch optical structure are provided.

The final chapter outlines some conclusions and recommendations for further study. Great care have been taken to create usable procedures for the test equipment. This information along with much of the analysis code is provided to future researchers in the Appendix.

II. Review of the Relevant Literature

2.1 Overview

There have been many recent research advances which have made the daunting task of placing a large optical quality mirror in space and maintaining a precise shape across its entire surface seem more attainable. Two areas of research are currently producing the most promising potential for meeting this ambitious goal. Advancements in materials and manufacturing techniques have greatly reduced the areal density of rigid, lightweight optical structures. Similarly, improvements in piezo-actuated polymer control and boundary control of membrane-like structures has paved the way for an order of magnitude decrease in areal densities by allowing the use of flexible, thin, deployable structures to create new lightweight mirror designs.

The areal density, ρ_{areal}, is useful as a comparison of mass per surface area for different optical structures. It is defined in Equation 3. Here ρ, m, h and V are defined as density, mass, height and volume, respectively.

$$\rho_{areal} = \rho h = \frac{m}{V} h \tag{3}$$

These large decreases in areal density are necessary if a large aperture space-based optical system is to be realized. Various U.S. Government agencies have proposed mission objectives which require optical surfaces up to 100 meters in diameter to be constructed [15].

Decreasing the areal density produces many design problems that have not been addressed with traditional optics. Structural vibration, durability, deployability and robustness are all important to consider. Active and adaptive control algorithms are necessary to constantly maintain the surface shape and quality.

This section outlines some of the recent advances, which have made this design problem more tractable. Two areas of research are considered: lightweight, rigid optical structures and membrane-like structures.

2.2 Lightweight, Rigid Optical Structures

Currently, the standard material used to produce space-based optical systems is monolithic glass, which can be polished to a very suitable optical surface. This polishing process is time consuming and costly. The systems are also heavy, often exhibiting areal densities in the hundreds (approximately 200 for the primary mirror on the Hubble Space Telescope). These traditional systems are relatively robust and do not require the amount of active stabilization that a lighter weight, flexible membrane-like system does.

The space shuttle serves as an appropriate benchmark for the size and lifting capacity of a typical modern day launch vehicle used to lift a telescope into orbit. The maximum cargo size for the space shuttle is approximately 3.25 meters and it can accommodate approximately 28,800 kg. These numbers will be assumed for future comparisons of areal density. As an example, a monolithic glass mirror which maximized both the weight and diameter specification would have an areal density of approximately 3,472 $\frac{kg}{m^2}$, as shown by Equation 4.

$$\rho_{areal} = \frac{28800}{\pi \left(\frac{3.25}{2}\right)^2} \approx 3472 \frac{kg}{m^2} \tag{4}$$

Similarly, an optical system with a primary mirror aperture of 100 meters would need an areal density of about 3.67 $\frac{kg}{m^2}$ to be lifted by the space shuttle.

One approach is to combine the positive aspects of monolithic glass mirrors with advanced material processing and fabrication methods to create thinner, light weight, rigid optical structures. These structures help to lower the launch weight of the optical system, but do nothing to increase the aperture size of the mirror.

Researchers at AFRL are looking into ways to fabricate a mirror using a spin casting technology to form the reflective surface in a shape close to that which it will be utilized. These methods emphasize the use of stress coatings applied to the optical surface coupled with boundary control techniques to ensure that an optical quality surface is maintained. Other approaches considered by this group include fabrication of the rigid support structure or mirror surface once deployed on orbit. This process may involve the use of shape memory alloys or electro-active materials (such as PVDF) to deploy the membrane-like structure to its usable state [4].

Another approach is to simply replace the heavy support structure of traditional monolithic glass mirrors with light weight alternatives. Researchers at Eastman Kodak Co. have produced a 1.4 meter mirror with an areal density of around 12 $\frac{kg}{m^2}$. This mirror uses a carbon fiber reinforced polymer matrix composite reaction structure to support the optical surface [15]. It is constructed in the shape of a hexagon, so that it can be fit with other similar pieces to form a larger primary mirror.

AFRL Materials Directorate researchers are also pursuing glass or ceramic syntactic foam [15]. These are structures which are made from glass, ceramic or polymer microballoons. The microballoons are suspended in a polymer resin matrix. These structures are stiff, very lightweight and can be coated with reflective material to form an optical quality surface.

2.3 Lightweight, Deformable Membrane-like Structures

While the diameter of lightweight, rigid mirrors are restricted by the cargo bay dimensions of today's launch vehicles, an optical surface which could be compressed in some way could be substantially larger. For this reason, several ideas are being considered to fold, roll or otherwise store flexible, membrane-like structures for launch. These structures are then deployed in orbit.

The flexible nature of these structures necessitates some means of tensioning and control in order to maintain an optical quality surface. The membrane-like structure can either be controlled with subtle deformations around the boundary or by control actuation applied to the interior of the membrane surface.

2.3.1 Boundary Manipulation Control Methods. One method of deploying a lightweight optical structure which has been studied, is to enclose it with an inflatable structure and simply pump positive pressure into the system. The pressure of the gas, shape of the structure and other actuation methods could be used to control the flexible surface. Figure 2 gives an illustration of such a system. One major drawback of this system is that the transparent canopy would be difficult to manufacture. To accommodate much of the visible spectrum, the total thickness and thickness variation across the structure would have to be kept to very tight tolerances [4].

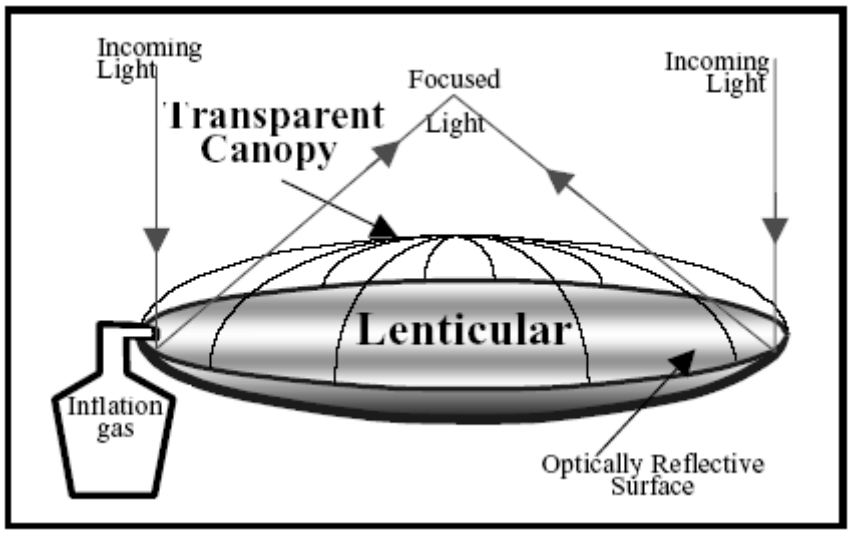

Figure 2: Lenticular Optics System [4]

Another design approach is to use a deformable boundary to enclose the membrane-like structure. This approach has been validated by the inflatable antenna experiment, which was carried out

by NASA in May, 1996. Systems similar to this, with piezoelectric control patches applied to the outer ring have been studied [10].

Work has also been done to develop analytical models to represent these boundary actuated flexible membrane optical structures [9] and [6].

Figure 3: Inflatable Optical System [8]

Experiments have been conducted to study the effects of stretching a membrane structure over a curved rail system. The rails can be actuated by forces and moments applied to their ends. The deformed rails alter the shape of the membrane and offer some measure of control [1].

2.3.2 Interior Manipulation Control Methods. Results from a test conducted at the University of Kentucky indicate that a non-contact electron gun can feasibly be used to deform a piezoelectric mirror [5]. The test subject for these experiments was a piezoelectric bimorph (PZT-5H) 2 mm thick and 2 inches in diameter. Deflections on the order of 3 μm positive deflection and 2 μm negative deflection were observed. This method of actuation requires complicated equipment in a controlled environment, therefore questions regarding the scaling of this approach are legitimate.

Another approach is to etch control patches directly onto the piezoelectric material. Research along these lines has been done at the Air Force Institute of Technology. It has been shown that static deformations on the order of 3.3 μm are possible using 5 inch membranes [22]. For these tests, membranes with a thickness of 4 to 6 mm were produced. Membranes were constructed of etched PVDF material. Due to the control patch placement directly on the optical membrane, layers of silicone substrate are needed to smooth the surface and create and optical quality mirror.

Analytical modeling of piezo-actuated material has also been an area of research. Researchers at NASA have developed an analytical solution to deform a flat piece of electro-active polymer into a predefined deformed state and have verified the results computationally [3].

Mirrors with actuation patches require less complicated equipment than non-contact methods, however etching the control pattern without imprinting onto the optical surface can be a problem. No one method is a clear best alternative, each possesses new problems that will require additional research efforts to solve.

Many potential solutions are currently under investigation within the scientific community. Previous work completed at AFIT demonstrated great promise for an advancement in the area of control of a tin deformable PVDF optical surface. Thus, the current research seeks to validate and extend this valuable effort by creating an acquisition system which will enable data to be processed in a more timely manner. This development is critical if any control algorithms are to be developed for control or stabilization of the mirror surface in the future.

III. Membrane Design and Fabrication

3.1 Overview

The design and fabrication process for the test articles is a very important phase of the project. Each mirror must be produced by hand, which is a time consuming process. There are many ways that each mirror could be produced, but simply changing one small technique during fabrication may produce separate mirrors with different dynamics. Great care was taken to follow the procedures outlined below for every mirror that was fabricated. Any deviation from this is noted and explained. By closely following the outlined procedures, wasted time and resources was minimized and mirrors with similar dynamics are produced for testing.

3.2 Control Pattern Design

Three control patterns are used for this research, 1-patch, 5-patch and 7-patch. The following sections describe the reasons that each control pattern was selected. A description of the dimensions of each control patch is also provided.

The width of all control leads was set at $\frac{1}{8}$ inch (3.2e-3 m). This dimension was chosen to minimize the area of the control lead, while still enabling fabrication by hand.

Design considerations for the 5 and 7-patch mirrors included the ability to actuate both symmetric and antisymmetric portions of the surface, patch spacing and ease of fabrication. The final design satisfied all design considerations. The mirror surface can be actuated symmetrically with only the central control patch, all outer patches or all patches acting in unison. The mirror can be actuated anti-symmetrically through the use of any combination of the outer control patches.

The control patches were carefully spaced, to provide the greatest actuation area, while still maintaining a minimal patch spacing. The minimum patch spacing was determined by fabrication constraints ($\frac{1}{8}$ in) and serves to provide insulation between charge on different patches.

The control patterns were designed with only one set of concentric patches because this is sufficiently complex to demonstrate both symmetric and antisymmetric motion, while it is simple enough to fabricate by hand.

The outer most edge of the patch design is located $\frac{3}{4}$ inch (1.9e-2 m) from the aluminum ring support, which serves two purposes. By using this inner portion, the slightly distorting effects of the meniscus can be minimized. The meniscus describes the slightly raised level of the silicone near the aluminum wall, which is formed during the cure process. Additionally, the wavefront sensing equipment has an optimal illumination of approximately 4 inches, so by localizing the control patches to this diameter, the maximum actuation effect can be observed.

The control patch pattern is designed only to be etched onto one side of the PVDF material. By placing the pattern onto the underside of the mirror surface and mounting the aluminum ring onto the other, a layer of insulation is maintained. This prevents shorting of one patch to another through the aluminum ring or by other means. It is important to note that PVDF can be actuated on both the top and the bottom, which may increase control input options for future researchers. Double sided actuation would require the development of an improved membrane support structure, which would maintain an insulated boundary between control patches.

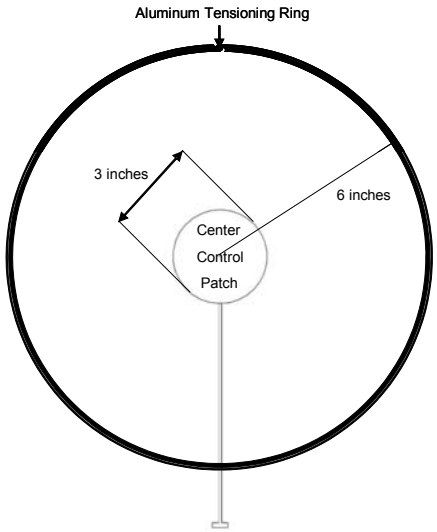

Figure 4: Schematic of 1-Patch Design

3.2.1 1-Patch, 12 inch Membrane. The 1-patch etch design (see Figure 4) was used primarily as a proof of concept. The diameter of the central control circle is 3 inches (07.62e-2 m) and the length of the control lead is 7 inches. The length of the lead is determined by the radius of the tensioning apparatus, which is 6 inches. The diameter of the control patch was decided upon in a somewhat arbitrary manner. The patch is large enough to actuate the tensioned membrane for the vibration phase of testing, yet small enough not to be cumbersome during fabrication.

This simple design was chosen as a starting point in order to serve as a learning device for some of the more complex control patterns which needed to be fabricated. This control pattern demonstrated that it is possible to etch thin, clean, straight lines for the control leads by hand.

3.2.2 5-Patch, 5 inch Membrane. The 5-patch control pattern was developed primarily for use as a final test mirror. The 5-patch design has larger control patches than the 7-patch, therefore it offers a larger actuation area as a test subject.

The dimensions of the 5-patch test subject are outlined in Figure 5. For identification, each control patch is given a number label 1 to 5 as shown in this diagram. The area of the central control patch is 0.7854 in^2 (5.067e-4 m^2), this represents approximately 4.0% of the mirror surface area. The area of the outer control patches is 1.19 in^2 (7.6826e-4 m^2), which is approximately 6.0% of the mirror surface area.

Two 5-Patch mirrors were etched for this project, however only one was given a silicone surface coating. These structures will be referred to as 5-Patch A and 5-Patch B, where only 5-Patch A was coated.

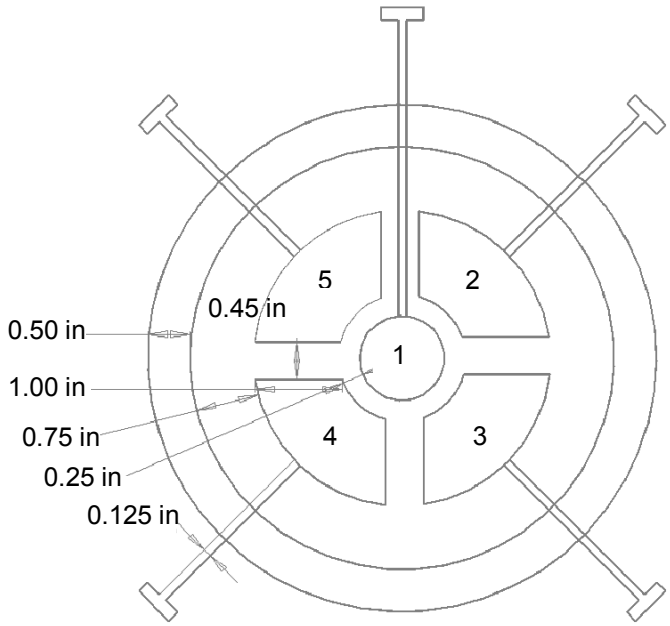

Figure 5: Schematic of 5-Patch Design

3.2.3 7-Patch, 5 inch Membrane. The 7-patch control pattern was developed primarily for use as a final test mirror. The 7-patch design has more control patches than the 5-patch, therefore it offers more actuation options as a test subject.

The dimensions of the 7-patch test subject are outlined in Figure 6. For identification, each control patch is given a number label 1 to 7 as shown in this diagram. The area of the central control patch is 0.7854 in^2 (5.067e-4 m^2), this represents approximately 4.0% of the mirror surface area. The area of the outer control patches is 0.866 in^2 (5.587e-4 m^2), which is approximately 4.4% of the mirror surface area.

Two 7-Patch mirrors were etched for this project and both membranes were coated with silicone for wavefront testing. These structures will be referred to as 7-Patch A and 7-Patch B.

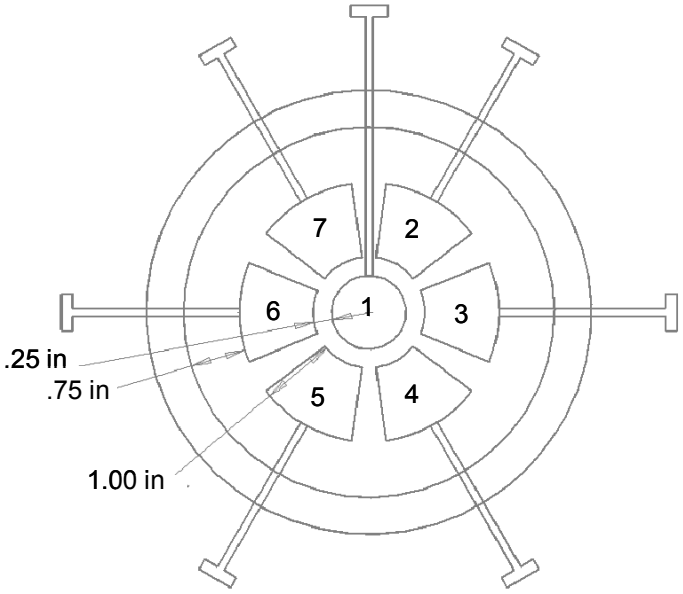

Figure 6: Schematic of 7-Patch Design

3.3 PVDF Material

The PVDF material used for this research is manufactured by Measurement Specialties, Inc. It is $52\mu m$ thick and can be purchased in an unprocessed 14 inch wide roll.

The material is typically rolled during processing and a usable center patch is cut out before delivery to the client. It was determined that the post-processed PVDF material is too small to fit AFIT's tensioning apparatus. The supplier agreed to provide the roll of PVDF material without this post-processing step. Only the center of the PVDF material is utilized once it is etched and epoxied to the aluminum ring, thus insuring a high quality piece of PVDF material for testing.

Each piece of PVDF has a thin layer of conductive copper and nickel coated on each side, see the illustration in Figure 7.

PVDF material is a piezoelectric polymer which responds by expanding when a voltage is applied to it. Conversely, if the material is deformed, it will produce a voltage. PVDF also exhibits

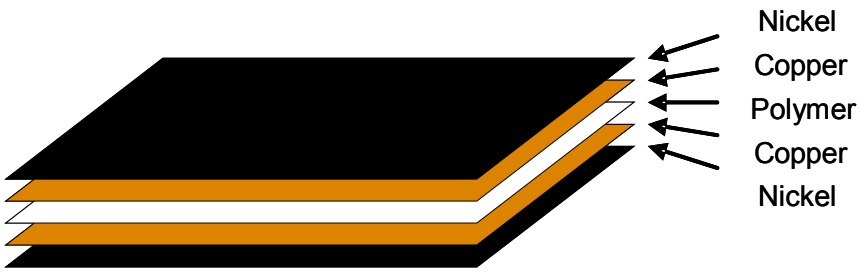

Figure 7: Schematic of PVDF Material Layers

a pyro-electric effect, where upon it will produce a voltage due to a change in temperature. For this reason the material is widely used in the sensors community.

The deformation of PVDF material is a result of the attraction (or repulsion) of internal dipoles due to an applied electric field. The PVDF material is anisotropic, therefore it will not expand the same in all directions. A positive polarity will cause the PVDF material to expand in length and contract in width and height. A negative polarity will cause the PVDF material to contract in length and expand in width and height. The coordinate system for the PVDF material has been defined in Figure 8.

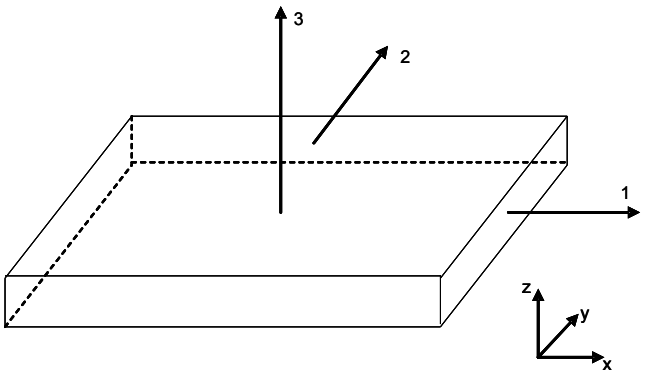

Figure 8: Definition of PVDF Coordinate System

$$\Delta L = \frac{L d_{31} v}{t} \tag{5}$$

In Equation 5, L, ΔL, d_{31}, v and h are length, length change, piezoelectric coefficient for length direction, applied voltage and thickness, respectively.

$$\Delta w = \frac{w d_{32} v}{t} \tag{6}$$

Where w, Δw and d_{32} are width, width change and piezoelectric coefficient for width direction.

$$\Delta t = \frac{t d_{33} v}{t} = d_{33} v \tag{7}$$

In Equation 7 d_{33} is the piezoelectric coefficient for the 3-direction (height).

PVDF material cannot generally be used to create large displacements, but it can be used over a large range of frequencies ($1e10^{-3}$ Hz to $1e10^{9} Hz$). Table 2 provides some of the useful coefficients that apply to the PVDF material. This data is taken directly from the Measurement Specialties, Inc., Piezo Film Sensors Users Manual [11].

Table 2: PVDF Coefficients and Material Properties

Symbol	Parameter	Value	Units
h	Thickness	52	μm (micron, 10^{-6} m)
d_{31}	Piezo Strain Constant (length)	23	10^{-12} $\frac{m}{V}$
d_{33}	Piezo Strain Constant (height)	-33	10^{-12} $\frac{m}{V}$
ρ_m	Mass Density	1.78	10^{3} $\frac{kg}{m}$

3.4 Mirror Etching

The fabrication process utilized for the optical membrane-like structures is an extension of that used in previous research [21]. The clean PVDF material is stored on a thick cardboard roller (to prevent creases in the material) with the positive side rolled on the inside.

The positive side of the PVDF material was marked with permanent masking marker to avoid confusion. This will help to make sure that the aluminum ring is epoxied to the correct side of the PVDF sheet. It will also help to predict the positive or negative displacement of the final mirror surface under an applied voltage.

To track the orientation of the material during fabrication, three parallel lines are marked in the corner near the positive side marking. The lines are drawn parallel to the length of the material, perpendicular to the cardboard roller and correspond to the 1 direction in Figure 8.

Computer generated masking patterns were created and used to form the mask for the etching process. The specifics of these masking patterns is covered in Section 3.2.1 to 3.2.3. A razor was used to cut the control patches out of the computer generated stencil. This was done extremely carefully to maintain the exact spacing of the control pattern design. The area that is to be the control pattern and therefore must be masked with a permanent marker must be completely removed.

A 14 inch piece of PVDF material is cut from the roll of clean material with a straight edge and the razor blade. The resulting PVDF piece is roughly 14 inches square. It is important to

maintain this size, because smaller dimensions will not fit on the tensioning stand and cannot be evenly tensioned.

The center of the PVDF piece is found by touching two pieces of string to each diagonal corner. This will form and 'X', which will mark the spot to center the membrane. A small mark is made at the center with the permanent marker.

The computer generated template is then taped down to the positive side of the PVDF material with Scotch tape. The lead for the center patch is always oriented perpendicular to the 1 direction. Eventually, the excess PVDF material will be trimmed away and this orientation will replace the positive side and parallel line markings which were made earlier. The middle control patch is then matched to the center of the PVDF material.

The PVDF material is masked with the permanent marker by tracing out the control patches and filling in the visible regions of the PVDF. Great care is taken not to smear the permanent marker while it dries. If the pattern is deformed in some way, it can be cleaned with isopropyl alcohol and reapplied.

The paper stencil is then carefully removed. The control pattern is then cleaned up by hand with the straight edge and the permanent marker. Typically, there are leads that need to be straightened and rounded edges that need smoothing by hand. Occasionally, a permanent mark was removed with the alcohol from a region not supposed to be masked. Great care was taken not to change the dimensions of the control pattern.

The PVDF material was then etched with Ferric Chloride by simply dipping a cotton ball in the etchant solution and wiping away the exposed copper and nickel on the PVDF surface. The reaction is stopped by applying water to the etched region. The PVDF is then dried by patting with a soft paper towel and hanging to dry.

The PVDF sheet was then flipped upside down, and small patches of the material were etched. These patches serve as windows (see Figure 9). Each window is strategically selected to allow the placement of the 6 inch aluminum ring onto the PVDF during the epoxy phase. This method is a crucial step in the centering of the control pattern in the middle of the ring. If the control etching was to be off center, the dynamics of the membrane would suffer accordingly and many of the theoretical symmetry assumptions which were made would not be valid.

Finally, the permanent marker is removed with the alcohol, leaving the etched control patch design on the sheet of PVDF. Since deformations of the sheet will cause charge generation, the sheet is stored loosely rolled and covered in poster board material.

Figure 9: Windows Etched into PVDF Material

3.5 Mirror Tensioning and Epoxy

Even tension around the circumference of the membrane is important to the dynamics of the final optical surface. This section will describe the methodology which was used to tension and epoxy the PVDF membrane to the 6 inch aluminum ring. There are, of course, many other options and variations for these tensioning methods, some of which will also be addressed in this section and some of which are beyond the scope of this research effort.

The etched PVDF membrane is placed over a 12 inch tensioning ring. The etched, positive side of the PVDF membrane is placed face down, so that the aluminum ring can be epoxied to the smooth negative side of the PVDF. The etched windows should provide the ability to center the aluminum ring over the control patches, without the need to see the control patches directly. The tensioning ring has a rubber o-ring set into a groove, which will be deformed when the PVDF is clamped. The deformation provides even tensioning around the circumference of the membrane. An aluminum top ring, which is flat, is placed on top of the PVDF. Four clamps are then spaced evenly around the circumference of the tensioning apparatus. Figure 10 illustrates this setup.

The PVDF material is carefully stretched by hand in all directions to remove any wrinkles which may be present. Great care is also taken to insure that the PVDF material is resting evenly on the o-ring around the entire perimeter.

The clamps are tightened slowly, two at a time. Opposing corners are tightened together and only one eighth of a turn is given to the clamp before switching sets. The clamps are tightened in this manner until it is difficult to tighten any more with the thumb and forefinger only.

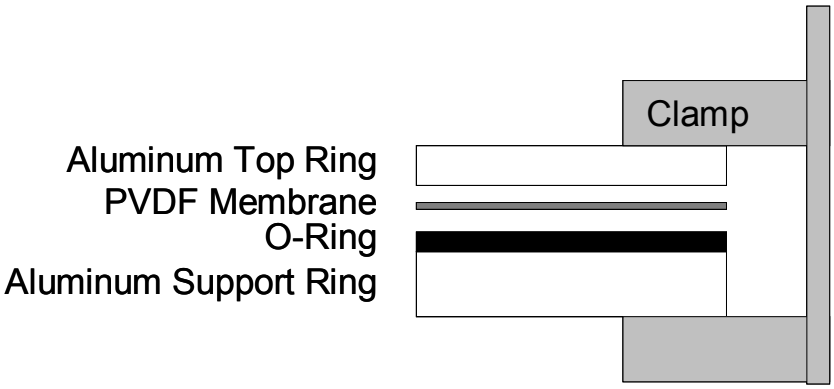

Figure 10: Tension Apparatus Setup Diagram

Other methods of tensioning which were considered include measuring the rotation angle of the clamp screw, measuring the torque of the clamp screw and placing force transducers between the PVDF and the aluminum top plate to measure the compression force. In the end this method of tensioning was decided upon because it had been used successfully in the past [21] and the tensioning apparatus was readily available.

One additional method of tensioning, which has been successfully used for fabrication of optical membranes by AFRL Researchers, is the use of a vacuum system to pull the PVDF material down around the 12 inch ring [10]. This method could potentially provide very even tensioning, however working in a vacuum introduces complications which are beyond the scope of this project.

An aluminum ring, which was specifically designed to allow excess epoxy to flow away from the membrane surface was used for the membrane support structure. Figure 11 shows the design of this ring. Notice the shallow epoxy groove, which is surrounded on either side by epoxy drain grooves.

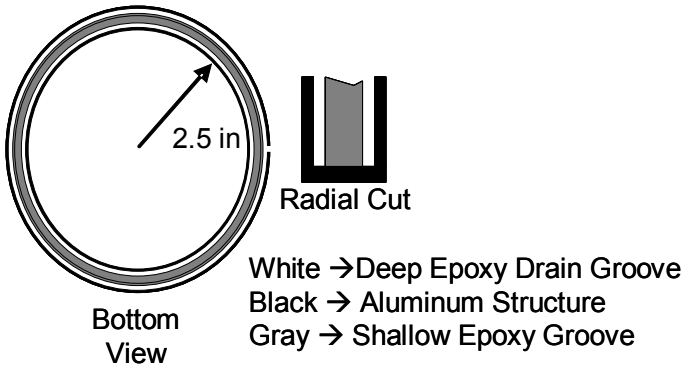

Figure 11: Aluminum Ring Diagram

The grooved area on the aluminum ring is cleaned with a compressed air canister to remove any particles which may prevent a solid bond between the membrane and the aluminum ring. Some

of the aluminum rings have been machined with wire support plates on the top surface (side opposite the grooves). These plates must be removed with a hex wrench so that the ring will lay flat on a surface. If the ring is tilted at all during cure, the epoxy will be unevenly distributed around the circumference of the mirror, which may jeopardize the bond strength.

M-bond 610 is a two part epoxy system. It was selected for the project based on its ability to bond securely to both aluminum and the PVDF material. This epoxy was also selected because of its low viscosity, which allowed the epoxy to easily fill the machined grooves of the aluminum ring. This is not a conductive epoxy, so a grounded lead was attached to the negative side of the PVDF sheet to bleed off any stored charge accumulated during testing.

A plastic dropper was used to carefully fill the inner groove of the aluminum ring. Once the groove is filled, the epoxy will naturally flow up to the shallower middle groove. Epoxy is added until the liquid has completely filled both the inner and the middle grooves. The outer groove is simply used for runoff. If too much epoxy is applied, it will flow into the outer groove and to the outside of the aluminum ring through the slit. This prevents the epoxy from running to the inside of the ring, which would destroy the surface of the mirror and distort the dynamics of the membrane.

The epoxy is allowed to set for a half of an hour. This process is important, because when the ring is turned right-side-up for placement on the PVDF membrane, the epoxy cannot be allowed to run out of the grooves onto the mirror.

After the epoxy has started to set up and the ring can be tilted without disrupting the epoxy in the aluminum grooves, the PVDF membrane is brushed with epoxy in the areas where the ring will be attached. The aluminum ring is then carefully turned right-side-up and placed in the center of the control patches. The windows etched on the PVDF membrane will help with the placement.

The epoxy between the aluminum ring and the PVDF is allowed to cure under its own weight for two or more days. The mirror can then be carefully removed from the tensioning apparatus. The excess PVDF material is then cut away from the 6 inch ring with sharp scissors. Care must be taken not to remove any of the control leads and also to insure that an appropriate space is left for the ground wire.

The membrane is placed in a 150° F oven for at lease 24 hours to further solidify the epoxy cure. Once the M-bond 610 is completely cured, the control lead wires are attached to the control leads on the PVDF membrane. The control lead wires are covered with electrical tape to insure a solid, isolated connection and protect against unintentional grounding during testing.

The membrane is now appropriately tensioned, epoxied to the six inch aluminum ring and ready for coating with silicone substrate.

3.6 Silicone Coating

After the etching and epoxy processes are complete, at 52 μm thick, the material cannot support a bending moment and behaves like a membrane. However, the surface of the mirror is not optical quality. Some surface roughness and inevitable foreign particles have accumulated on the mirror surface. The mirror surface is thoroughly cleaned and coated with silicone substrate to reduce the surface impurities and increase the optical quality of the surface. A smooth coating of gold is applied to the finished substrate to create the needed reflective properties on the mirror.

Before each mirror is coated, a few measurements are taken. In order to estimate the thickness of the silicone layer, a weight measurement before and after coating is taken. Also, vibration testing can be used to predict the tension that was applied to the PVDF during the epoxy phase (see Section 3.5). This information is valuable to the characterization of the membrane structure and is easiest to collect before coating.

Coating the mirror surface with the silicone substrate requires a great deal of care and experience. The process used was highly iterative and experimental. An outline of the procedure as well as comments about some of the problems that were faced are discussed below.

The silicone substrate that was selected for the coating process is GE Silicones RTV615. This product is a two part compound which requires thorough mixing. The mixture requires precisely 10 parts (by weight) RTV615A resin to one part RTV615B curing agent. RTV615 was selected because of its low shrink rate and room temperature cure. It is clear and colorless, pours easily after mixing and cures in one week.

The flexibility of RTV615 is similar to rubber and therefore will certainly have an effect on the dynamics of the membrane. Silicone substrate can carry a bending moment, where the uncoated PVDF membrane could not. This alters the dynamics of the optical structure from those of a membrane to something closer to a thin, deformable plate. In order to maximize the membrane-like behavior of the plate, the thinnest possible layers were applied. Each layer was approximately 1 to 2 mm thick, however, two to three layers were needed to create an optical quality surface. Table 3 provides some useful material properties for RTV615.

Two configurations are possible for the curing process. The first is to lay the PVDF membrane on a flat sheet of glass, pour the silicone substrate and allow it to cure with the weight of the resin supported by the glass sheet. This configuration would provide a coat of even thickness of silicone when supported by the glass. However, during suspension by the aluminum support ring for testing the PVDF membrane would have to support the weight of the resin and may sag. This would certainly affect the optical quality of the reflective surface. Figure 12 illustrates this deformation problem. The second method is to pour the resin and allow it to cure in the testing configuration (i.e.

Table 3: GE Silicones RTV615 Material Properties

Parameter	Value
Specific Gravity	1.02
Viscosity	4000 cps
Shrinkage	0.2%
Useful Temperature Range	-60° C to 204° C
Work Time @ 25° C	4 hr
Cure Time @ 25° C	7 days
Cure Time @ 100° C	1 hr

suspended by the aluminum ring). In this case, the weight of the resin is supported by the PVDF during the cure process. The silicone will cure unevenly (thicker in the middle) to compensate for the sag in the PVDF. Figure 13 shows an approximation to the surface shape. The result is a flat surface when suspended, but an uneven distribution of the silicone substrate. Ultimately, the second approach was utilized because it will provide a flatter surface in the testing configuration.

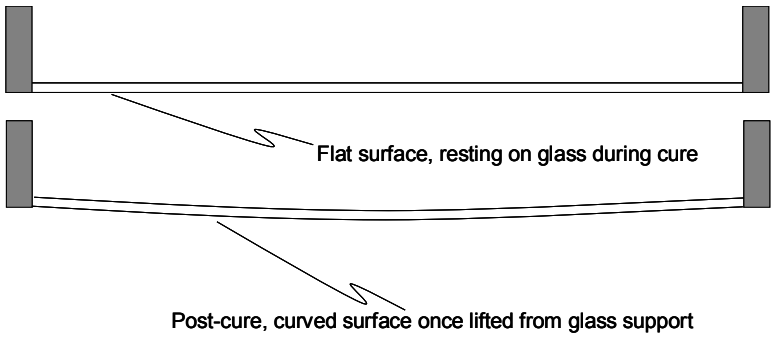

Figure 12: Glass Cure Configuration

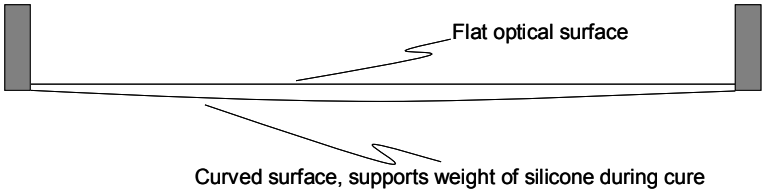

Figure 13: Suspended Cure Configuration

The silicone substrate is very susceptible to contamination during the curing process, therefore the uncoated PVDF mirror surface must be thoroughly cleaned before the silicone substrate is poured. An air jet sprayer is used to clean the surface. Any chemicals or oils on the surface may prevent the silicone from properly bonding to the PVDF material. Additionally, all tools and mixing containers are cleaned before working with the substrate. The lubricating powder on latex gloves also seems to spoil the cure process, so no gloves are used (the substrate is chemically very neutral, so a good washing is enough to remove any silicone from the hands).

The uncoated PVDF mirror is weighed to serve as a baseline. This will enable an inference of the thickness of the silicone layer, see Section 3.7. The raw PVDF surface is coated with GE Silicones SS4120 priming compound. This will help to ensure that the surface is ready to accept the resin with a tight bond and that no air bubbles are formed on the bond surface. Simply brushing on the primer with the provided brush was enough to coat the surface. The mirror is then placed on 4 support blocks which contact only the outer aluminum ring. A sheet of glass is placed over the top of the mirror structure to prevent dust and other contaminants from collecting on the primed mirror surface.

Next, 25 g of RTV615A are poured into the clean stirring container. 2.5 g of RTV615B curing agent is then added, ensuring a ten to one ratio of resin to cure agent. The curing agent and the resin are mixed for ten minutes with a clean stirring implement. The mixture is then poured into a second mixing container and mixed with a second stirring implement for another ten minutes. Finally the mixture is poured into clean test tubes (two to four test tubes are needed for this amount), placed in a centrifuge and spun for ten minutes. The centrifuge will pull all of the entrained bubbles out of the mixture.

The resin mixture is carefully poured onto the PVDF membrane. Pouring is done in one puddle, in the center of the membrane and care is taken to place the lip of the test tube as close as possible to the surface of the membrane. These precautions will help to prevent entrained bubbles, which could work to the surface during cure and destroy to optical quality of the mirror.

After the resin mixture is poured onto the PVDF, the mirror is carefully tipped at a slight angle to encourage the mixture to flow over all parts of the exposed surface.

At this point, some of the early mirrors were placed into a vacuum chamber as recommended by the manufacturer [7]. This process was thought to help remove any remaining bubbles from the mixture, however both mirrors which went through this procedure exhibited visible surface wrinkles after the resin cured. The visible surface wrinkles prevented the surface from being optical quality and necessitated an additional resin coat for smoothing. This vacuum process seems to have resulted in loss of time and material and was not utilized in the fabrication of the most advanced mirrors (7-Patch A and B mirrors).

The silicone resin is shielded from dust by a glass sheet and allowed to cure for seven days at room temperature. The manufacturer specifies that this time could be greatly reduced if a heat treatment is used, however the longer cure time was used to allow the entrained bubbles time to work themselves out of the resin. Accelerating the cure time may have resulted in entrained bubbles and a disrupted optical surface.

After the silicone is completely cured, the mirror is coated with a thin layer of gold to increase the reflectivity of the primary optical surface. The specimen is placed in a vacuum chamber and a small amount of solid gold is evaporated. This process evenly coats the mirror which is suspended in the vacuum.

The optical surface quality is then evaluated. In some instances, visible wrinkles or surface imperfections could be seen with the naked eye. These specimen were selected for recoating and the above procedure was repeated to obtain a smoother surface. If no imperfections were visible on the surface with the naked eye, a small interferometer was used to obtain a rough measurement of the surface quality. Finally, if the surface appeared flat using these methods, the subject was tested in the AFIT test facility with the Shack-Hartman system and wavefront measurements were obtained (Section V).

The final optical structure consists of a base layer of etched PVDF material, one or more layers of silicone substrate and a very thin surface layer of gold. Details of the silicone coating thickness are closely related to the areal density of the mirror and are therefore given in Section 3.7.

3.7 Areal Density Calculation

The areal density, ρ_{areal}, is useful as a comparison of mass per surface area for different optical structures. It is defined in Equation 3:

$$\rho_{areal} = \rho h = \frac{m}{V} h$$

$$V = h * A = h\pi r^2 \tag{8}$$

Volume of a cylinder is defined in Equation 8, where r and A are the mirror radius and surface area, respectively. The equation for areal density can now be reduced:

$$\rho_{areal} = \frac{m}{h\pi r^2} h = \frac{m}{\pi r^2} \tag{9}$$

It is now clear that the areal density relates the mirror mass to surface area. For a space application, where payload weight is at a premium, a lower areal density is desirable.

Table 4 includes mass measurements for all the membranes that were produced. Measurements were taken after the silicone substrate and gold reflective coating were applied, as outlined in Sections 3.2.3 through 3.2.2. Notice that mirror 5-PatchB was not coated and therefore does not have

Table 4: Mirror Mass Data

Mirror	Uncoated Mass (kg)	Coated Mass (kg)	Difference (kg)
7-PatchA	0.357	0.400	0.043
5-PatchA	0.354	0.410	0.056
7-PatchB	0.355	0.375	0.020
5-PatchB	0.355	-	-
Solid Mirror	0.370	-	-

coated measurements. The radius of all mirrors was 2.5 inches (0.0635 m). Given this data we can calculate the areal densities for the three membrane-like mirrors which were constructed, Table 5 gives this data.

Table 5: Calculated Areal Densities

Mirror	Areal Density $\left(\frac{kg}{m^2}\right)$	Substrate Thickness (mm)
5-PatchA	4.42	4.3
7-PatchA	3.39	3.3
7-PatchB	1.57	1.5
Solid Mirror	45.63	-

The density of GE Silicones RTV615 substrate is known to be 1200 $\frac{kg}{m^3}$. The estimated substrate thickness is then calculated using Equation 3. These values are also included in Table 5.

Previous fabrication efforts performed at AFIT have produced mirrors with thicknesses of 4 to 6 mm [22]. The use of these improved fabrication methods have resulted in mirror thicknesses of 1.5 to 3.3 mm, which is a reduction of more than 50 percent in thickness. Because the previous research was done with exactly the same mirror size and materials, the areal density will also be improved. Results indicate that areal densities of 1.57 to 3.39 $\left(\frac{kg}{m^2}\right)$ can be obtained using these methods.

IV. Modal Analysis of Membranes

4.1 Overview

Modal analysis gives essential information about the dynamics of a system. A vibrational analysis of a membrane optical structure can be used as a comparison to the theoretical prediction. This analysis also allows for a comparison between test articles, which enables verification that the fabrication process used for all test articles has been carried out in a similar fashion. Finally, this information can be used to calculate the in-plane tension in the PVDF layer of the optical structure, which is valuable information to numerical researchers.

This chapter first provides a theoretical development of circular membrane theory and gives a description of what results are expected from modal analysis based on that theory. Next a detailed description of the test setup and data collection methods is discussed. Then a calculation of the tension in the membrane is performed.

The modal analysis data is then used to compare many aspects of the vibration tests. Attributes such as actuation method, input signal and orientation of the test article on the test stand are compared. The silicone coated test mirror is also subjected to modal analysis and the results are presented for completeness.

4.2 Theoretical Development

4.2.1 Modes of Vibration of a Circular Membrane. Consider a circular membrane, such as Figure 14, described by polar coordinates (r, θ). Please note that the formulation of this section closely follows that given in Meirovitch [13].

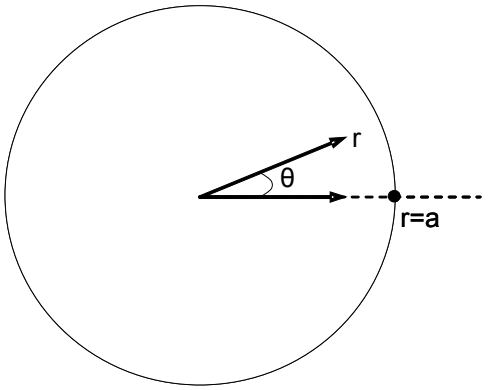

Figure 14: Circular Membrane with Polar Coordinates

The differential equation that describes membrane motion is as follows:

$$\nabla^2 W(r,\theta) + \beta^2 W(r,\theta) = 0 \tag{10}$$

The Laplacian and β are defined as follows:

$$\nabla^2 = \frac{\partial^2}{\partial r^2} + \frac{1}{r}\frac{\partial}{\partial r} + \frac{1}{r^2}\frac{\partial^2}{\partial \theta^2}$$

$$\beta_{mn}^2 = \left(a\frac{\omega_{mn}}{c}\right)^2$$

Here $W(r,\theta)$ is the displacement of the membrane surface, ω is the natural frequency of the membrane and c is the wave speed. Ultimately the solution is attained through a separation of variables. In order to apply this technique, assume a solution of the form:

$$W(r,\theta) = R(r)\Theta(\theta)$$

Make a substitution for $W(r,\theta)$ into Equation 10 and rearrange.

$$\nabla^2 R(r)\Theta(\theta) + \beta^2 R(r)\Theta(\theta) = 0$$

$$\frac{\partial^2}{\partial r^2}\left(R(r)\Theta(\theta)\right) + \frac{1}{r}\frac{\partial}{\partial r}\left(R(r)\Theta(\theta)\right) + \frac{1}{r^2}\frac{\partial^2}{\partial \theta^2}\left(R(r)\Theta(\theta)\right) + \beta^2 R(r)\Theta(\theta) = 0$$

Next, carrying out the partials and factoring, one attains:

$$\Theta(\theta)\left[\frac{\partial^2 R(r)}{\partial r^2} + \frac{1}{r}\frac{\partial R(r)}{\partial r}\right] + \frac{R(r)}{r^2}\frac{\partial^2\Theta(\theta)}{\partial\theta^2} + \beta^2 R(r)\Theta(\theta) = 0 \tag{11}$$

Separate 11 into two equations, starting from:

$$\Theta(\theta)\frac{\partial^2 R(r)}{\partial r^2} + \frac{\Theta(\theta)}{r}\frac{\partial R(r)}{\partial r} + \frac{R(r)}{r^2}\frac{\partial^2\Theta(\theta)}{\partial\theta^2} + \beta^2 R(r)\Theta(\theta) = 0$$

Multiplying by $\frac{r^2}{R(r)}$ one obtains

$$\Theta(\theta)\frac{r^2}{R(r)}\frac{\partial^2 R(r)}{\partial r^2} + \frac{r\Theta(\theta)}{R(r)}\frac{\partial R(r)}{\partial r} + \frac{\partial^2\Theta(\theta)}{\partial\theta^2} + r^2\beta^2\Theta(\theta) = 0$$

Now solve for $\frac{\partial^2\theta}{\partial\theta^2}$, obtain

$$\frac{\partial^2\Theta(\theta)}{\partial\theta^2} = -\Theta(\theta)\left[\frac{r^2}{R(r)}\frac{\partial^2 R(r)}{\partial r^2} + \frac{r}{R(r)}\frac{\partial R(r)}{\partial r} + \beta^2 r^2\right]$$

Now, let m^2 be defined as follows:

$$m^2 = \frac{r^2}{R(r)}\frac{\partial^2 R(r)}{\partial r^2} + \frac{r}{R(r)}\frac{\partial R(r)}{\partial r} + \beta^2 r^2$$

This leads to two partial differential equations:

$$\frac{\partial^2 R(r)}{\partial r^2} + \frac{1}{r}\frac{\partial R(r)}{\partial r} + R(r)\left(\beta^2 - \frac{m^2}{r^2}\right) = 0 \tag{12}$$

$$\frac{\partial^2 \Theta(\theta)}{\partial \theta^2} + \Theta(\theta)m^2 = 0 \tag{13}$$

Equations 12 and 13, taken together, are equivalent to Equation 11. The value of m^2 was chosen to give a harmonic equation in θ. The solution of (13) must be continuous, therefore

$$\theta = \theta_o \sim \theta = \theta_o + 2\pi j, \quad j = 1, 2, 3 \ldots \tag{14}$$

So for any value of θ_o, m must be an integer, or relation (14) would be false and the solution could not be harmonic (which is a contradiction and cannot occur). Now solve (12) and (13) separately.

As previously discussed, the solution to (13) must be periodic and is therefore best represented as a trigonometric function of the form:

$$\Theta_m(\theta) = C_{1m} sin(m\theta) + C_{2m} cos(m\theta), \quad m = 0, 1, 2, \ldots \tag{15}$$

Equation 12 is of a form that has a known solution involving Bessel functions:

$$R_m(r) = C_{3m} J_m(\beta r) + C_{4m} Y_m(\beta r), \quad m = 0, 1, 2 \ldots \tag{16}$$

Where J_m is a Bessel function of the first kind and of order m and Y_m is a Bessel function of the second kind and of order m. Finally, write the general solution by combining 15 and 16.

$$W(r, \theta) = R(r)\Theta(\theta)$$

$$W(r,\theta) = A_{1m}J_m(\beta r)sin(m\theta) + A_{2m}J_m(\beta r)cos(m\theta) +$$
$$A_{3m}Y_m(\beta r)sin(m\theta) + A_{4m}Y_m(\beta r)cos(m\theta), \quad m = 0, 1, 2\ldots \tag{17}$$

Where,

$$A_{1m} = C_{1m}C_{3m}$$

$$A_{2m} = C_{2m}C_{3m}$$

$$A_{3m} = C_{1m}C_{4m}$$

$$A_{4m} = C_{2m}C_{4m}$$

Now the boundary conditions can be applied, to obtain the values of the constants. Assume that a fixed boundary condition exists at the rim, therefore:

$$W(a,\theta) = 0, \quad m = 0, 1, 2, \ldots$$

Since all points of the interior of the membrane must remain finite and Bessel functions of the second kind tend to infinity as the argument approaches zero ($r \approx 0$ at center of membrane), $A_{3m} = A_{4m} = 0$ is the only condition which will prevent the displacement from blowing up. Rewrite Equation 17 as:

$$W(r,\theta) = A_{1m}J_m(\beta r)sin(m\theta) + A_{2m}J_m(\beta r)cos(m\theta), \quad m = 0, 1, 2, \ldots \tag{18}$$

Equation 18 can be written at the boundary, $r = a$, as:

$$W(a,\theta) = A_{1m}J_m(\beta a)sin(m\theta) + A_{2m}J_m(\beta a)cos(m\theta), \quad m = 0, 1, 2, \ldots$$

This can only be satisfied for all θ, if

$$J_m(\beta a) = 0, \quad m = 0, 1, 2, \ldots \tag{19}$$

This equation represents an infinite set of characteristic equations, for any given m, there are infinite solutions, β_{mn}, which correspond to the zeros of the Bessel function of the first kind, J_m.

The subscript m indicates the number of divisions through the center of the membrane for a given mode shape, while n indicates the number of circumferential divisions. There are two modes for each frequency, ω_{mn}, but only one mode for $m = 0$. Therefore, the natural modes are degenerate. The modes can be written as:

$$W_{on}(r,\theta) = A_{on} J_o\left(\frac{\omega_{on}}{c} r\right), \quad n = 1, 2, 3 \ldots \tag{20}$$

$$W_{mnc}(r,\theta) = A_{mnc} J_m\left(\frac{\omega_{mn}}{c} r\right) cos(m\theta), \quad m, n = 1, 2, 3 \ldots \tag{21}$$

$$W_{mns}(r,\theta) = A_{mns} J_m\left(\frac{\omega_{mn}}{c} r\right) sin(m\theta), \quad m, n = 1, 2, 3 \ldots$$

Where W_{mnc} is the cosine component of the solution and W_{mns} is the sine component. Notice that this problem is self-adjoint (i.e. the complex conjugate transpose of a matrix is equal to that matrix), positive definite (i.e. $x^T A x > 0$ where $x \in C^n$) and has orthogonal natural modes (i.e. $AA^T = 1$). From the properties of orthogonality:

$$\int_D \rho W_{on}^2 dD = 1$$

$$\int_0^{2\pi} \int_0^a \rho A_{on}^2 J_o^2\left(\frac{\omega_{on}}{c} r\right) r dr d\theta \equiv 1$$

$$\pi \rho a^2 A_{on}^2 J_1^2\left(\frac{\omega_{on}}{c} a\right) = 1$$

$$A_{on}^2 = \frac{1}{\pi \rho a^2 J_1^2\left(\frac{\omega_{on}}{c} a\right)}$$

Similarly,

$$\int_D \rho W_{mnc}^2 dD = 1$$

$$\int_0^{2\pi} \int_0^a \rho A_{mnc}^2 J_m^2\left(\frac{\omega_{mn}}{c} r\right) cos^2(m\theta) r dr d\theta = 1$$

$$\frac{\pi}{2}\rho a^2 A_{mnc}^2 J_{m+1}^2\left(\frac{\omega_{mn}}{c}a\right)=1$$

$$A_{mnc}^2=\frac{2}{\pi\rho a^2 J_{m+1}^2\left(\frac{\omega_{mn}}{c}a\right)}$$

and finally,

$$\int_D \rho W_{mns}^2 dD=1$$

$$\int_0^{2\pi}\int_0^a \rho A_{mns}^2 J_m^2\left(\frac{\omega_{mn}}{c}r\right) sin^2(m\theta) r dr d\theta=1$$

$$\frac{\pi}{2}\rho a^2 A_{mns}^2 J_{m+1}^2\left(\frac{\omega_{mn}}{c}a\right)=1$$

$$A_{mns}^2=\frac{2}{\pi\rho a^2 J_{m+1}^2\left(\frac{\omega_{mn}}{c}a\right)}$$

Having obtained the necessary A coefficients, substitute these values into 20 and 21 to form the particular solution.

$$W_{on}(r)=\frac{J_o\left(\frac{\omega_{on}}{c}r\right)}{\sqrt{\pi\rho}aJ_1\left(\frac{\omega_{on}}{c}a\right)},\quad n=1,2,3\ldots \tag{22}$$

$$W_{mnc}(r,\theta)=\frac{J_m\left(\frac{\omega_{mn}}{c}r\right)cos(m\theta)}{\sqrt{\pi\rho}aJ_{m+1}\left(\frac{\omega_{mn}}{c}a\right)},\quad m,n=1,2,3\ldots \tag{23}$$

$$W_{mns}(r,\theta)=\frac{J_m\left(\frac{\omega_{mn}}{c}r\right)sin(m\theta)}{\sqrt{\pi\rho}aJ_{m+1}\left(\frac{\omega_{mn}}{c}a\right)},\quad m,n=1,2,3\ldots \tag{24}$$

4.2.2 Undamped Response of a Circular Membrane. The undamped response of a circular membrane will be developed in this section. This development is included for completeness and is not strictly necessary for the modal analysis comparisons which will be used to support the experimental results in the remainder of the chapter.

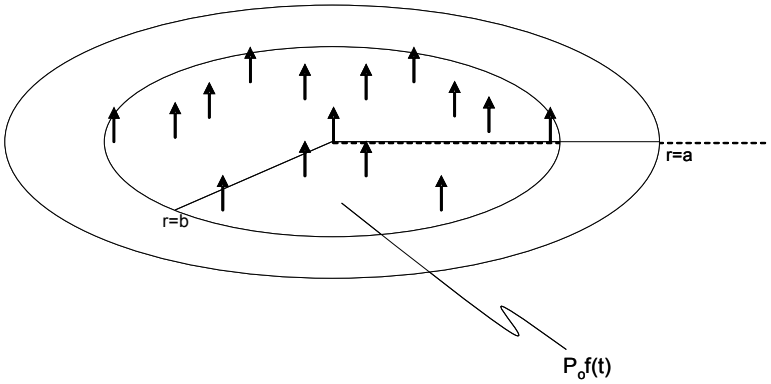

Figure 15: Circular Membrane with Axisymmetric Pressure Distribution

Consider a circular membrane, such as Figure 15. The membrane is assumed to be uniform thickness and clamped at the boundary. The membrane is subject to time-dependent uniform pressure because this is similar to that which a loud-speaker actuator will produce. This pressure is described by:

$$p(r,\theta,t) = p_o f(t), \quad 0 \leq r \leq b$$

$$p(r,\theta,t) = 0, \quad b \leq r \leq a$$

The general solution to the partial differential equation describing membrane motion can be written in the following form through the use of the expansion theorem:

$$W(r,\theta,t) = \sum_{m=0}^{\infty} \sum_{n=1}^{\infty} W_{mn}(r,\theta)\eta_{mn}(t) \tag{25}$$

using the previously developed membrane solution (Equation 22 to 24):

$$W(r,\theta,t) = \sum_{n=0}^{\infty} W_{on}(r,\theta)\eta_{on}(t) + \sum_{m=0}^{\infty} \sum_{n=1}^{\infty} W_{mnc}(r,\theta)\eta_{mnc}(t) + \sum_{m=0}^{\infty} \sum_{n=1}^{\infty} W_{mns}(r,\theta)\eta_{mns}(t)$$

where $W(r,\theta)$ are displacements and $\eta(t)$ are generalized temporal coordinates:

$$\eta_{on}(t) = \frac{1}{\omega_{on}} \int_0^t N_{on}(\tau) sin(\omega_{on}(t-\tau)) d\tau \tag{26}$$

$$\eta_{mnc}(t) = \frac{1}{\omega_{mn}} \int_0^t N_{mnc}(\tau) sin(\omega_{mn}(t-\tau)) d\tau \tag{27}$$

$$\eta_{mns}(t) = \frac{1}{\omega_{mn}} \int_0^t N_{omns}(\tau) sin(\omega_{mn}(t-\tau)) d\tau \tag{28}$$

N_{on}, N_{mnc} and N_{mns} are generalized forces. Recall that the natural frequencies have the form:

$$\omega_{mn} = c\frac{\beta_{mn}}{a} = \sqrt{\frac{T}{\rho}}\frac{\beta_{mn}}{a} \tag{29}$$

Here, T is the tension per unit length, ρ is the mass per unit area and c is the membrane wave speed. Also, recall that β_{mn} are the roots of the Bessel function, $J_m(\beta_{mn})$=0. The generalized forces are given by,

$$n_r(t) = \int_D W(r,\theta) f(r,\theta,t) dD(r,\theta) + \sum_{j=1}^{l} W(r_j,\theta_j) F_j(t) \tag{30}$$

Here, l is the number of constrained forces, $N(t)$ are generalized forces associated with the generalized coordinates, $\eta(t)$. The first term in Equation 30 is associated with the distributed forces, while the second term is associated with the concentrated forces. The current problem as posed above involves no concentrated forces, therefore we are left with:

$$N_{on}(t) = \int_0^{2\pi} \int_0^a W_{on}(r,\theta) p(r,\theta,t) r dr d\theta = \frac{2\pi p_o f(t)}{\sqrt{\pi\rho} a J_1\left(\frac{\omega_{on}}{c}a\right)} \frac{bc}{\omega_{on}} J_1\left(\frac{\omega_{on}}{c}b\right)$$

$$N_{mnc}(t) = \int_0^{2\pi} \int_0^a W_{mnc}(r,\theta) p(r,\theta,t) r dr d\theta = 0 \tag{31}$$

$$N_{mns}(t) = \int_0^{2\pi} \int_0^a W_{mns}(r,\theta) p(r,\theta,t) r dr d\theta = 0 \tag{32}$$

It is indeed reasonable that Equations 31 and 32 are equal to zero because of the axisymmetric distributed force that is assumed in the problem statement.

Substitute back into 26 to 28:

$$\eta_{on}(t) = \frac{2\pi p_o bc J_1\left(\frac{\omega_{on}}{c}b\right)}{\sqrt{\pi\rho} a \omega_{on}^2 J_1\left(\frac{\omega_{on}}{c}a\right)} \int_0^t f(t) sin(\omega_{on}(t-\tau)) d\tau$$

$$\eta_{mnc}(t) = \eta_{mns}(t) = 0$$

Finally, substitute back into the displacement Equation (25):

$$W(r,\theta,t) = \frac{2p_o bc}{\rho a^2} \sum_{n=1}^{\infty} \left[\frac{J_1\left(\frac{\omega_{on}}{c}b\right) J_o\left(\frac{\omega_{on}}{c}r\right)}{\omega_{on}^2 J_1^2\left(\frac{\omega_{on}}{c}a\right)} \int_0^t f(t) sin(\omega_{on}(t-\tau)) d\tau \right] \tag{33}$$

So Equation 33 is the solution for the displacement of the membrane under an axisymmetric distributed load with a clamped boundary condition.

4.2.3 Predicted Surface Deflection. Equation 33 demonstrates the fact that the roots of the Bessel functions play an important part in predicting the the natural frequencies and surface deflections of a circular membrane structure. Figure 16 shows the first few Bessel functions, with the zeros clearly labeled. Note that m corresponds to the order of the Bessel function and n corresponds to the n^{th} zeros crossing of the Bessel function. Table 6 provides the roots of these functions for reference.

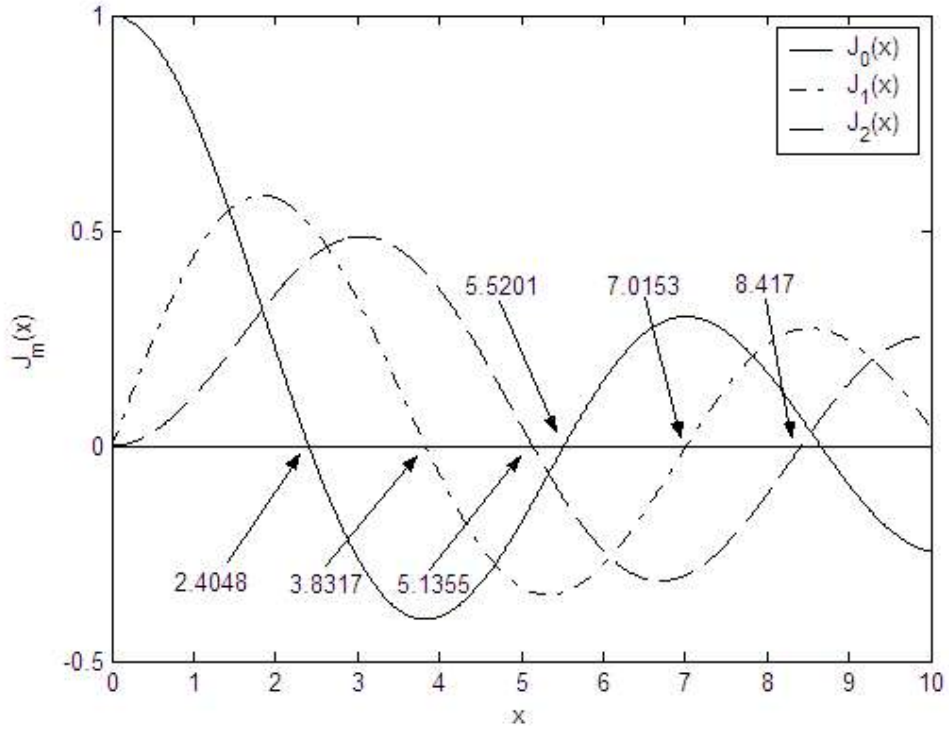

Figure 16: Example of Bessel Functions $J_m(x)$, for m=0:2

Table 6: Table of Bessel Zeros

	n=1	n=2	n=3	n=4	n=5
m=0	2.4048	5.5201	8.654	11.791	14.931
m=1	3.8317	7.0153	10.173	13.324	16.471
m=2	5.1355	8.417	11.620	14.796	17.960
m=3	6.3799	9.761	13.015	16.224	19.409
m=4	7.5884	11.065	14.373	17.616	20.827
m=5	8.7716	12.339	15.700	18.98	22.218

The deformation patterns given in Figure 17 are generated with a Matlab® code (see Appendix B.6), which uses Equation 33. The x, y and z-axis have all been scaled from -1 to 1 because Figure 17 is only intended to illustrate the primary modes of surface deformation. It is important to note that the theory predicts that these modes will appear in the order of the coefficient values given in Table 6. So $m = 0$, $n = 1$ is expected to appear first in a frequency profile, followed by $m = 1$, $n = 1$, then $m = 2$, $n = 1$ and so on.

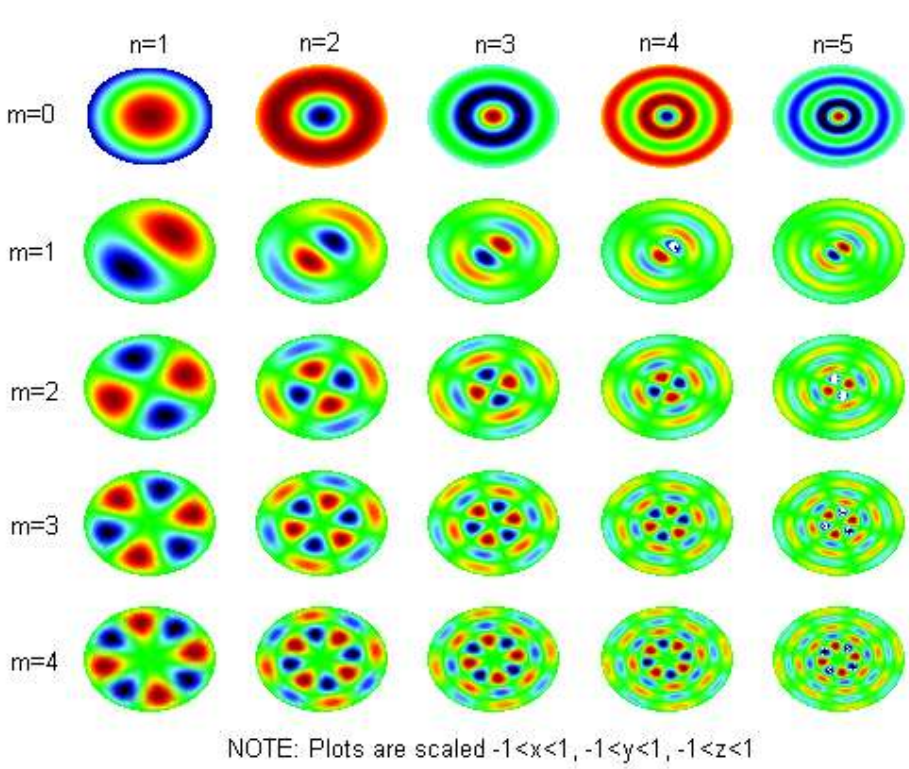

Figure 17: Predicted Surface Deflections given by Bessel Functions

It is worth noting that the use of thin membrane theory as a model for the test subjects is only a rough approximation to the actual dynamics of the system. There are two primary reasons that

this standard theory only approximates the model. First, the thickness of the final optical structure (with the silicone coating) is typically a few millimeters. This structure will support some small bending stress, due to this thickness and is therefore a slight violation of thin membrane theory as it was developed in this section. The second reason involves the actuation method. When the optical structure is actuated with the speaker, on average there is a normal force on the surface. This is the same as the actuation direction which was assumed in the development of the thin membrane theory. However, actuation with the PVDF patches causes the patch to expand in the plane, the deformation out of the plane is a result of bending moments due to the thickness of the optical structure. This actuation direction is different than that assumed in thin membrane theory and may result in additional discrepancies from predicted results for membrane actuated in this manner. Since the structure is overall relatively thin and flexible, membrane theory was still utilized to model the dynamics of this system.

4.3 Test Setup

The test setup which was used for all vibrations tests is shown in Figures 18 and 19. The scanning laser vibrometer was positioned directly above the test membrane. The membrane support ring was then placed onto the support structure with the test article suspended in the middle by heavy iron bars. The actuating speaker was then placed on supports below the membrane and was rested on rubber isolators, which helped to damp vibration in the test structure. Figure 19 illustrates the setup of the test structure with a close side view of the equipment.

The iron support bars were carefully wrapped in electrical tape to isolate the membrane from any electrical connection and vibration in the structure. Heavy iron bars were used to help isolate the excitation of the membrane support structure from that of the membrane surface. The wrapped bars can be seen in the lower image of Figure 18.

This test setup was not changed for any membrane. The exact location and orientation of every piece of equipment was marked before testing and this orientation was verified before every test was performed. These efforts helped to ensure that the test setup and vibration in the support structure were similar for every membrane which was tested. The speaker was left in place on the test setup even if acoustic actuation methods were not used.

4.4 Data Collection

A scanning laser vibrometer manufactured by Polytec Inc. was used for modal analysis of the test membranes. A signal generator integrated with the laser vibrometer software was used to

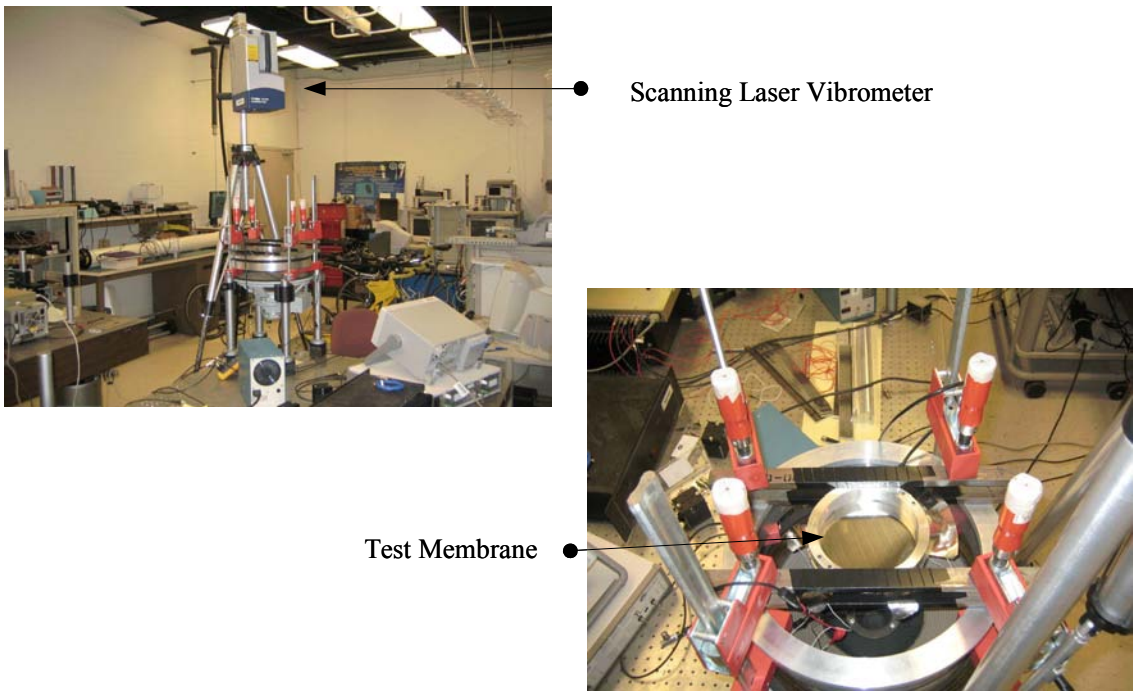

Figure 18: Vibration Test Setup: Global View

provide an input signal to the system (see Figure 21). The power amplifier used for all tests was manufactured by Active Control Experts (ACX). A characterization of this amplifier is given in Appendix C.1. The signal was then used to power either a speaker or the PVDF material directly. The scanning laser sampled 541 points on the membrane surface. Figure 20 illustrates the pattern of data points which were scanned by the laser vibrometer. Software provided by the manufacturer was used to view the data. Frequency response curves, max deformation plots and real time movies were generated using this software. The data was then post-processed using Matlab® code.

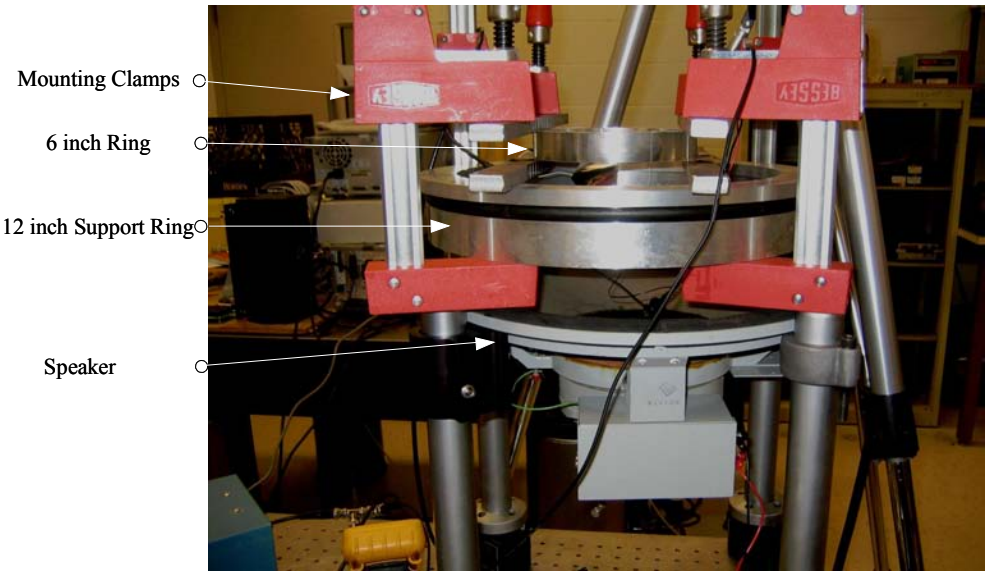

Figure 19: Vibration Test Setup: Side View

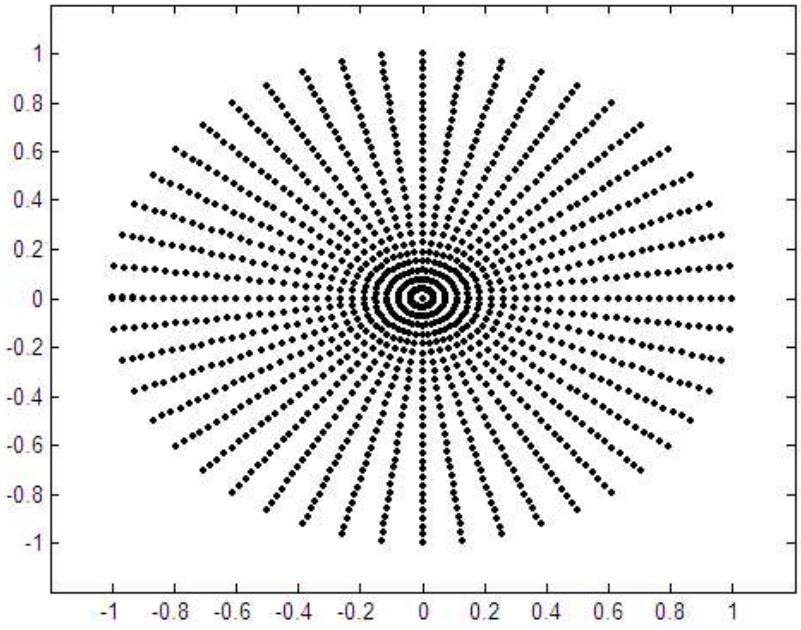

Figure 20: Data Collection Pattern for the Scanning Laser Vibrometer

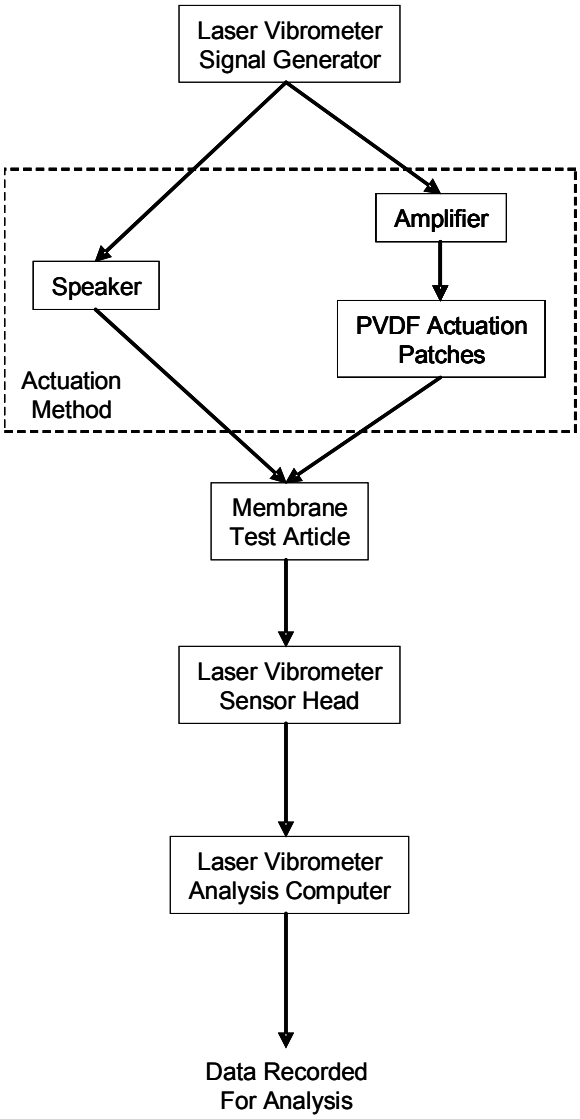

Figure 21: Flow Chart of Vibrometer Experiment

4.4.1 Test Parameters. Table 7 provides an overview of the test parameters which were used for data collection with the scanning laser vibrometer. These parameters remained the same for every test which was run.

Table 7: Table of Test Parameters

Parameter	Setting
Scan Points	541
Optimal Reading	100 %
Scanning Head	PSV-I-400 LR
Front End Software	PSV-E-400-3D (1D)
Acquisition Board	National Instruments PCI-4452
Acquisition Mode	FFT
Averaging	Complex
Average Count	10
Cosine Correction	Active
Bandwidth	50 Hz to 1.25 kHz
Sampling Lines	3200
Sampling Frequency	3.2 kHz
Sample Time	2.56 s
Resolution	390.6 mHz
Window	Rectangular

4.4.2 Description of Test Runs Performed. A summary of the tests performed with the vibrometer is given below:

- 12 Inch Test Article
  - Speaker actuation, chirp, standard orientation, optical surface up
  - 1-patch actuation, chirp, standard orientation, optical surface up
- 5 Inch Uncoated Test Article
  - 5-Patch Control Pattern
    - Speaker actuation, chirp, standard orientation, optical surface up
    - Speaker actuation, noise, standard orientation, optical surface up
    - PVDF actuation (all patches), chirp, standard orientation, optical surface up
    - PVDF actuation (all patches), chirp, rotated 180°, optical surface up
    - PVDF actuation (all patches), chirp, rotated 180°, optical surface down
  - 7-Patch Control Pattern
    - Speaker actuation, chirp, standard orientation, optical surface up
    - PVDF actuation (center patch), chirp, standard orientation, optical surface up

        * PVDF actuation (all patches), chirp, standard orientation, optical surface up

- 5 Inch Coated Test Article
  - 7-Patch Control Pattern (membrane A)
    * Speaker actuation, chirp, standard orientation, optical surface down
  - 7-Patch Control Pattern (membrane B)
    * Speaker actuation, chirp, standard orientation, optical surface down

4.5 Tension Calculation

One of the primary goals of this research is to obtain an estimation of the tension entrained in the PVDF material during fabrication. The results of the vibration tests can be utilized to calculate this tension.

Recall from Section 4.2.2 that Equation 29 gives the theoretical natural frequencies of the circular test article. This equation can be rearranged for the tension as given in Equation 34:

$$T = \rho \left(\frac{\omega_{mn} r}{\beta_{mn}} \right)^2 \tag{34}$$

The zeros of the Bessel Function, β_{mn} are known quantities, given in Table 6. The radius, r, and density per unit area, ρ, are known quantities. Therefore, final piece of the puzzle is the natural modes, ω_{mn}, for the structure.

The natural modes are easily identified through the FFT's and surface deflection plots produced by the laser vibrometer testing (see Section 4.6.4 for these results). The task is to simply pick a mode, examine the surface deflection plot, match it to the theoretical surface deflection plots given in Figure 17 to find β_{mn} for that mode and then to use Equation 34 to calculate the tension.

This procedure has been done for selected uncoated test articles and the results are tabulated in Table 8. The tension calculation presented is an average of the calculated tension for the first five identifiable modes for each test article.

Table 8: Calculated Average Tension

Mirror	Avg Tension $\frac{N}{m}$	Std Deviation $\frac{N}{m}$	Modes Identified (m,n)
12 Inch Test Article	1.9128	0.56359	(0,1) (1,1) (2,1) (1,2) (3,1)
5-Patch A	3.0049	0.50113	(0,1) (1,1) (2,1) (1,2) (2,2)
7-Patch A	4.5874	1.0303	(0,1) (1,1) (2,1) (0,2) (3,1)

4.6 Comparison of Testing Attributes

Several tests were conducted using membranes of different orientations, actuation methods and input signals. Membranes were also tested with and without the silicone surface coatings. Results and comparisons that illustrate these aspects will be described within this section. Presentation of all results and data is simply not economical, therefore only the best illustrative examples have been chosen.

4.6.1 Actuation Method. Two different actuation methods are possible for the test articles. The first is actuation with the speaker, mounted in close proximity to the membrane. The second are the PVDF patches etched on the membrane surface. Actuation with the center patch alone and actuation with seven patches simultaneously were examined.

In order to test the dependence of actuation method, three cases were tested using an uncoated 5 inch, 7-patch membrane. All actuation tests were run with the chirp input signal.

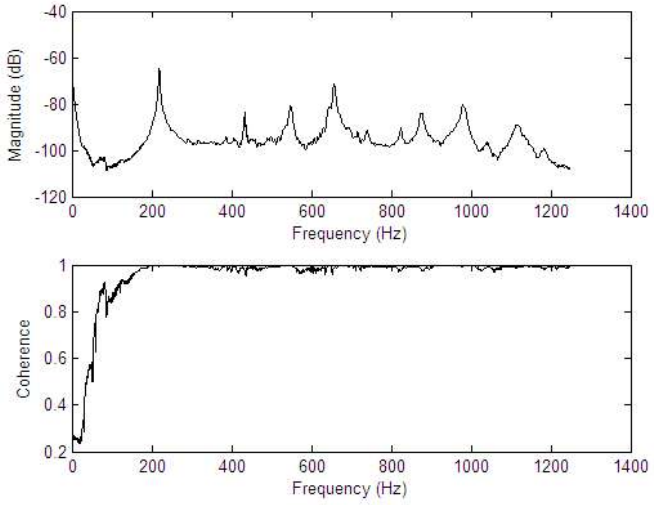

Figure 22: FFT and Coherence Plot for Speaker Actuated Case

Figure 22 shows the Fast Fourier transform (FFT) and coherence data for the speaker actuated case. The FFT data represents the average FFT for every point on the surface, sampled by the vibrometer. The coherence data is of particular interest. Notice that below 150 Hz, the coherence drops off rapidly, but for the rest of the spectrum the coherence is near to one. This indicates that the data is well correlated, therefore it is more likely to give accurate results.

The coherence plot for the 1-patch actuated case (Figure 23) is well below 80% over the entire domain of the spectrum. This indicates that the data has low correlation. This is expected because

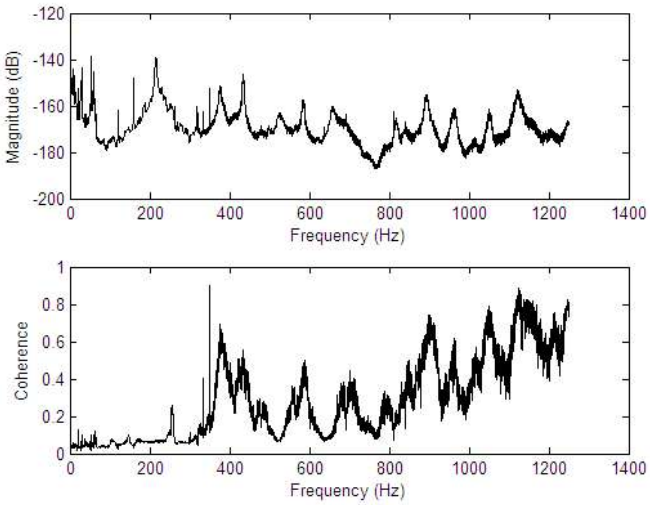

Figure 23: FFT and Coherence Plot for 1-Patch Actuated Case

only a small patch in the center of the membrane is being actuated. The time delay that it takes the waves to propogate to the exterior of the membrane may reduce the correlation of the data.

Figure 24 gives the FFT and coherence data for the 7-patch actuated case. Here the coherence is solidly above 80% after 350 Hz, but relatively shakey prior to that. This indicates that at lower frequencies, the data is still not correlated very well, despite the additional control patch actuation. The data indicates that the use of more control patches gives better correlated data over the entire spectrum. This is due to a larger area of the membrane being actuated, which gives a reduced time delay and larger displacement.

Table 9: Comparison of Speaker, 1-Patch and 7-Patch Frequencies with Circular Membrane Theory

	Theory	Avg Freq	Speaker Freq	1-Patch Freq	7-Patch Freq
m=0, n=1	213.6 Hz	213.6 Hz	215 Hz	218 Hz	208 Hz
m=1, n=1	331.4 Hz	429.6 Hz	433 Hz	433 Hz	423 Hz

The observed frequencies of the first two modes are given in Table 9. These frequencies are averaged and this value is given in the 'Avg Freq' column. The theoretical value is obtained based on the theory presented in Section 4.2.3.

Equation 29 gives the relationship between the theoretical natural frequency and the physical parameters associated with the membrane test subject (i.e. T, ρ, $r = a$). The zeros of the Bessel functions are given in Table 6. Since the tension, radius and density are constant during this test, the values in this table can simply be used to predict the subsequent modes of the structure. Note

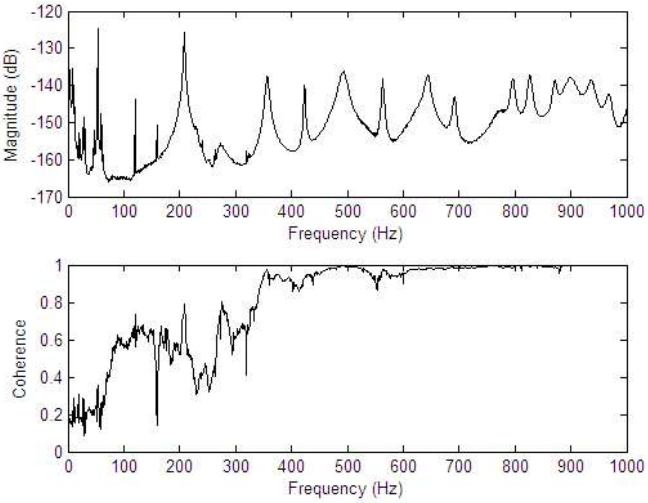

Figure 24: FFT and Coherence Plot for 7-Patch Actuated Case

that the first theoretical frequency must be used to find the constant multiplier and therefore is set equal to the frequency of the first average mode. Equation 35 is an illustration of how this method can be used to predict the $m = 1$, $n = 1$ natural frequency.

$$\omega_{mn} = \sqrt{\frac{T}{\rho}}\frac{\beta_{mn}}{a} = K\beta_{mn}$$

$$K = \frac{\omega_{01}}{\beta_{01}}$$

$$\omega_{11} = K\beta_{11} = \frac{\omega_{01}}{\beta_{01}}\beta_{11} \tag{35}$$

4.6.2 Input Signal. The input signal typically used for vibrations testing is random noise. This is a signal that contains the same power at every frequency. Since the natural frequencies of the optical structures was predicted to be in the hundreds of Hertz, exciting the entire frequency spectrum could prove inefficient. For this reason, both a pseudo random noise signal and a periodic chirp signal were used to excite the test articles.

A pseudo random noise signal has equal power only over a specified frequency range. A periodic chirp signal emits sinusoidal oscillations over a specified frequency range. The chirp signal begins with the low end of the frequency range and ends at the high end.

In order to test the dependence of the vibration data on the type of input signal, these signals were run over the frequency range from 50 to 1400 Hz.

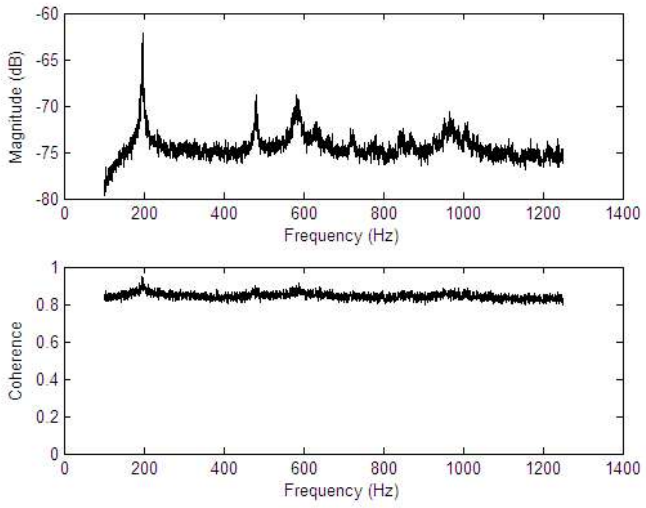

Figure 25: FFT and Coherence Plot for Pseudo Random Noise Input Case

In total, the coherence plots for both test cases are relatively good, averaging values above 80%. The noise generated FFT of Figure 25 compares closely with that of the chirp generated FFT in Figure 26 with respect to location and magnitude of the first mode. At higher frequencies, the noise generated FFT suffers a loss of detail and the peaks are not as pronounced. The chirp generated FFT has the most detailed information about these primary modes.

Due to the clean data pattern relative to a pseudo random noise input signal, the periodic chirp input signal is determined to be slightly better for acquisition. For this reason, all further tests use the chirp signal generator.

4.6.3 Orientation. In order to test the orientation dependence of the membrane test article, tests were performed in the 'standard' orientation and then the specimen was rotated 180° and tested again. In order to protect the coated mirrors, they were tested in the upside-down position. Therefore, the test membrane was also flipped upside-down and tested.

The 'standard' position was chosen by convenience and is arbitrary. For this discussion it will be defined as the control lead for the center patch running parallel to the iron bar supports and

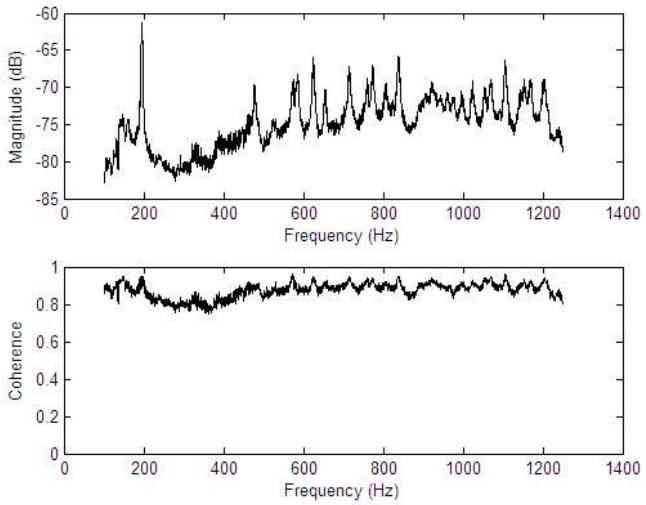

Figure 26: FFT and Coherence Plot for Periodic Chirp Input Case

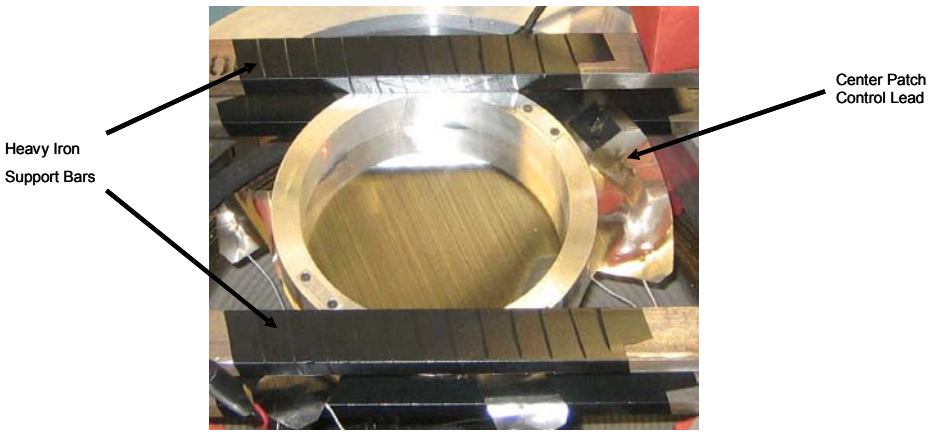

Figure 27: Definition of 'Standard' Orientation

toward the nearest table edge. This orientation is clearly illustrated in Figure 27. Notice the PVDF flap where the center patch control lead runs and the grounding wire (covered by electrical tape) can be seen on the right of the membrane.

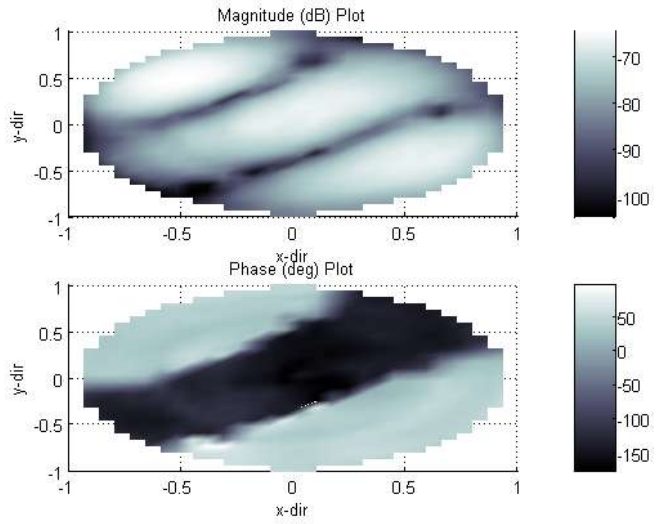

Figure 28: Magnitude and Phase for 'Standard' Orientation Case (Freq=467Hz, m=2, n=1)

Figure 28 shows the m=1, n=2 mode for the standard orientation. It is clear from Figure 29 that the rotation changed the vibration of the membrane. The darkened lines indicating zero crossings on the membrane surface have rotated in accordance with the membrane support structure, as is expected.

After the membrane is flipped up-side down (Figure 30) the zero crossing lines on the magnitude plot return to the orientation of the original standard position. This is also as expected since the membrane is now in an upside-down, 180° rotated orientation.

The dark bands on the phase plots, which indicate 180° out of phase are also important to notice. The right side-up test articles show that the center portion is out of phase, while the upside-down membrane shows the sides out of phase, as expected.

The mean for the first and second natural frequencies were calculated and compared to the theoretical value (obtained as in Table 9). This information is given in Table 10.

Table 10: Comparison of Standard, Rotated and Flipped Frequencies Data with Circular Membrane Theory

	Theory	Avg Freq	Standard Freq	Rotated Freq	Flipped Freq
m=0, n=1	191.3 Hz	191.3 Hz	191 Hz	192 Hz	191 Hz
m=2, n=1	410 Hz	476.3 Hz	467 Hz	478 Hz	484 Hz

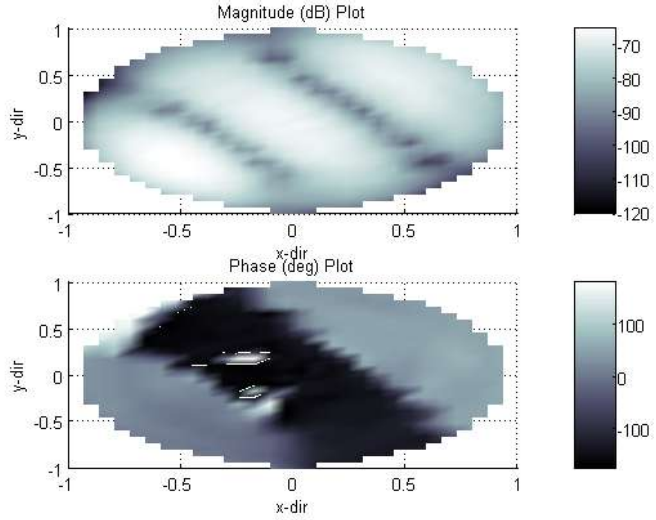

Figure 29: Magnitude and Phase for Rotated Case (Freq=478Hz, m=2, n=1)

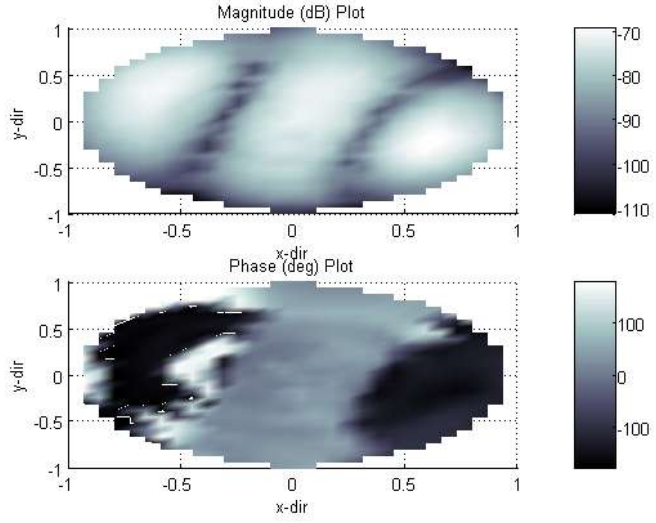

Figure 30: Magnitude and Phase for Upside-down Case (Freq=484Hz, m=2, n=1)

Since the results of these tests show almost no variation in the fundamental frequencies of the test article, the orientation of the test article is shown to be largely arbitrary for a given test. Therefore, testing the coated membrane optical structures in an inverted position to protect the optical surface are assumed to yield very similar results to tests run in the 'standard' test configuration.

4.6.4 Membrane Coating. Each membrane must be coated with silicone to improve the optical quality of the surface. This coating drastically changes the dynamics of the membrane. For this reason, a comparison between an uncoated mirror and a coated mirror is justified. The 7-patch mirror was used for the comparison.

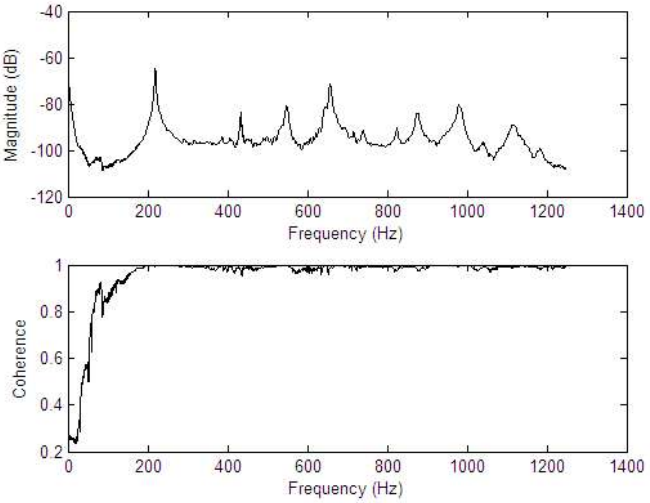

Figure 31: FFT and Coherence Plot for Uncoated Case

Figure 31 shows the Fast Fourier transform (FFT) and coherence data for the uncoated case. Figure 32 gives the same information for the silicone coated membrane. Notice that the high frequency vibrations (above 400 Hz or so) are severely damped out by the silicone coated membrane.

The first three peaks in both the coated and uncoated cases represent the same modes of vibration. These frequencies can be compared to the theoretical prediction of the fundamental frequencies for these modes. This comparison will enable an estimation of how the presence of the silicone substrate affects the dynamics of the membrane. Table 11 provides a comparison of the first three modes for the uncoated case (obtained as in Table 9). The first three peaks for the uncoated case a

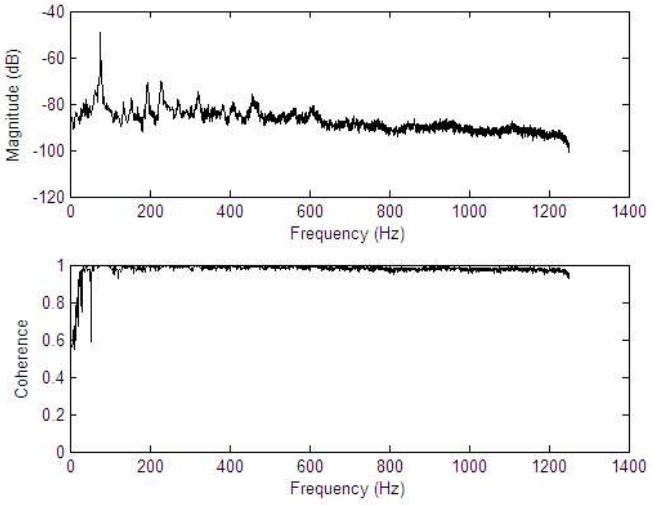

Figure 32: FFT and Coherence Plot for Coated Case

Table 11: Uncoated Comparison of Membrane Frequencies with Circular Membrane Theory

	Theory	Experimental	% Difference
m=0, n=1	218 Hz	218 Hz	0.0%
m=2, n=1	465.5 Hz	547 Hz	17.5%
m=0, n=2	500.4 Hz	656 Hz	31.1%

Table 12: Coated Comparison of Membrane Frequencies with Circular Membrane Theory

	Theory	Experimental	% Difference
m=0, n=1	64.5 Hz	76 Hz	17.8%
m=2, n=1	137.85 Hz	194 Hz	40.0%
m=0, n=2	148.1 Hz	228 Hz	53.8%

Table 12 gives the experimentally observed fundamental frequencies for the coated case. The theoretical prediction is obtained by the use of Equation 29, where tension, mass and the zeros of the Bessel function are known quantities, addressed in Table 8, Table 4 and Table 6, respectively.

The results indicate that a frequency shift of approximately 142 Hz occurs after the surface is coated with silicone. Theory predicts that a shift of 153.5 Hz should occur due to the added mass on the membrane. There is approximately 11.5% error, which is well within the error deviations that have been recorded for these tests. This indicates that even with the silicone substrate, the system is still modeled well by the membrane equations, as long as the additional mass is acounted for in the system.

4.7 Summary

In this chapter, a modal analysis of the test articles has been carried out and the data has provided information regarding the dynamics of the optical structure. The theoretical development was relied upon for the prediction and calculation of fundamental frequencies and mode shapes. These theoretical values were compared to the experimentally observed values. The modal analysis data was also utilized to calculate the tension in the membrane.

The tension in the membrane was determined to be 3.0 to 4.6 $\frac{N}{m}$ with a standard deviation of 0.5 to 1.0 $\frac{N}{m}$. The orientation of the test article was determined to have little to no impact on the frequency analysis data. The silicone coated test membrane was determined to match the values obtained by pure membrane theory to about 11.5%, which indicates that the coated membrane can still be well approximated by membrane theory.

The insight gained through this modal analysis is useful to the development of understanding about thin deformable structures and numerical researchers studying this membrane system. An improved data acquisition system would allow some of this insight to be applied to the control problems associated with this optical system.

V. Wavefront Imaging of Membrane Surface

5.1 Overview

This chapter provides an explanation of the testing procedure and results for the wavefront imaging experiments. Included sections describe the test setup, data collection and data processing tools that are developed and utilized. Static deformation results are given a statistical treatment and compared to previous research. Dynamic measurements are also made of the surface and the results are used to characterize the data acquisition system.

5.2 Surface Deflection in Terms of Zernike Polynomials

The classical formulation for the expression of the displacement of the surface in terms of Bessel functions (as explained in Section 4.2.3) is not the only way to mathematically express the surface deformation. Another orthogonal set of polynomials which are often used to express the surface are called Zernike Polynomials. This set is often used in the optics community.

Appendix C.3 gives a list of the first 42 Zernike Polynomials. Since the surface is described by a linear combination of the polynomials, additional terms in the sum increases the accuracy of the surface match to the data. 42 polynomials were chosen in order to capture the most significant deflection of the surface.

The Zernike polynomials are functions of radius, r, and angle, θ. Given a polar coordinate, Equation 36 will return a surface deflection. The data taken during the wavefront experiments was Zernike coefficients, this data is scaled by the WaveScope® software to give a solution in terms of microns of surface deflection (see Section 5.4.1).

$$W(r,\theta) = \sum_{i=1}^{n} \zeta_i Z_i(r,\theta) \tag{36}$$

Here ζ is the Zernike coefficient and Z is the Zernike polynomial. Figure 33 provides a surface plot of the first 25 Zernike polynomials for comparison with Figure 17. These plots illustrate the $Z_i(r,\theta)$ polynomials, which are eventually scaled by the wavefront data, ξ_i. The x, y and z-axis have all been scaled from -1 to 1. The mathematics required to obtain a mapping from the set of Bessel functions to the set of Zernike polynomials is beyond the scope of this thesis. For the purpose of this research, data will be transformed into terms of surface displacements before analysis, through the use of one of the methods described above.

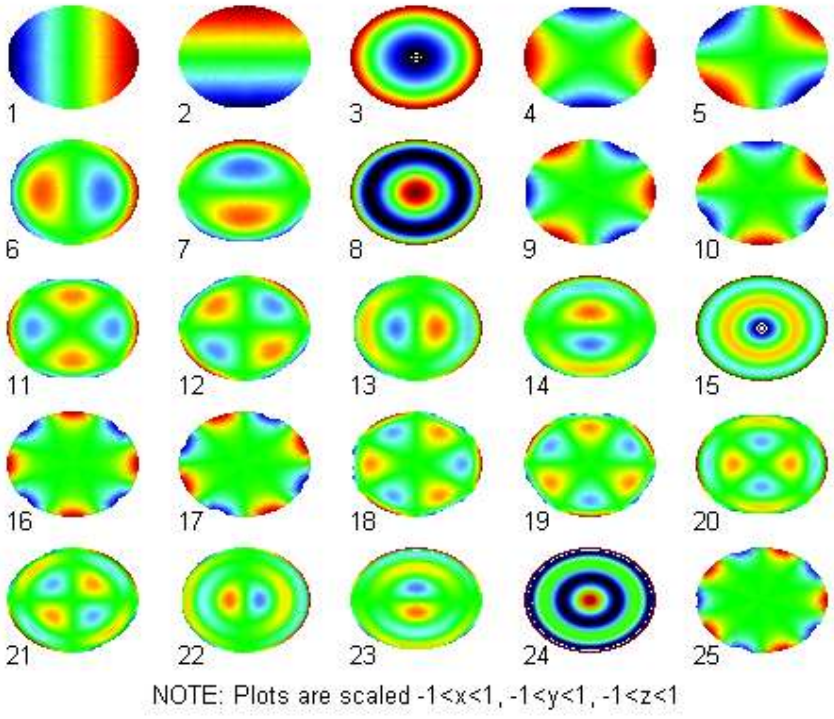

Figure 33: Component Breakdown of Zernike Polynomials

5.3 Test Setup

The test setup on the optical table is an extension of a prior arrangement used by previous researchers at AFIT [21]. For completeness, the setup of the optical table will be described again here. Any significant deviations from this setup will also be noted.

A 20 mWatt helium-neon laser (λ = 633 nm) was used to illuminate the test subjects. The optical path of the laser is outlined in Figure 34 through 36.

Light from the laser first passes through a set of neutral density filters, which alter the intensity of the beam to a usable level for the wavefront sensor. The filter set includes a primary filter wheel, with lenses ranging from 10% to 80% transmission and two variable gradient filter wheels which can be used for fine adjustments. These filters are shown in Figure 35. Due to differences in optical quality and reflectivity, the filter wheels are tuned for every test article.

The optical path is then turned 90° by a $\frac{\lambda}{20}$ flat mirror (Small Pivot Mirror A, 34). The beam passes through a spatial filter, which produces a clean Gaussian wavefront to illuminate the test

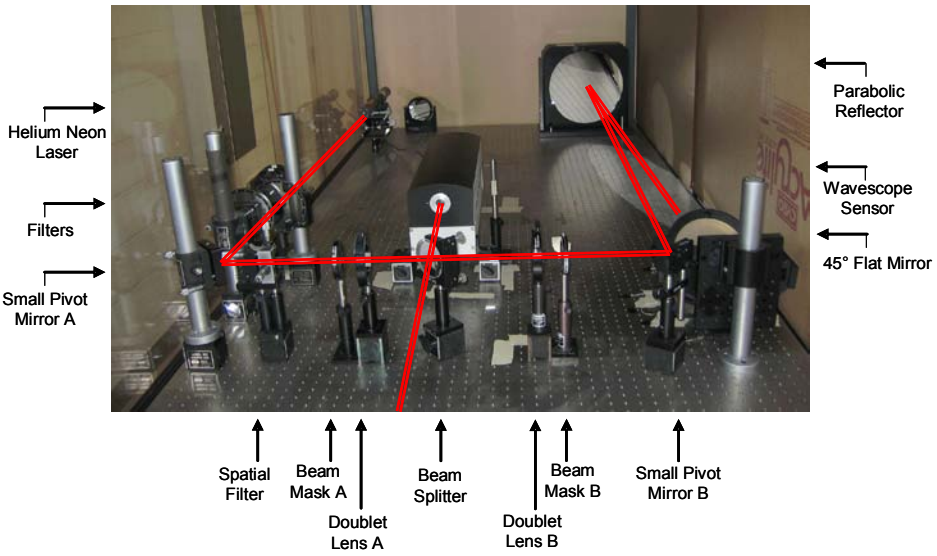

Figure 34: Optical Table Test: Global View

article. At this point, the laser light is expanding. A 1 inch achromatic doublet lens (Doublet Lens A) is utilized to collimate the expanding beam. This lens has a focal length of 200 mm.

A Shack-Hartmann type wavefront sensor, requires two beams for wavefront measurement. The first beam is the image from the optical surface under investigation and will be referred to as the test beam. The second beam is a reference beam from a flat optical surface and will be referred to as the reference beam. In order to generate these two beams from the same source, a beam splitter is utilized.

The collimated laser light now meets a 3 inch $\frac{\lambda}{5}$ wedge beam splitter, which separates the beam into two equal intensity beams. The reference beam is turned 90°, reflected off of a $\frac{\lambda}{20}$ flat mirror (Reference Beam Flat Mirror, 36), back through the beam splitter and into the wavefront sensor.

The test beam is allowed to pass through the beam splitter. This beam is focused using a 1 inch doublet lens, with a focal length of 250 mm. The focal point of the test beam is located on a $\frac{\lambda}{10}$ flat mirror (Small Pivot Mirror B, 36), which turns the expanding beam toward the end of the table. A 12.5 inch parabolic reflector, with a focal length of 75.125 inches, is used to stop the expansion of the beam and to direct the beam path onto the test article. Finally, a 6 inch flat mirror, mounted at 45° from vertical, was used to turn the test beam 90° downward onto the test article.

The test beam is reflected off of the test article and allowed to follow the same optical path back to the beam splitter. The beam splitter turns the test beam 90° into the wavefront sensor. The test article is suspended over the optics table by spacers, which allows the membrane to vibrate freely.

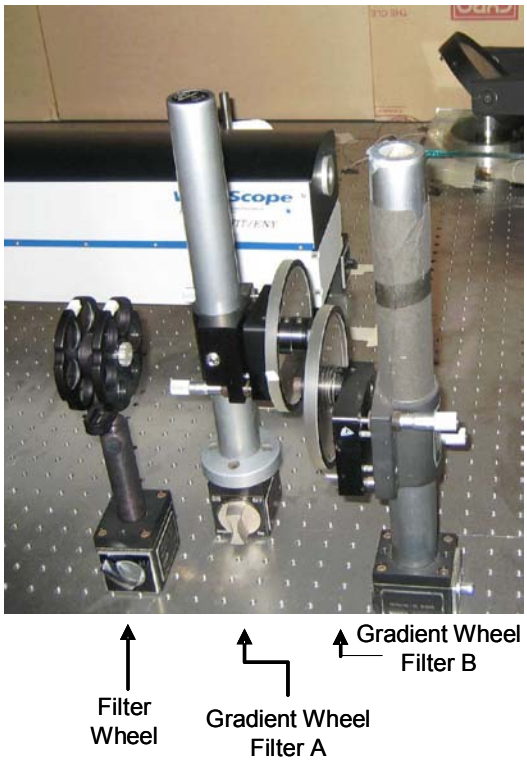

Figure 35: Optical Table Test: Filter View

5.4 Data Collection

Data collection from the wavefront sensor can be completed with the WaveScope® electronics box and acquisition software, however for situations where greater versatility is needed a data acquisition methodology was developed to use Matlab® running on a separate computer. This methodology lays the foundation for future development of the system for use with Simulink® controls software and dSpace® control system prototyping hardware. This section provides an outline of the new data acquisition setup. The system is illustrated in the form of a flow chart in Figure 37.

All wavefront measurements utilized a Shack-Hartmann type, WaveScope® wavefront sensor, manufactured by Adaptive Optics Associates. Data is generated from the test and reference beams (see Section 5.3) and processed by the WaveScope® electronics box (Figure 38).

The data is then used to calculate various coefficients and images by the WaveScope® software. For the present system, it is desirable to disable all unnecessary calculations and image displays on the WaveScope® computer. This will save time and allow the data to stream as quickly as possible to the Matlab® acquisition computer.

Software engineers at Adaptive Optics Associates graciously provided a script to enable Zernike coefficients generated by the WaveScope® computer to be exported via an ethernet connection. This

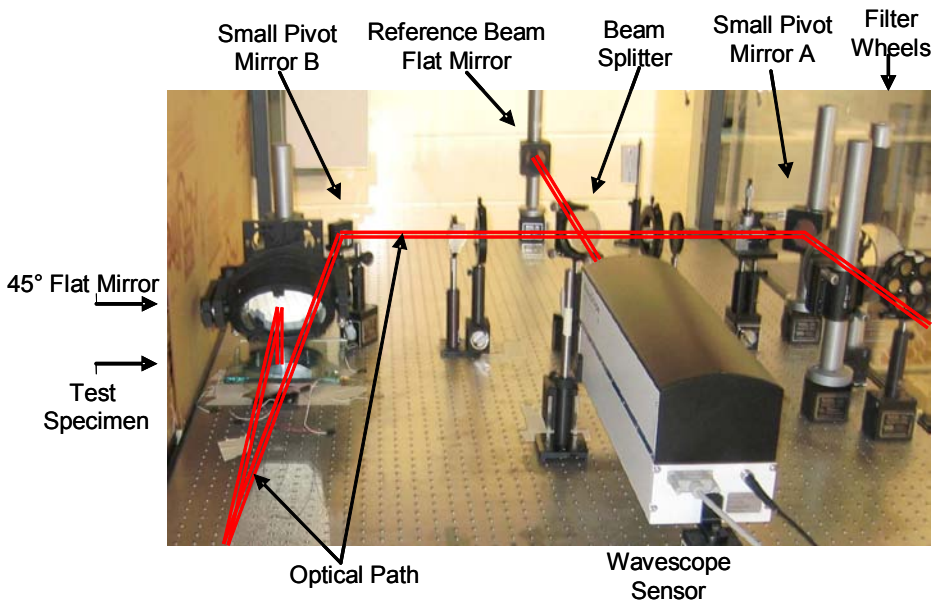

Figure 36: Optical Table Test: Test Specimen View

data stream from the WaveScope® computer's ethernet port was converted into a serial data stream using the Nport® Serial to ethernet conversion box.

This was a necessary step because the dSpace® hardware does not currently support data acquisition through an ethernet connection. In order to insure future compatibility with the dSpace system, the conversion to the serial data was made.

The input signal for all tests was generated by an Hewlett-Packard 1.5 MHz function generator and amplified by a stack of 4 Trek PZD Duel Channel Amplifier (see Figure 39). Transfer functions for these amplifiers are given in Appendix C.1. The output of the amplifier is verified using an Agilent 6.5 digit multimeter before being used to actuate the control patches. Data from the wavefront is received and processed using the acquisition and control hardware pictured in Figure 40.

5.4.1 Data Processing. The WaveScope® software allows the user to choose the number of Zernike coefficients to be calculated, with a maximum of 42 values. To obtain the most information possible with the given equipment, 42 Zernike coefficients are exported at a rate of approximately 10 Hz. No averaging is performed by the WaveScope® software.

Once the WaveScope® software has been configured to export the Zernike Coefficients (see Appendix A.6), the SerialInit.m (see Appendix B.11) script file is run on the Matlab® computer. This script initializes the communication to the serial port and defines some characteristics of the incoming data stream.

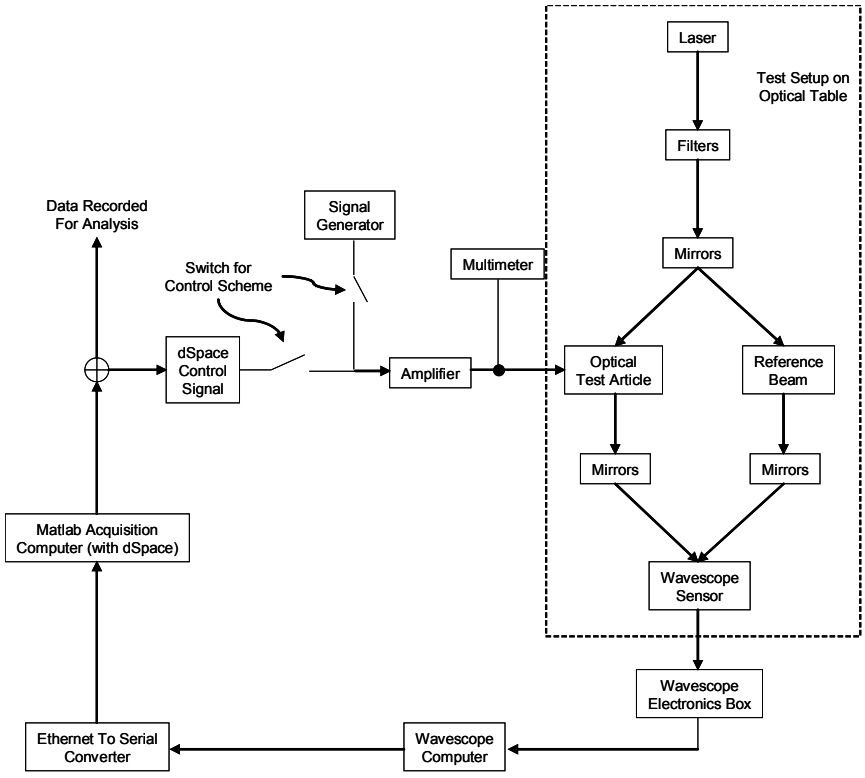

Figure 37: Flow Chart of Wavescope Experiment

The basic command to grab a set of coefficients from the serial port is given in the script SerialGrab.m (see Appendix B.10). This script simply looks for the start of a set of data and takes 42 lines after that from the buffer. A provisional output has been included to tell the user if noncontiguous frames have been taken. This lets the user know if sets of Zernike coefficients are being corrupted or overwritten due to an improper communication setting.

The data processing is done with the SerialPlot.m script (see Appendix B.12). This script serves as the user interface to the data acquisition system. The program first calls a function (see Appendix B.18 to calculate a surface mesh of Zernike Polynomials (see Appendix C.3). The program then asks the user to shut off all inputs to the system so that a static reference frame of the mirror surface can be taken. This reference frame is an average of 30 sets of Zernike polynomials and is subsequently subtracted from all measurements of the surface.

Next the SerialPlot.m will prompt the user to turn on equipment again, if needed. A specified number of Zernike coefficient, n, sets are then read from the serial port. Each set used to obtain the deviation of the surface from the static reference frame with Equation 37.

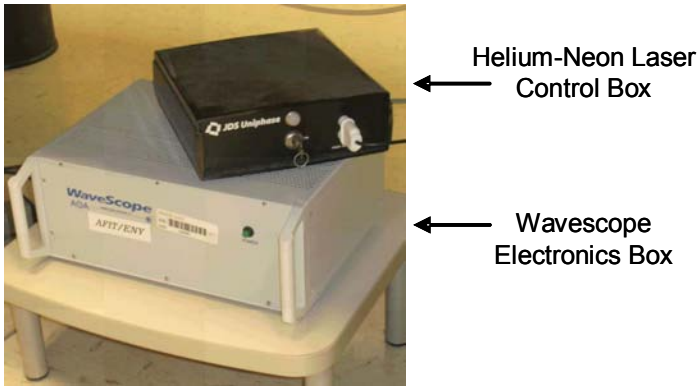

Figure 38: Electronic Control Boxes

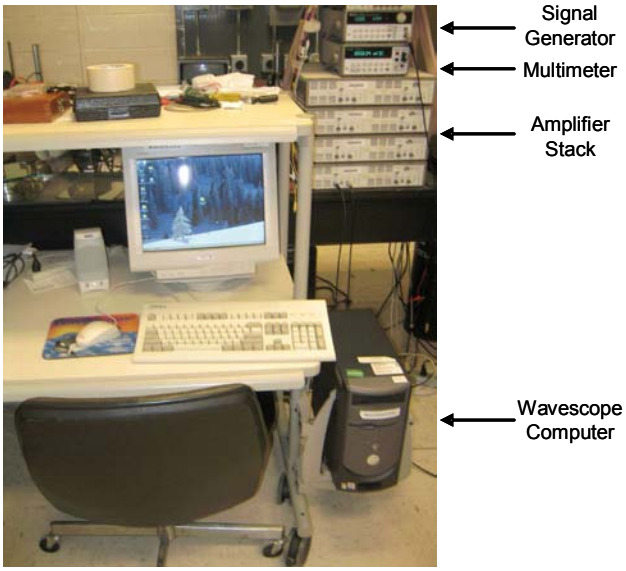

Figure 39: Signal Generation and Data Processing Hardware

$$W(r,\theta) = \sum_{i=1}^{n} \zeta_i Z_i(r,\theta) \tag{37}$$

The set of n surface shapes is then stored in a *.MAT file for later analysis and a movie of the deformation is created. Additional post-processing is accomplished using the StaticPlotter.m and StaticFramePlot.m script files (see Appendix B.14 and B.15). The data manipulation used for these files will be explained as the results are discussed in the remaining sections in this chapter.

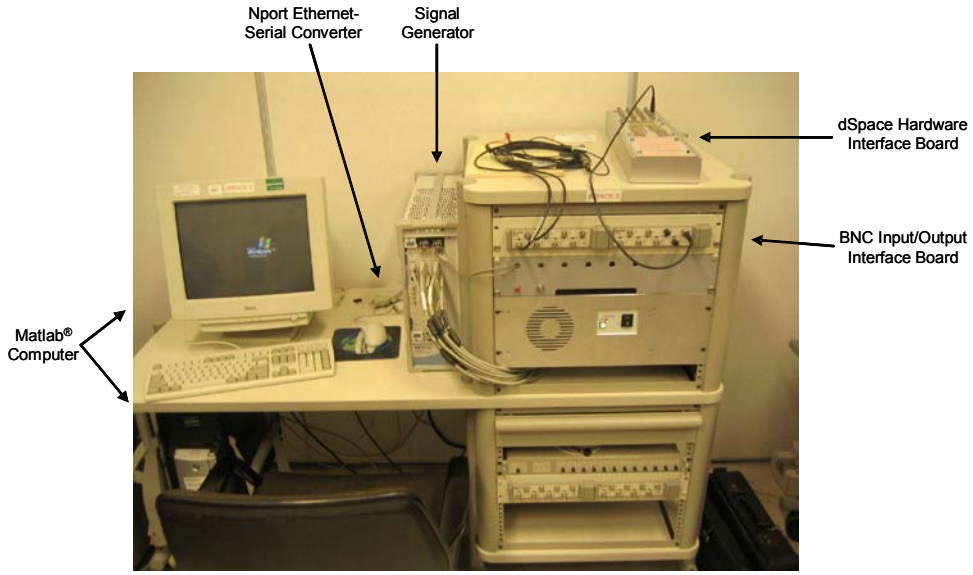

Figure 40: Data Acquisition and Control Hardware

5.5 Data Analysis: Static Imaging

The behavior of the membrane-like optical structure under static voltage can be investigated using the dynamic sampling acquisition system to generate enough data for statistical analysis. Mean Static deformation plots will be discussed for each of the patches. A calculation of the standard deviation in the data is provided. Finally, the dependence of the deformation with respect to applied voltage is discussed.

5.5.1 Mean Surface Deformation. The mean deformation of the surface with respect to the static reference is an important measurement. This information is obtained by averaging the surface deformation data calculated with the SerialPlot.m script. The code which was developed to perform this analysis is called StaticPlotter.m (see Appendix B.14).

This script file first prompts the user for the *.MAT file to be loaded. It discards the first and last surface profiles and takes the average and standard deviation of the remaining sets. For these experiments 30 sets of data were taken, therefore 28 sets of data are averaged to obtain the mean surface deformation.

The laser could not be expanded enough to sample the entire surface of the mirror, therefore area that could be reliably illuminated was centered on the middle of the membrane and sampled with the wavefront sensor. In order to match the scale of the mirror and give an accurate representation of the area where data was acquired from the optical surface, the sampled data is padded with

zeros around the outside. The zero displacement region in the images represents the area where no wavefront measurements were taken, however, the surface is surely deformed in these regions.

The control patch design was then overlaid on the surface deformation plots. This information is calculated based on the scale of the original computer design for the control patch and is not simply a drawing of what appears to fit the data. The data set is rotated clockwise until a close match with the overlaid control pattern is obtained. Typically the data needed rotation of about 15° to match the control pattern. This rotation is simply a matter of how the mirror was oriented on the test stand during testing and has no effect on the actual data.

The maximum and minimum deformation is calculated over the entire surface and this information is provided in Table 13.

Table 13: Maximum and Minimum Surface Displacements

Patch	Min Disp (μm)	Max Disp (μm)	PV Value (μm)	PV Value (λ)
1	-1.0121	0.79105	1.80314	2.84857
2	-0.70536	0.67029	1.37565	2.17322
3	-1.4521	0.98718	2.43926	3.85349
4	-1.6321	0.98338	2.61553	4.13196
5	-1.7879	0.83931	2.62723	4.15044
6	-2.0969	1.0568	3.15369	4.98214
7	-1.1939	0.73168	1.92555	3.04194

Peak to valley (PV) calculations can be calculated for each data sample by simply adding the absolute value of the minimum deflection to the maximum deflection. This information is useful for comparison and gives a good idea of the total variation of the mirror surface. The PV value can also be used to describe the surface quality of the membrane-like structure. This information is also provided in Table 13.

Figure 41 is the 'static reference frame' which was subtracted from every measurement which was taken. This is due to the surface roughness present on the membrane's silicone coating. The frame is taken prior to every measurement and simply subtracted from the measurement to remove the bias due to this roughness. The PV value of the resting surface is determined to be 1.7 μm.

The actuated center control patch did not show very good agreement with the predicted displacement area. The actuated area appeared between control patches 4 and 5, with maximum deflection of -1.01 microns. One possible cause of this displacement is that the test beam is not centered on the mirror surface. This, however, is unlikely to be the case because the centering was verified with measurement equipment at the time of testing and the other control patch actuation results all appear centered on the surface. This patch may have been shorting to one of the other patches through some unforeseen mechanism in the test setup.

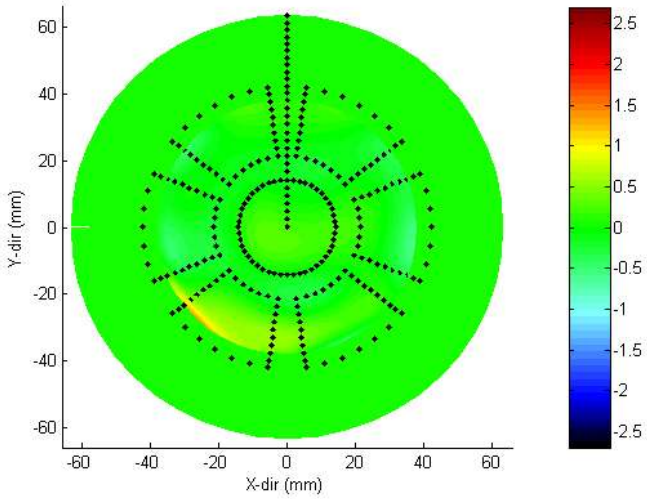

Figure 41: Mean Surface Deformation of Zero Voltage Reference

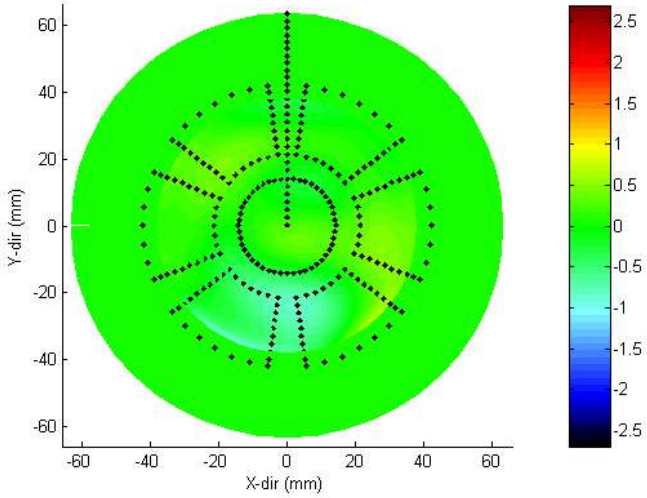

Figure 42: Mean Surface Deformation with Patch 1, Actuation at 0 Hz, 400 V

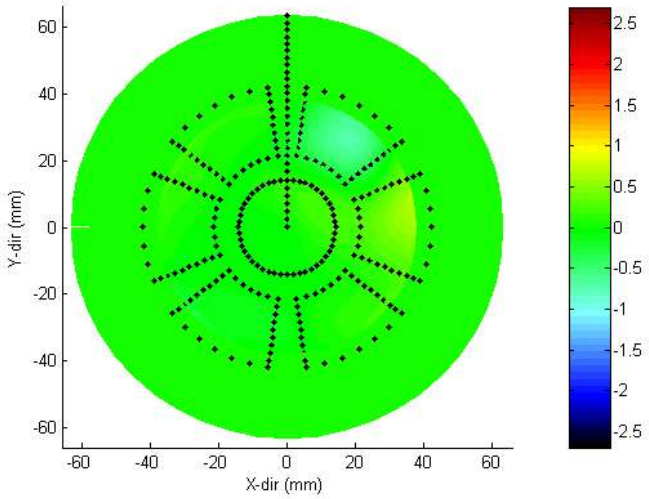

Figure 43: Mean Surface Deformation with Patch 2, Actuation at 0 Hz, 400 V

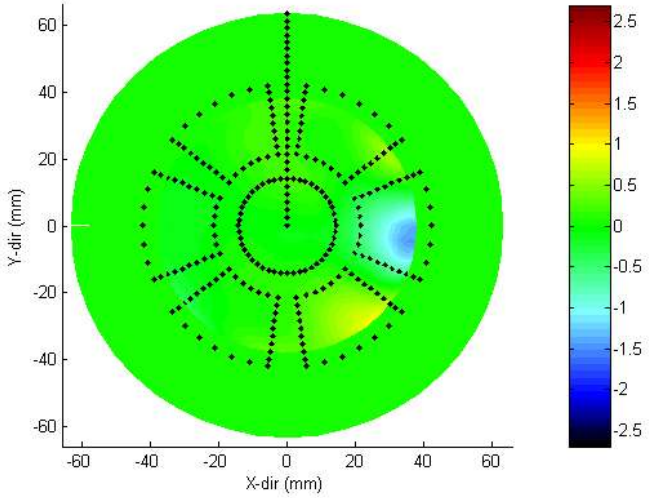

Figure 44: Mean Surface Deformation with Patch 3, Actuation at 0 Hz, 400 V

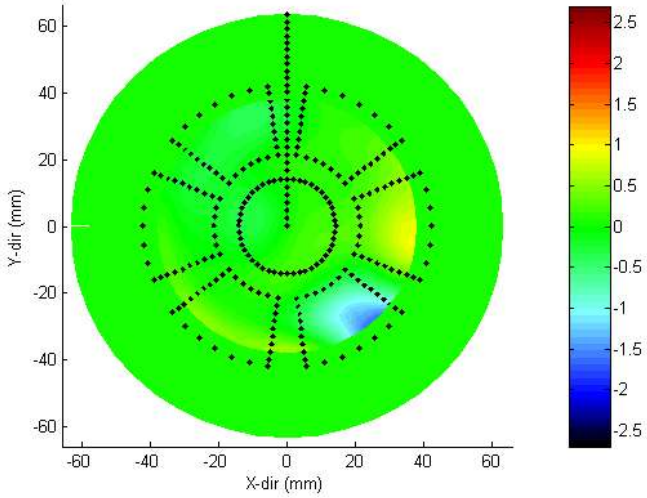

Figure 45: Mean Surface Deformation with Patch 4, Actuation at 0 Hz, 400 V

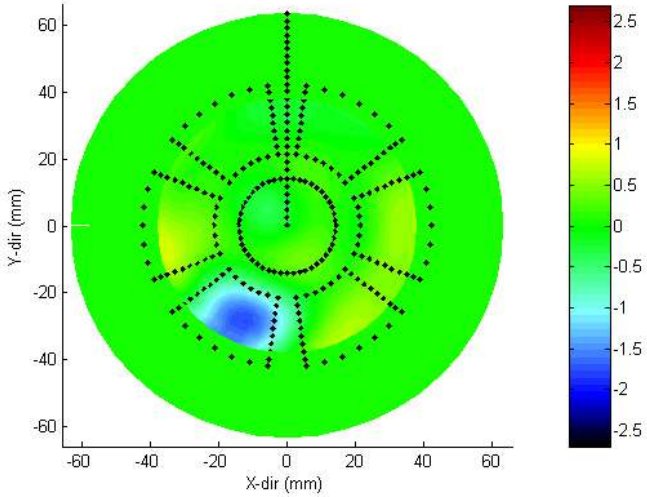

Figure 46: Mean Surface Deformation with Patch 5, Actuation at 0 Hz, 400 V

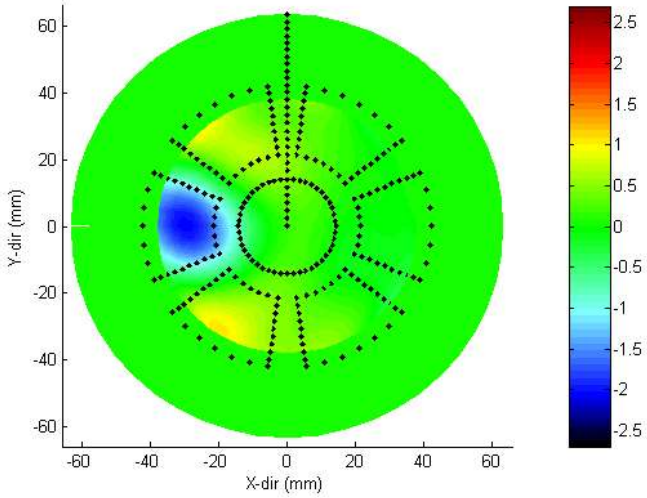

Figure 47: Mean Surface Deformation with Patch 6, Actuation at 0 Hz, 400 V

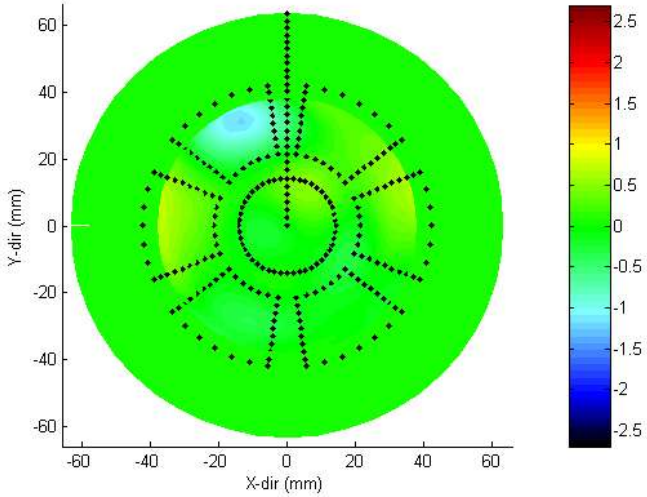

Figure 48: Mean Surface Deformation with Patch 7, Actuation at 0 Hz, 400 V

Figures 42 through 48 represent the surface deformation patterns for patches 1 through 7, respectively. Each patch is actuated at a static voltage of 400 V. All exterior control patch actuation results appear to fall in the predicted region. The low area in each plot falls within the lines of the control patch overlay, which is expected. The displacements in the membranes range from to -0.71 to -2.1 microns.

5.5.2 RadialCuts. Since the out of plane deformation is most interesting in the area of each patch, a diagram has been designed to show this deformation for a radial cut pattern around the mirror. There are 6 radial cuts made, one through each of the outer control patches. Each cut is located on the line connecting the of the control patch and the center of the mirror. By examining these patterns, details regarding the relative displacements of the surface when a given patch is actuated are brought out. The post-processed data used in Section 5.4.1 is used to create these plots and no additional processing was required. The data points represent the mean deformation from the static reference frame and the error bars are figured by a calculation of the standard deviation from that mean.

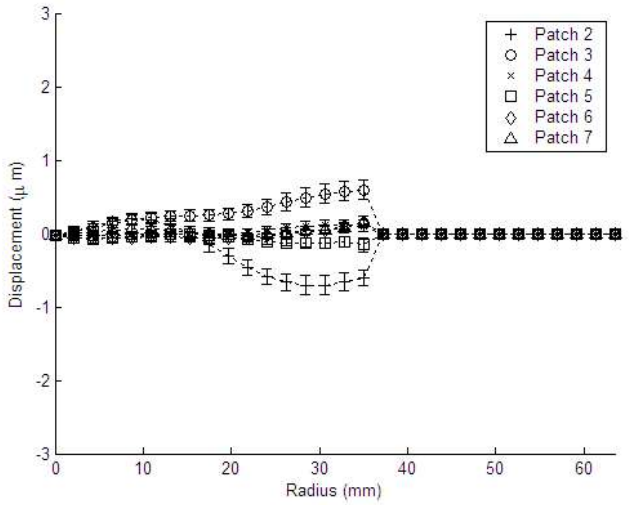

Figure 49: Radial Cut of Patch 2, Actuation at 0 Hz, 400 V

Figures 49 through 54 represent the radial cut patterns for patches 2 through 7, respectively. These plots are simply glimpses of the data contained in the surface deformation plots and therefore exhibit similar statistical characteristics.

These figures highlight a unique behavior. The actuated control patch has a negative deflection, as expected, but the neighboring control patches often exhibit a positive compensative deflection. A great example is the plot of the actuation of control patch 3. This surface exhibited a large positive

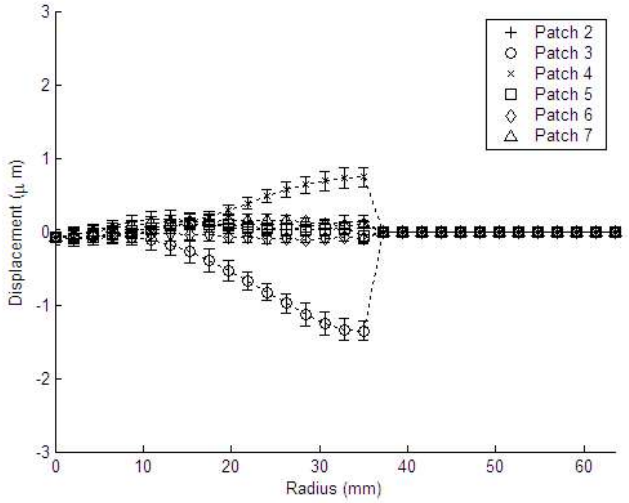

Figure 50: Radial Cut of Patch 3, Actuation at 0 Hz, 400 V

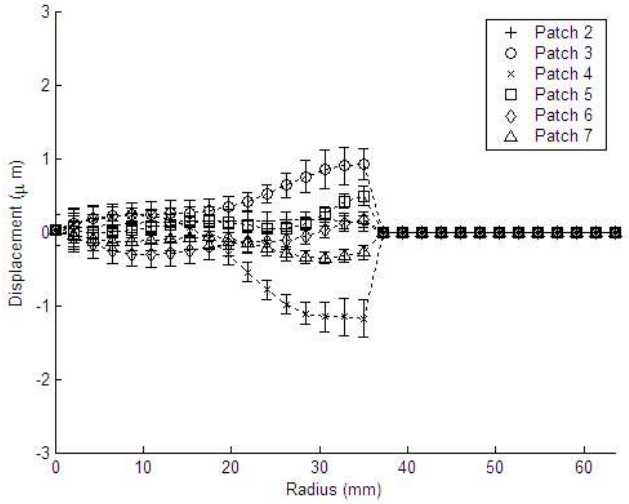

Figure 51: Radial Cut of Patch 4, Actuation at 0 Hz, 400 V

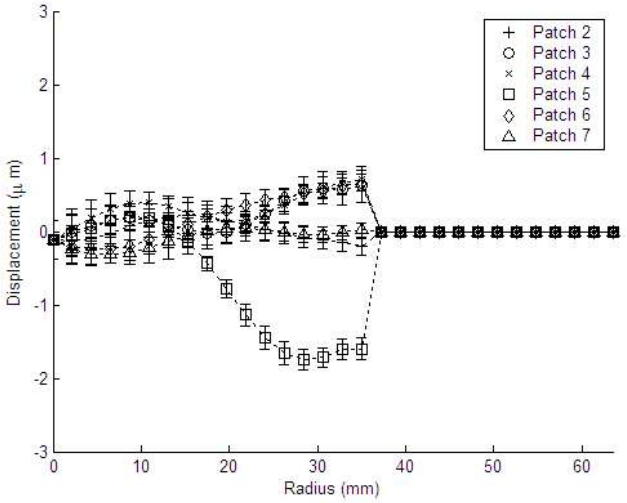

Figure 52: Radial Cut of Patch 5, Actuation at 0 Hz, 400 V

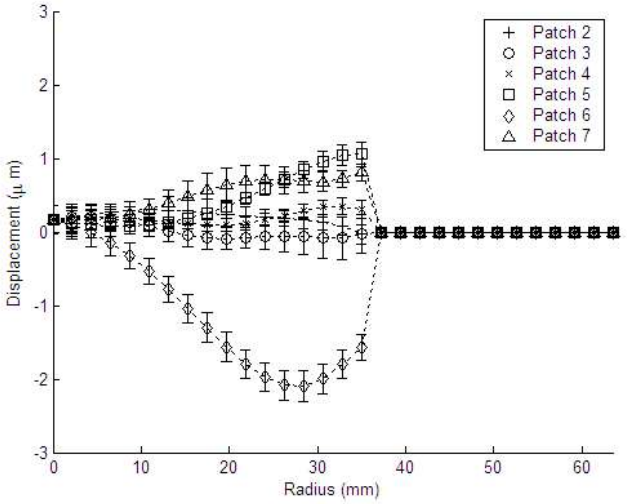

Figure 53: Radial Cut of Patch 6, Actuation at 0 Hz, 400 V

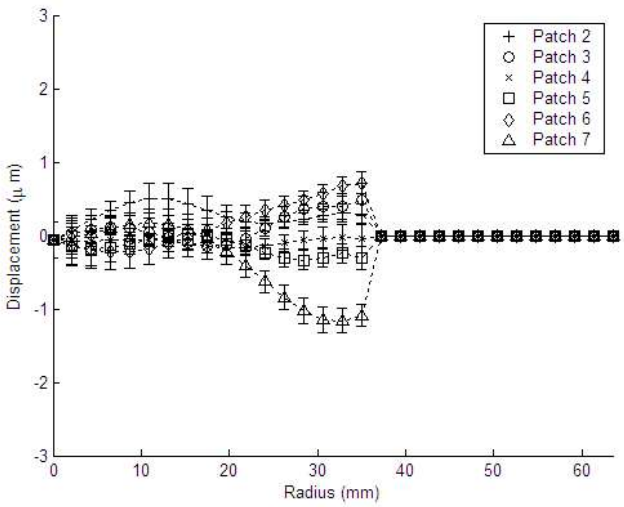

Figure 54: Radial Cut of Patch 7, Actuation at 0 Hz, 400 V

deformation in the region of control patch 4. This behavior is most likely tied to the fact that the membrane coating cannot return to zero deformation very quickly in the interface regions of the membrane (in fact the reason it is on the surface at all is for the smoothing effect).

5.5.3 Standard Deviation. The standard deviation from the mean surface deflection is calculated using the Equation 38.

$$s = \sqrt{\frac{1}{1-n}\sum_{i=1}^{n}\left(x_i - x_{avg}\right)^2} \tag{38}$$

This information gives an idea of what kind of variance can be expected in the measurement. A low variance translates to a higher certainty that deformed surface will be close to the stated mean.

Actuation on the center, or right side of the membrane (Figures 55 to 58 showed a maximum standard deviation toward the outer edge of the right hemisphere. The cases where the actuation was applied to the left patches (Figures 59 to 61) show a shift in the maximum standard deviation to the center section of the membrane. These shifts may be caused by slightly uneven tensioning or non-uniformities in the optical system. This data indicates a combination of two results. First, the area is actuated seems to have an increased standard deviation. Second, the right hemisphere of this mirror seems to have an increased variance. The increased standard deviation for the patch 5 to 7 in the center region may be a result of a combination of these two effects.

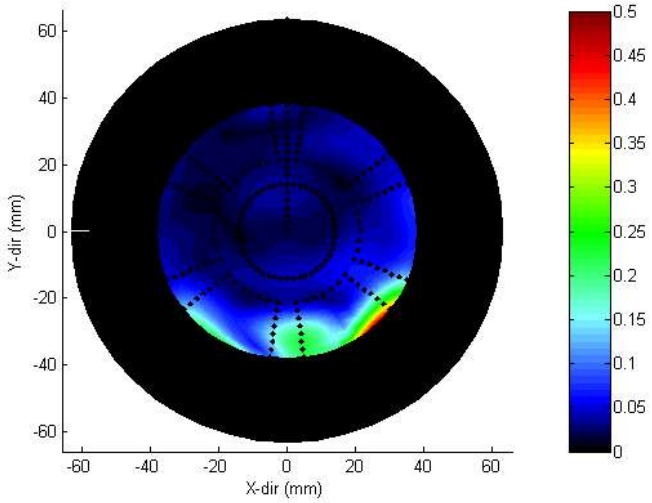

Figure 55: Standard Deviation from Mean Deformation of Patch 1, Actuation at 0 Hz, 400 V

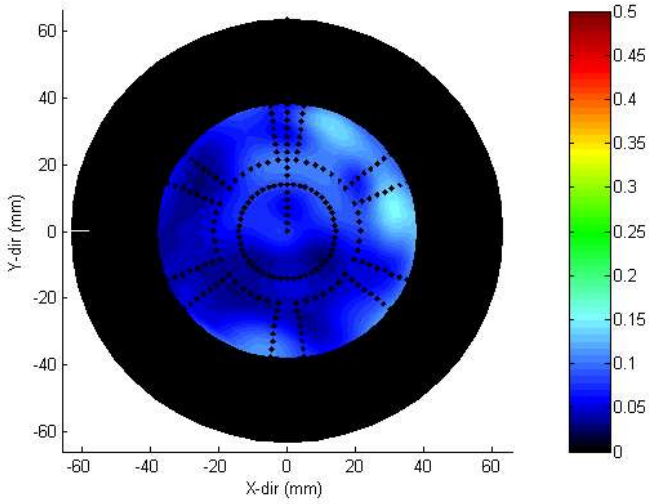

Figure 56: Standard Deviation from Mean Deformation of Patch 2, Actuation at 0 Hz, 400 V

Table 14: Maximum Standard Deviation from Mean Surface Deflection

Patch	Max Standard Deviation from Mean (μm)
1	0.47799
2	0.15178
3	0.1921
4	0.39651
5	0.27748
6	0.40928
7	0.38451

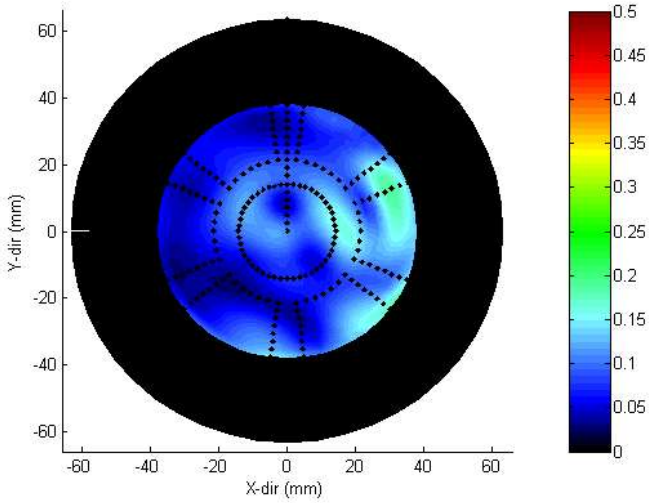

Figure 57: Standard Deviation from Mean Deformation of Patch 3, Actuation at 0 Hz, 400 V

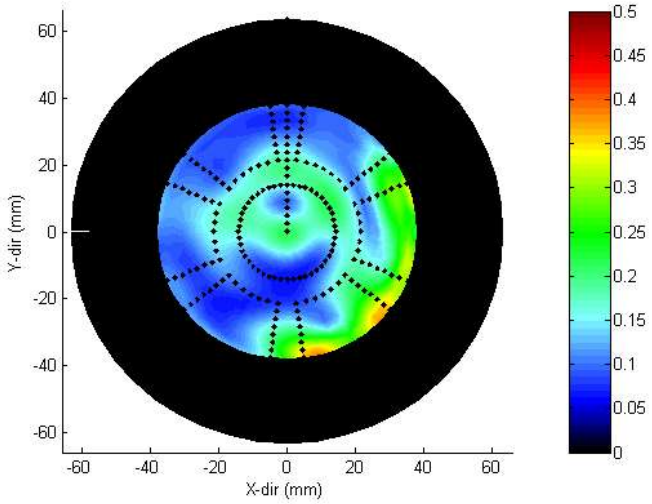

Figure 58: Standard Deviation from Mean Deformation of Patch 4, Actuation at 0 Hz, 400 V

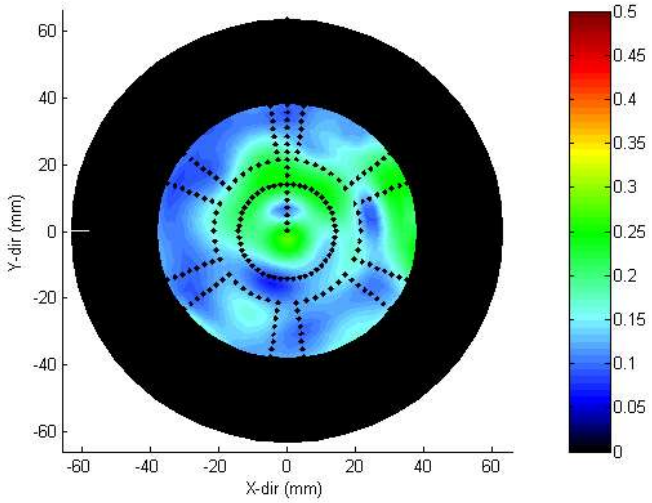

Figure 59: Standard Deviation from Mean Deformation of Patch 5, Actuation at 0 Hz, 400 V

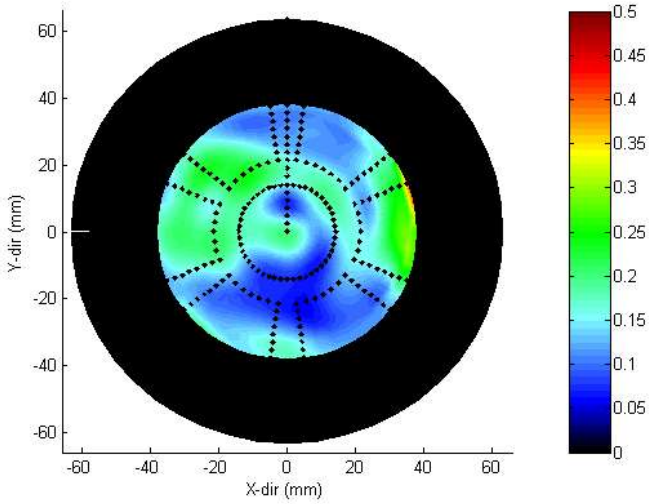

Figure 60: Standard Deviation from Mean Deformation of Patch 6, Actuation at 0 Hz, 400 V

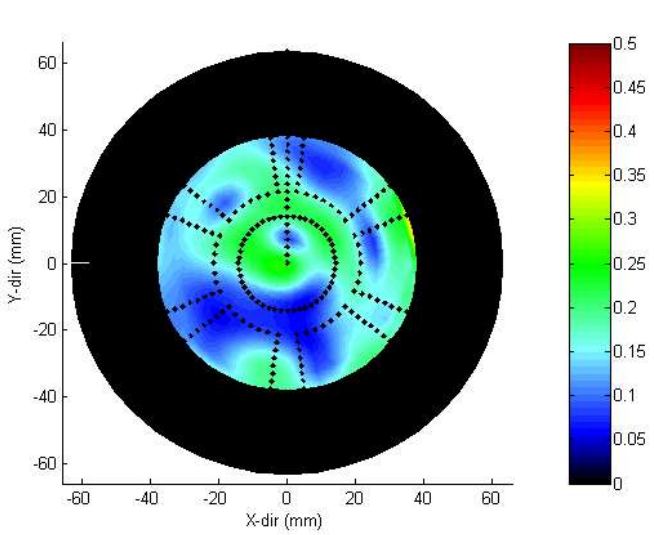

Figure 61: Standard Deviation from Mean Deformation of Patch 7, Actuation at 0 Hz, 400 V

The standard deviation has an average value of 0.3271 μm. The maximum values for the standard deviation of each plot are given in Table 14.

5.5.4 Voltage Dependence. Figure 62 is a plot of the observed surface deformation as the voltage is increased from 100 to 600 volts. Each measurement is an average of the max or min value of the seven patches. The negative values are the displacement of the surface in the control region. The positive values represent the compensatory effect of the surrounding region. The trend is very linear in the region from 200 to 600 V and an increase in voltage gives a larger deflection.

5.6 Data Analysis: Active Imaging

The primary objective of this section is to characterize the sampling rate of the new data acquisition system. The Zernike coefficients describe the surface deformation and can be examined in time to characterize the vibration of the surface. Significant surface deflection were observed during static actuation for patch 5, therefore this patch was selected for this analysis. Figure 63 shows the values for the first 42 Zernike coefficients. This plot illustrates the fact that larger coefficients typically have less impact (lower values) when compared to the small coefficients. This is due to the larger coefficients being defined to describe more and more complex surface deformation patterns.

The 4^{th} Zernike coefficient is chosen for tracking due to its large magnitude. By keeping the relative size of the tracked coefficient large, compared to the measurement error and background noise, the results are isolated from those errors.

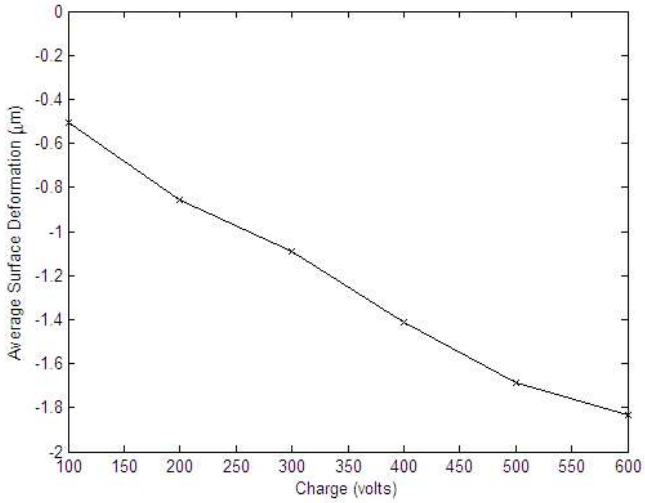

Figure 62: Average Surface Deformation as a Function of Voltage

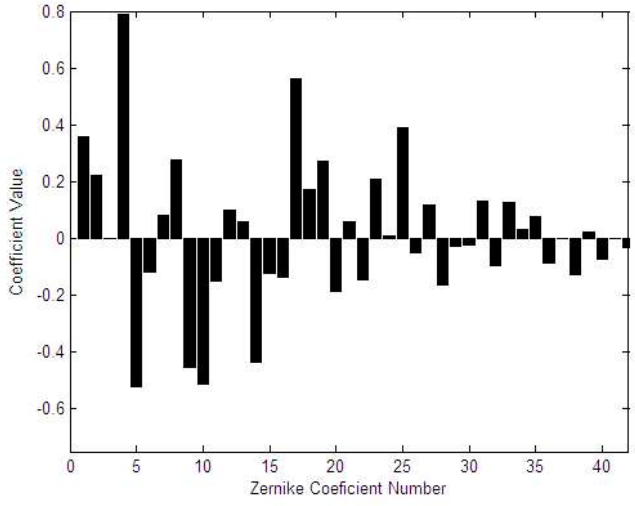

Figure 63: Bar Chart of all 42 Zernike Coefficients for Patch 5 at 400 V

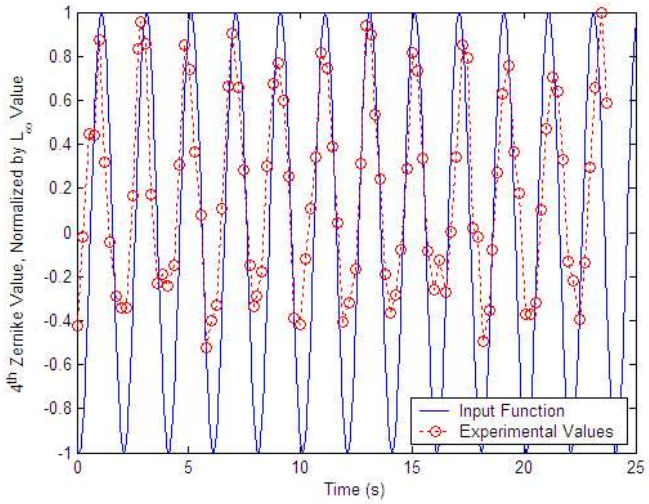

Figure 64: Time Signature of 4^{th} Zernike Coefficient with $\frac{1}{2}$ Hz Input Signal

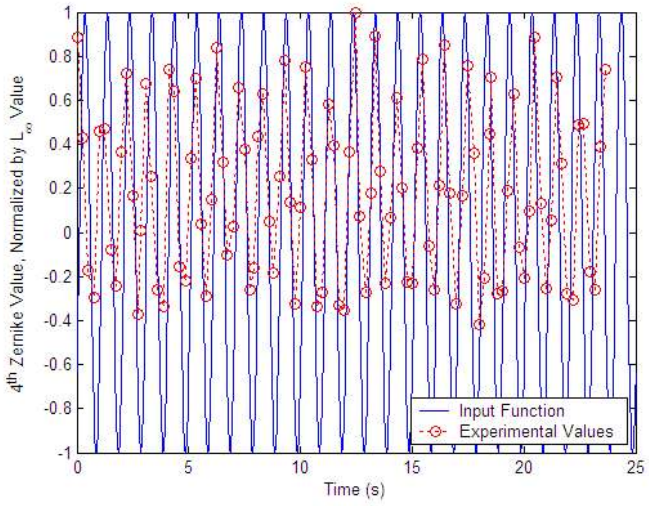

Figure 65: Time Signature of 4^{th} Zernike Coefficient with 1 Hz Input Signal

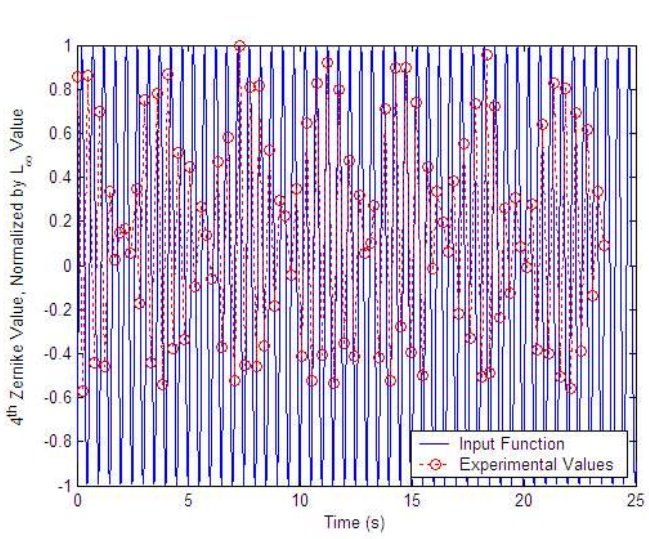

Figure 66: Time Signature of 4^{th} Zernike Coefficient with 2 Hz Input Signal

Figure 64, Figure 65 and Figure 66 show the experimental data as a function of time for the 4^{th} Zernike coefficient. This data was obtained by taking a time signature every time the data acquisition system read a line from the serial port data stream. This signature is then processed to obtain a time span for the data read, which is a measurement of the sampling rate of the system. The Matlab® code which was used to make these calculation is provided in Appendix B.3.

The input signal is also plotted on Figures 64 to 66. Since no knowledge of where the data is in the sinusoidal cycle can be easily obtained, a fit of the sinusoidal input curve is made based on an L_2 norm from a difference with the data sample. This effectively finds the best fit of a sinusoidal curve to the provided data. As illustrated by the figures, all data matches the input signals very closely.

The $\frac{1}{2}$ Hz and 1 Hz signals were slow enough that the data acquisition system could sample then more than one time per cycle. In the case of the 2 Hz input signal, the data acquisition is not able to sample fast enough to hit every cycle, which is why the oscillatory pattern in the data is apparent. This behavior is called aliasing and is associated with any data acquisition system.

The Nyquist frequency is said to be half of the sample frequency and provides a line below which aliasing does not occur. The fact that a 2 Hz input is exhibiting this aliasing phenomenon indicates that the Nyquist frequency for our system is slightly less than 2 Hz. Therefore, the sample frequency of the data acquisition system is approximately 4 Hz.

The sample frequency was also calculated analytically based on the time signatures which were obtained during testing. The average sample rate was determined to be 4.2406 Hz, with a standard

deviation of 0.029414 Hz. This sample rate is slightly higher than that predicted by the graphical method.

The system acquisition speed was also tested based on workload. The number of Zernike coefficients calculated by the WaveScope® computer and processed by the Matlab® were reduced to investigate is a sample rate speed increase was possible in the system.

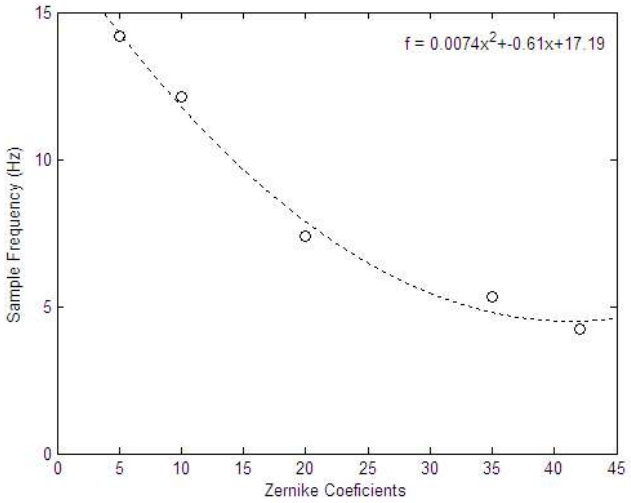

Figure 67: Sample Rate as a function of Zernike Coefficients Computed

Figure 67 gives the relationship between the Zernike coefficients sampled and the sample rate of the system. For convenience, a second order trend line has been fit to the data and the equation for this line is given in the upper right corner of the figure. This figure illustrates the fact that as fewer coefficients are computed, the sample speed in increased. A maximum sample speed of approximately 14 Hz can be obtained, however, so few Zernike coefficients would be available that the surface deformation prediction could not accurately represent the actual surface.

5.7 Summary

In this chapter, the new data acquisition was described in detail. This new system is capable of taking data at sample rates as high as 14 Hz, though 4 Hz was average for the computation of 42 Zernike coefficients. The acquisition system was used to perform a statistical measurement of the static surface deformations. The maximum static deformation was determined to be -2.1 μm and occurred for the actuation of patch 6. All exterior patches appeared to actuate in the region predicted by the placement of the control patches. The center patch did not actuate as expected and a possible short circuit in the control lead is suspected as the cause.

VI. Conclusion

6.1 Overview of Experiments

This project contained two distinct experimental test setups. A scanning laser vibrometer was used to characterize the optical structures over a wide range of frequencies and to calculate the tension in the membrane. An active wavefront sensor was used to characterize the optical surface subject to static and periodic applied voltages. In addition to the outline of these two experiments, an overview of the fabrication and design process is provided.

6.1.1 Fabrication and Design. The fabrication and design process included the design of the control pattern etched onto the membrane, the selection and description of the PVDF actuator material, mirror etching and tensioning and coating of the optical surfaces. The areal densities of each mirror produced is also provided as a benchmark for the fabrication methods used in this project.

6.1.2 Modal Analysis. Next a modal analysis of each membrane was performed. An extensive theoretical treatment of circular membrane theory is provided along with an overview of the test equipment and setup, data collection and data analysis methods. Frequency response curves and surface deformation plots are provided to characterize the primary modes of each surface. A estimation of the tension in the PVDF membrane is provided. Comparisons are also made based on actuation method, input signal, orientation and membrane coating.

6.1.3 Wavefront Analysis. Finally measurements of the optical wavefront were performed. A description of the test setup an data acquisition system is provided and static and dynamic experimental test results are presented and discussed.

6.2 Conclusions Drawn

6.2.1 Fabrication and Design. While an established fabrication methodology was followed, some improvements to the technique were noted. Thin layers of silicone are not necessarily the best. A minimum thickness seems to exist around 1.5 mm, beyond which a print through of the control pattern could be observed and the surface was not considered testable. Exposing the curing membrane to vacuum pressure to siphon out the bubbles is not a valid technique. This seemed to create a myriad of surface wrinkles which rendered the surface untestable. It was verified that additional layers of silicone can be applied directly to previous gold coated silicon layers, with no apparent problem of wrinkling or bubble formation at the interface. Finally, structures with optical quality reflecting surfaces can routinely be produced using this methodology. These structures have

been calculated to have an areal density of 1.5 - 4 $\frac{kg}{m^2}$ and thicknesses of 1.5 to 3.3 mm, which represents a 50% reduction in thichness over previous research completed at AFIT.

6.2.2 Modal Analysis. The tension is a valuable parameter for numerical modeling of membrane structures. Modal analysis results were used to estimate the tension in the PVDF membrane. This tension was estimated to be 3.0 to 4.6 $\frac{N}{m}$ with a standard deviation of 0.5 to 1.0 $\frac{N}{m}$.

Various other attributes of the test articles were also investigated. The results indicate that the silicone coated membrane is well approximated by thin membrane theory. Orientation of the test article on the test stand was also determined to have little to no impact on the modal analysis results.

6.2.3 Wavefront Analysis. A new data acquisition system was developed for use with AFIT's wavefront imaging hardware. This system enables static data to be taken at sample rates up to 14 Hz. The number of Zernike coefficients calculated is found to have a large impact on the sample rate of the system. 42 Zernike coefficients give a reasonable approximation to the surface deformation and can support a sample rate of approximately 4 Hz.

Static deformations at 400 volts were used for comparison. This actuation method produced surface deformations of -0.71 to -2.1 microns. Each exterior control patch deformed in the region which was expected. The redial cut diagrams showed that often times when a particular patch is actuated, its neighboring patches are adversely affected. A calculated average standard deviation was determined to be 0.3271 microns. The largest deviations were also noted to be in the patch which was being actuated or toward the outside of the observed region on the membrane. Finally, the surface deformation was determined to go nearly linearly with increased voltage in the range of 200 to 600 volts.

6.3 Areas for Further Development

It is the author's hope that this research will serve as an appropriate stepping stone for the future. There are many possible areas which seem to show promise for possible lines of research, a few are discussed below.

6.3.1 Fabrication and Design. The silicone substrate which was utilized for this experiment is not rated for use in space. This temperature range would severely change the dynamics of this coating and another material must be found as a replacement. Also the PVDF etching pattern is time consuming and relatively inefficient to do by hand. Other methods for masking the etch pattern onto the PVDF material would allow for more intricate control designs and speed up the fabrication

process. Finally, better methods of approximating the tension in the membrane could be developed. The use of force transducers or other methods could be used to verify the results obtained from modal analysis.

6.3.2 Wavefront Analysis. The largest area of possible advancement is in the area of control. Now that a way of collecting data in 'real time' has been demonstrated, a control system to damp out vibrations on the surface or otherwise shape the structure are within reach. Careful attention has been paid to making the system compatible with the most obvious control implementation tools, namely Simulink® and dSpace®.

6.4 Summary

This project consists of three major parts: Fabrication and Design, Modal Analysis and Wavefront Analysis. The relevant information has been presented and discussed regarding each of these three areas. Significant advances have been made in the area of data acquisition and processing using AFIT's wavefront analysis hardware.

The development of this methodology has brought within reach the seemingly distant goal of 'real time' investigation of the wavefront for a thin deformable membrane-like structure. This research is critical to the overall goal of placing large aperture optical structures in space. Such systems could provide valuable information for the mission planners and war-fighters of tomorrow.

Appendix A. Laboratory Notes

A.1 Etching the Membrane

A.1.1 Supplies.

- Razor blade, sharpie, straight edge, tape, cotton balls, cutting board, paper towel
- computer generated membrane template
- rubber safety gloves
- Isopropyl Alcohol (91% by volume)
- Ferric Chloride Etchant Solution
- 14 by 14 inch piece of PVDF material ($52\mu m$, with Cu Ni coating)

A.1.2 Procedures and Comments.

1. Mark the positive side of the PVDF with a (+) in the corner of the piece with the black marker. Packaging of PVDF indicates that 'positive inside' when on the roll.
2. Measure and cut a 14 inch piece from the roll with the straight edge and knife.
3. Use the knife to cut the computer generated membrane template out as cleanly as possible. The area that is to be masked with the permanent marker must be completely removed.
4. Mark the orientation of the PVDF sheet with 3 parallel lines, parallel to the direction that the PVDF was rolled up.
5. Tape down the template in the appropriate position.
6. Mask the PVDF by tracing the template and shading in with permanent marker.
7. Remove the template.
8. Carefully clean up the edges of the mask with the straight edge and marker. Note: It is easy to smudge the marker at the point, be sure to remove unwanted marks with alcohol before etching.
9. Put on the rubber gloves and ventilate the area.
10. Dip cotton ball in etchant solution and rub the PVDF to remove metallic coating. You will need only a little solution. Do not touch skin clothes or furniture.
11. After the PVDF is etched and metal coating is dissolved, rinse in water to stop the reaction.
12. Pat with paper towel to dry and hang to dry completely.
13. Remove the permanent marker with the alcohol and allow to evaporate.
14. Store loosely rolled (do not fold) and away from dust and contamination.

A.2 Tensioning the Membrane

1. Place the membrane over the large ring in the following order (bottom to top): bottom of clamp, 12 inch aluminum ring, rubber o-ring, PVDF membrane, aluminum top ring, top of clamp.
2. Space clamps at equal increments around the circumference of the 12 inch ring. Do not tighten yet.
3. Gently pull all wrinkles out of the membrane. Pull in all directions, multiple times. Be sure not to pull the PVDF material out from between the o-ring and the aluminum top ring (the PVDF must rest on the o-ring at every point around the circumference).
4. Slowly tighten the clamps in opposing corners until the slack is out of the membrane. Alternate the corners after every eighth turn of the clamp handle.
5. Tighten until the PVDF is stretched tightly in all directions. Typically, until it is hard to tighten the clamp handles anymore with only two fingers.

A.3 Epoxy the PVDF membrane to the 6 inch ring

1. Begin with an etched piece of PVDF stretched over the 12 inch ring and under appropriate tension.
2. Be sure that the top of the membrane has windows etched in, so that you can easily center the aluminum ring.
3. Clean and prep the grooved area.
4. Unscrew the wire support plates on the top of the 6 inch rings (2 or 3 plates, 2 hex screws each). This will allow the ring to sit more level.
5. Be sure to wear gloves and be in a well ventilated area.
6. M-bond 610 epoxy was used.
7. Use the plastic dropper to carefully fill the inner groove on the 6 inch ring.
8. Fill until the shallow groove at he center of the other two grooves is completely covered with epoxy.
9. Any excess epoxy will run around the outer groove and drain out the side, so have a towel there to catch the runoff (keep the ring level though).
10. Allow the epoxy to set up for about half an hour, so that the ring can be turned up side down without the epoxy running all over everything.
11. Use the epoxy brush to coat the PVDF with epoxy in the area that will contact the ring. Do not coat any PVDF that will be on the interior of the ring (the membrane dynamics could be affected).
12. Flip the aluminum ring over and gently place it on the stretched PVDF. Line the sides of the ring up with the pattern shown in the PVDF window.
13. Allow the aluminum ring to cure to the membrane for two days.
14. Gently loosen the clamps and lower the membrane onto the table.
15. Remove all tensioning hardware and examine the epoxy bond of the membrane
16. Carefully cut the excess PVDF material away from the edge of the aluminum ring. Be careful to leave all of the electrical leads in tact and to leave a space for the ground wire on the top of the PVDF sheet. Sharp scissors work best.
17. Place the membrane upside down in the oven for 24 hours at 150° F to cure the epoxy.
18. Adhere the copper lead wires to the PVDF material. Cover with electrical tape for safety and don't forget the ground lead.

19. Membrane is ready for coating.

A.4 Coating the Membrane with Silicon Rubber Resin

1. Thoroughly clean the surface with an air jet duster. Silicon rubber is very susceptible to contamination.
2. Suspend the membrane on supports around the circumference of the 6 inch ring. This method should create a flat surface that compensates for the sag in the membrane due to gravity. The other method is to set the membrane on a very smooth glass surface, which will create a more evenly distributed coating, but will deform once lifted for testing.
3. Prime the surface of the PVDF with GE Silicones (SS4120 01P). Simply paint this substance over the entire surface of the membrane. This will prevent the silicon from separating from the surface due to air bubble or impurities on the surface.
4. Mix two test tubes of the GE Silicon (Ten parts RTV615A resin (by weight) and one part RTV615B curing agent). Stir for ten minutes, transfer into another mixing dish and stir for another ten minutes. Pour into the test tubes and place in a centrifuge for ten minutes to remove all bubbles.
5. Carefully pour the mixture onto the clean membrane surface. Pour in the center of the membrane, with the lip of the test tube as close as possible to the membrane surface. Any disturbance will cause bubble that may be hard to remove later. Pour only the minimum amount of resin needed to coat the surface.
6. Tilt the membrane smoothly to completely coat the membrane surface.
7. Pour any excess silicon off of the membrane surface. This will ensure the thinnest coating that is possible.
8. Carefully wipe the excess silicon rubber off of the walls of the 6 inch ring.
9. Optional: Use a vacuum chamber to suck out the majority of the bubbles. This technique was attempted for the first 7-patch membrane, however the longer the silicon is under suction, the more its composition seemed to change. This seems to be a very fragile step, to much suction seemed to create wrinkles in the surface, but no suction may leave entrained bubbles in the resin. This step is assumed responsible for the wrinkled membrane surface and should be exercised with caution.
10. Place the membrane back on the support post.
11. Cover the silicon with a glass shield. This will keep the dust and other contaminants away from the mirror when it is curing.
12. Allow to cure for 3 to seven days at room temperature.

13. Coat with gold in the vacuum coating chamber. This will put a shiny reflective surface on the membrane.

Research shows that a 250μm surface depression can be reduced to approximately 1 μm with the first coat [14]. Visible depressions on the surface have a magnitude of tens of microns at least (minimum that the human eye can discern), so this is motivation for coating the surface with at least one coating. A reflective layer placed directly on the PVDF would have to have surface imperfections of this order of magnitude.

A.5 Turning on the Laser

1. Turn on the pressurized air table. Maintain 25 psi.
2. Turn on the WaveScope® computer.
3. Turn on the WaveScope® electronics box.
4. Start WaveScope® software (link on desktop).
5. Remove all reflective objects (jewelry, watches and hard rank) from the room.
6. Verify that the door is locked and closed.
7. Put on protective eye wear (correct for the wavelength of the laser).
8. Turn off the lights.
9. Turn on the laser.

A.6 'Real Time' Data Collection with the MATLAB Computer

1. Turn on WaveScope® computer.
2. Turn on WaveScope® electronics box.
3. Turn on Matlab® computer.
4. Turn on all dSpace® hardware.
5. Make sure that the Nport® ethernet to serial adapter is plugged in and properly configured.[1]
6. Start the WaveScope® software on the WaveScope® computer. You should hear the sensing unit cycle through different lenses at startup.
7. Start Matlab® on the dSpace® computer.[2]
8. Setup the test subject, turn on the laser and calibrate the WaveScope® as normal.
9. Open test with at least a Zernike display.
10. Open the TCL command prompt, from the Misc menu on the WaveScope® toolbar.
11. Start a live display.[3] Data should now be streaming to the dSpace® computer. This is evident by the rapidly flashing lights on the Nport® ethernet to serial connector.
12. On the Matlab® computer, initialize the serial port in Matlab®. The SerialInit.m (Section B.11) script can be used for this.
13. Grab and process the streaming data with the Matlab® computer. The SerialGrab.m (Section B.10) and SerialPlot.m (Section B.12) scripts can be used. The WavefrontZernikes.m (Section B.18) script is needed to make the Zernike's for multiplication with the coefficients grabbed from the WaveScope® computer.

[1] Proper configuration for the Nport® has all 'dip' switches off, the device is in TCP Client mode and the data flow control is turned off.

[2] dSpace® was never utilized to close a control loop, however it is definitely a tool that warrants further study.

[3] The data collection variables, such as frame rate and number of Zernike's calculated, can still be configured from within the WaveScope® software.

Appendix B. MATLAB Code

B.1 AvgRead

This code is used to process the data from the laser vibrometer. It reads in data text files and was used to create Figures 22 to 24.

```
%%%%%%%%
% Name: AvgRead.m
%%%
% This program opens up the Average FFT and Coherence data
% files collecetd from the scanning laser vibrometer and
% creates a plot.  Data must be exported using ascii format.
%%%
% Author: Eric M. Trad
%%%

clc;
clear all;
close all;
format short g;

%Get file to read the FFT Files for Laser Vibrometer
[File,Path] = uigetfile('*.txt','Choose File for Average Spectrum');
[Freq,Mag]=textread(File,'%f %f','headerlines',5);
[CFile,CPath] = uigetfile('*.txt','Choose File for Coherence');
[CFreq,CMag]=textread(CFile,'%f %f','headerlines',5);

figure
subplot(2,1,1)
plot(Freq, Mag, 'k');
xlabel('Frequency (Hz)')
ylabel('Magnitude (dB)')
subplot(2,1,2)
plot(CFreq, CMag, 'k');
xlabel('Frequency (Hz)')
ylabel('Coherence')

%Save to the clipboard
print -dbitmap
close all
```

B.2 BesZeros

This code is used to find the zeros of the Bessel function. It returns the values in Table 6.

```
function BesselTable=BesZeros(Mmax,Nmax)

%%%%%%%%
% BesZeros.m
%%%
% This function will return  a matrix of values
% that zero the bessel function of the first kind
% of size(Bes0)=[Nmax,Mmax].
%%%
% VARIABLE DEFINITIONS
% Bes0
%   Rows are n = 1,2,3...
%   Coulmns are m=0,1,2...
%%%
% Author: Eric M. Trad
%%%

BesselTable=zeros(Nmax,Mmax);

m=0;
nu=0;
while m <= Mmax
    Starter=0;
    n=1;

    %Fill the column of n values to Nmax
    while n <= Nmax
        TestString=linspace(Starter,Starter+30,50000);
        Bes0=besselj(nu,TestString);
        BesselTable(n,m+1)=NextZero(TestString,Bes0);
        Starter=BesselTable(n,m+1);
        n=n+1;
    end
    m=m+1;
    nu=nu+1;
end
```

B.3 DynamicDataFit

This code is used to process the dynamic data in Section 5.6. It was used to create Figures 64 to 66.

```
%%%%%%%%
%DynamicDataFit.m
%%%
% This program plots a bar chart of a Zernike in time.  This
% provides a comparison for the read rate of the system and other
% dynamic qualities.
%%%
% Author: Eric M. Trad
%%%

clc
clear all
close all
format short g

File='7PatchB_Patch5_HalfHz_600V';
load(File)
Freq=.5;

%Create the time hack
Hack=Timer(1:42:4200)/42; %Pick out one time hack per Zcoef Set
Hack=Hack-min(Hack); %Shift to the origin
Zc=Zcoef(4,:); %Look at the first Zcoef value as it changes in time
[ZcMax,ZcIndex]=max(Zc);
Zc=Zc/ZcMax; %Normalize between -1<Zc<1

%Find a Best Fit to Data
A=1;
w=2*pi*Freq;
t=linspace(0,25,1000);
Nlast=10;
for phi=0:.0001:2*pi
    f=abs(A*cos(w*Hack+phi)-Zc);
    N=norm(f);
    if N<=Nlast
        Nlast=N;
        FinalPhi=phi;
    end
end
f=A*cos(w*t+FinalPhi);


figure(1)
plot(t,f,'b-',Hack,Zc,'or:')
xlabel('Time (s)')
ylabel('4^{th} Zernike Value, Normalized by L_\infty Value')
legend('Input Function','Experimental Values',4)
```

```
%Look at the first set of Zcoef
figure(2);
for iii=1:16
    subplot(4,4,iii)
bar(Zcoef(1:10,iii))
axis([.5 10.5 -1 1])
end
text(-35,9.5,'Bar Charts for the 1^{st} 10 Zernike Coefficients, Frames 1:16')
figure(1)
```

B.4 DynamicVisual

This code is used to process the dynamic data in Section 5.6. It can be used to create animations of the surface deforming. This code was used for presentations, but not for any figure in this document.

```
%%%%%%%%
%DynamicVisual.m
%%%
% This program plots each frame of the surface deflection.
%   It can be used to create animations. Requires 'plotman'
%   function to plot the surface.  Use movie2avi() to
%   create the avi's.
%%%
% Author: Eric M. Trad
%%%

%%%%%%%%
% Initialize
%%%
clc
clear all
close all
format short g

global moviefile b

%%%%%%%%
%Load File
%%%
% [File,Dir]=uigetfile('*.mat','Choose the MAT file you want to load');
% load(strcat(Dir,File));
% disp(File);
load('7PatchB_Patch5_2Hz_600V.mat')

[tmp1, tmp2, tmp3]=size(Zsurf);
Zs=Zsurf(:,:,2:tmp3-1);

%%%%%%%%
%Expand the data with zeros to fill the membrane
%%%
R=28-16;
P=48;
radius = linspace(1,2.5/1.5,R+1);
theta = [-pi:(2*pi)/P:pi];
for i = 1:R+1;
for j = 1:P+1;
        r = radius(i);
        t = theta(j);
x(17+i,j) = r*cos(t);
y(17+i,j) = r*sin(t);
Zs(17+i,j,:) = 0;
end
```

```
end

%%%%%%%%
%Multiply by in2m() and 1.5 to fit to actual membrane size
%%%
x=in2m(x*1.5)*1e3; %Want the x axis in mm
y=in2m(y*1.5)*1e3; %Want the y axis in mm

%%%%%%%%
%Shift the data one or more points, rotate to align with control outline
%%%
S=0; %Shifter, clockwise, 0<S
Zs_shift=zeros(size(Zs));
for kkk=S+1:49
    Zs_shift(:,kkk-S,:)=Zs(:,kkk,:);
end
for kkkk=1:S
    Zs_shift(:,49-(S-kkkk),:)=Zs(:,kkkk+1,:);
end
Zs=Zs_shift;

%PLOT THE ABSOLUTE MAX DEFORMATION
for b=1:98
plotman(x,y,Zs,b);
moviefil(b)=getframe(1);
end
```

B.5 MagPhaseRead

This code is used to process the data from the laser vibrometer. It reads in data text files and was used to create Figures 28 to 30.

```
%%%%%%%%
% Name: MagPhaseRead.m
%%%
% This program opens up the magnitude and phase surface plot
% data files collected from the scanning laser vibrometer
% and creates a plot.  Data must be exported using ascii format.
%%%
% Author: Eric M. Trad
%%%


clc;
clear all;
close all;
format short g;

%Get file to read the FFT Files for Laser Vibrometer
[File,Path] = uigetfile('*.txt','Choose File for Magnitude and Phase');
[u, v, Mag, Phase]=textread(File,'%f %f %f %f','headerlines',11);

%Shift the center of the circle to x=0, y=0
Ushift=min(u)+(max(u)-min(u))/2;
Vshift=min(v)+(max(v)-min(v))/2;
u=u-Ushift; %Center the data
v=v-Vshift; %Center the data

%Scale the axes between -1 and 1
u=u./max(u);
v=v./max(v);

tmp = linspace(min(min(u,v)),max(max(u,v)),30);
[U,V] = meshgrid(tmp,tmp);

figure(1)
subplot(2,1,1)
M = griddata(u,v,Mag,U,V);
surf(U,V,M)
xlabel('x-dir')
ylabel('y-dir')
title('Magnitude (dB) Plot')
colormap bone
colorbar
shading interp
axis([-1 1 -1 1])

subplot(2,1,2)
P = griddata(u,v,Phase,U,V);
```

```
surf(U,V,P)
xlabel('x-dir')
ylabel('y-dir')
title('Phase (deg) Plot')
colormap bone
colorbar
shading interp
axis([-1 1 -1 1])

%Save to the clipboard
print -dbitmap

%Close the plot
close 1
```

B.6 MembraneSurface

This code is used to calculate the surface deflection. It is based on Equations 22 to 24.

```
function [x,y,W]=MembraneSurface(m,n,Radius,rho,Tension,Frequency)

%%%%%%%%
% MembraneSurface.m
%%%
% This function will return the surface deflection of a circular
% membrane made of PVDF, given a tension and a radius.
%%%
% VARIABLE DEFINITIONS AND UNITS
% x=x-coordinate (m)
% y=y-coordinate (m)
% W=vertical surface deflection (m)
% Frequency is in radian
% tta=theta (rad)
%%%
% Author: Eric M. Trad
%%%

rn = 30;
pn = 48;
R = [0:Radius/rn:Radius];
P = [0:2*pi/pn:2*pi];
for iii=1:length(R) %x loop
    for jjj=1:length(P) %y loop
        r=R(iii);
        tta=P(jjj);
        W(iii,jjj)=inv(sqrt(pi*rho)*Radius*...
          besselj(m+1,Frequency/sqrt(Tension/rho)*Radius)) ...
             *besselj(m,Frequency/sqrt(Tension/rho)*r)*(cos(m*tta)+sin(m*tta));
        if abs(r)>Radius
            W(iii,jjj)=0;
        end
    x(iii,jjj) = r*cos(tta);
    y(iii,jjj) = r*sin(tta);
    end
end
```

B.7 ModeShape

This code is used to predict mode shapes of fundemental natural frequencies.

```
%%%%%%%%
% This program first calculates a tension from an
% experimentally observed mode shape.  Next it predicts
% the shape of any other mode of vibration given
% an m and n value.
%%%
% Author: Eric M. Trad
%%%
% Required Functions Include:
%   BesZeros.m
%   FreqCalc.m
%   MembraneSurface.m
%   NextZero.m
%   TensionCalc.m
%%%

%%%%%%%%
% Initialize
%%%
clc
clear all
close all
format short g
tic

%%%%%%%%
%Define Parameters
%%%
Radius=in2m(6); %(m)
rho=1.78e3*52e-6; %(kg/m^3)*(m)=(kg/m^2) multiply by thickness

%%%%%%%%
%Normalize by the observed mode shape
%%%
iii=1
FFF=[218,434,547,656,875,979,1114];
MMM=[0,1,2,0,4,2,0];
NNN=[1,1,1,2,1,2,3];
BBB=[2.405,3.8314,5.1365,5.5206,7.5878,8.4158,8.6529];
Frequency_obs_Hz=FFF(iii);
Frequency_obs=BBB(iii); %Frequency observed in the experiment(rad/s)
m_obs=MMM(iii); %m value for the observed mode shape
n_obs=NNN(iii); %n value for the observed mode shape
Tension=TensionCalc(Frequency_obs,m_obs,n_obs,Radius,rho);

%%%%%%%%
%Find the max of the first mode to scale by
%%%
m=0;
```

```
n=1;
BesselTable=BesZeros(m,n);
Omega_mn=FreqCalc(BesselTable,Frequency_obs_Hz,Frequency_obs); %(rad/s)
[x,y,W_on]=MembraneSurface(m,n,Radius,rho,Tension, ...
BesselTable(n,m+1)); %(m)
Scaler_x=max(max(abs(x)));
Scaler_y=max(max(abs(y)));
Scaler_z=max(max(abs(W_on)));

%%%%%%%%
%Extrapolate to Surface Prediction
%%%
clear x y W_on
m=0;
n=1;
BesselTable=BesZeros(m,n);
Omega_mn=FreqCalc(BesselTable,Frequency_obs_Hz ...
   ,Frequency_obs); %(rad/s)
disp(sprintf('The predicted frequency for this mode
    is: %0.2f Hz',Omega_mn(n,m+1)))
[x,y,W_on]=MembraneSurface(m,n,Radius,rho, ...
   Tension,BesselTable(n,m+1)); %(m)
x=x/Scaler_x;
y=y/Scaler_y;
W_on=W_on/Scaler_z;

%%%%%%%%
% PLOT
%%%
x_in=x;
y_in=y;
W_on_in=W_on;

figure
subplot(2,1,1)
contour(x_in,y_in,W_on_in,10)
shading interp
colorbar
grid on
xlabel('X-dir')
ylabel('Y-dir')

subplot(2,1,2)
surf(x_in,y_in,W_on_in)
shading interp
colorbar
xlabel('X-dir')
ylabel('Y-dir')
zlabel('Surface Deflection')
axis([min(min(x_in)),max(max(x_in)),min(min(y_in)), ...
max(max(y_in)), min(min(W_on_in)),max(max(W_on_in))])
```

```
% Stop the clock
disp(sprintf('\n It took %f seconds to run' ...
   ' this code...end transmission.\n',toc))
```

B.8 NextZero

This code is used to find the next zero of a function and is called by the BesZero.m code.

```
function min=NextZero(t,x)

%%%%%%%%
% NextZero.m
%%%
% This function will return the next [MIN] zero of a function.
% Note: Developed for use with Bessel Fn and not
% thouroughly tested for other functions
%%%
% Author: Eric M. Trad
%%%

go=1;
iii=1;
min=0;
x=abs(x);
while go==1
    iii=iii+1;
    if x(iii)<=x(iii-1)
        min=t(iii);
    elseif min==0
        x=x*-1;
        go=1;
    elseif abs(x(iii))>=.1
        x=x*-1;
        go=1;
    else
        go=0;
    end
end
```

B.9 plotman

This function is used to plot the deformation of the membrane surface and is called by DynamicVisual.m.

```
%%%%%%%%
%plotman.m
%%%
% This function plots the deformation of the membrane surface
%   and is called by DynamicVisual.m to create movies.
%%%
% Author: Eric M. Trad
%%%
function plotman(x,y,Zs,frame)

%%%%%%%%
%PLOT the Surface Shape
%%%
hh=figure(1);
% surf(x,y,Zs(:,:,frame)); %Plot whole surface
surf(x(1:17,:),y(1:17,:),Zs(1:17,:,frame)) %Plot only interior region
xlabel('X-dir (mm)');
ylabel('Y-dir (mm)');
% axis([-in2m(2.6)*1e3 in2m(2.6)*1e3 -in2m(2.6)*1e3 in2m(2.6)*1e3 -2.7 2.7]);
axis([-30 30 -30 30 -2.7 2.7]);
caxis([-2.7 2.7]);
colorbar;
% view(0,90);
colormap(getmap);
shading interp;
grid off;

%%%%%%%%
% Draw the control pattern
%%%
% hold on;
% plot3(x(7,:),y(7,:),Zs(7,:,frame), 'k.') %Plot the center circle
% plot3(x(:,37),y(:,37),Zs(:,37,frame),'k.') %Plot the center patch control lead
% rad=[1:4,6:12,14:20,22:28,30:36,38:44,46:48];
% rad2=[4,6,12,14,20,22,28,30,36,38,44,46];
% plot3(x(10,rad),y(10,rad),Zs(10,rad,frame),'k.') %Draw r=0.75 inch lines
% plot3(x(20,rad),y(20,rad),Zs(20,rad,frame),'k.') %Draw r=1.75 inch lines
% plot3(x(10:20,rad2),y(10:20,rad2),Zs(10:20,rad2,frame), 'k.') %Draw lower radials
% plot3(x(10:20,rad2),y(10:20,rad2),Zs(10:20,rad2,frame), 'k.') %Draw upper radials
% hold off;
drawnow
```

B.10 SerialGrab

This code is used to grab the wavefront data from the serial port on the Matlab® computer.

```
function A=SerialGrab2()

%%%%%%%%
% Eric M. Trad
%%%
% Date: 14 Jan 05
%%%
% This function grabs Zernike Coefficients that are streaming
%   through a serial connection.  The serial connection must be
%   defined as type SERIAL in the variable 'port' (use the
%   SerialInit.m file to accomplish this).  Function returns a
%   vector of data equal in length to the number set in 'NumZern'
%   variable and should match the number of coefficients sent from
%   the Wavescope side.
%%%

clear A data

global NumZern port Frames Timer

%%%%%%%%
% GRAB THE DATA FROM THE SERIAL PORT
%%%
count=1;
iii=0;
corrupt=0;
WholeSet=0;
c=0;
A=zeros(NumZern,2,Frames);
cnt=1;
tic

while WholeSet == 0 %Check if the SAMPLE set is complete
    for jjj=1:Frames %Takes a whole SAMPLE set
        while corrupt == 0 %Check if the ZERN set is complete
            while count<=NumZern %Grab all the ZERN coef's
                data=fgets(port);
                Timer(cnt)=toc;
                cnt=cnt+1;
                if length(data)<=28 | length(data)>=35
                    iii=iii+1;
                    if iii>2
%                         disp('Frame Grab Disrupted...')
                    end
                else
                    A(count,1,jjj)=str2num(data(7:10));
                    if A(1,1,jjj)==1
                        tmp=length(data)-2;
                        A(count,2,jjj)=str2num(data(16:tmp));
```

```
                        count=count+1;
                    end
                end %Check the ZERN set
            end %End Grab
            %Check for a corrupted set
            for tester=1:NumZern
                if A(tester,1,jjj)~=tester
%                     disp('Corrupt Set...')
                    c=c+1;
                    corrupt=0;
                    count=1;
                    iii=0;
                    break
                else
                    corrupt=1;
                end
            end %Corruption Test
        end %While Corrupted
        corrupt=0;
        if c>0
            break
        end
    end %Take the whole SAMPLE set
    if c >0 %Check the SAMPLE set
%         disp('Not a Whole Set...')
        WholeSet=0;
        c=0;
    else
        WholeSet=1;
    end
end %While SAMPLE set is not complete
disp(sprintf('Grabbed %i consecutive sets of Zernike Coefficients',Frames))
```

B.11 SerialInit

This code initializes communication with the serial port on the acquisition computer.

```
function port=SerialInit()

%%%%%%%%
% Eric M. Trad
%%%
% Date: 14 Jan 05
%%%
% This function initializes the SERIAL type variable port for use
%   with the SerialPlot and SerialGrab M-files.  Note:  Occasionally
%   there are instances where the COM PORT will not be properly
%   initialized, usually running this script again will take care of
%   the problem.
%%%
%Note: Be sure to set port=SerialInit() at the command line when running,
%   because all other scripts assume this name for the connection.
%%%


%%%%%%%%
% INITIALIZE
%%%
clear all;
close all;
format short g;
clc;

%%%%%%%%
% INITIALIZE AND OPEN COM PORT
%%%
% Sets the COM PORT to COM1
% Sets the Baud Rate to 115200, which is the max on the Nport
% Sets the ByteOrder to Little End In
% Sets the Timeout to 10 seconds
% Sets the Terminator to Carriage return
% Pauses 3 seconds to allow time to establish the connection before opening
% the port
%%%
port = serial('COM1','BaudRate',115200,'ByteOrder','LittleEndian' ...
              ,'TimeOut',10,'Terminator','CR');
pause(3);
fopen(port);
```

B.12 SerialPlot

This code is used to acquisition the wavefront data on the Matlab® computer.

```
%%%%%%%%
% Eric M. Trad
%%%
% Date: 14 Jan 05
% Update: 15 Feb 05 - Include Matlab v6 export and
%   coefficient grab.
%%%
% This script sets up environment varibles and runs a number
%   of functions to grab Zernike data from the AFIT Wavescope
%   box, process it and display it in 'real time'.
%%%
% NOTE: This script uses the make_zernikes.m function
%   to make the Zernike definitions.
%%%

%clear all;
close all;
format short g;
clear A Movie Zcoef Zpoly Zsurf filename h hh i j k x y Timer;
clc;
tic;

global NumZern port Frames Timer

%%%%%%%%
% Initialize
%%%
NumZern=42;
FrameInterval=.1; %Seconds from Wavescope
% ShowZern=questdlg('Would you like to show the Zernike Component Plots?', ...
%     'Question','No');
ShowZern='No';
% NewRef=questdlg('Would you like to take a static reference?', ...
%     'Question','No');
NewRef='No';
% NewRef='Yes';
% MakeMovie=questdlg('Would you like to make a movie and save the run?', ...
%     'Question','Yes');
MakeMovie='Yes';
Frames=100;
Pnum=3;

%%%%%%%%
% Call the fn to put the polynomials together
%%%
R = 16;
P = 48;
radius_area = 1.0;
[x,y,Zpoly] = Wavefront_Zernikes(R,P,radius_area);
```

```
if strcmp(ShowZern,'Yes')==1;
    figure(1)
    for i=1:NumZern;
        subplot(5,ceil(NumZern/5),i);
        mesh(x,y,Zpoly(:,:,i));
    end
end

%%%%%%%%
% Grab a reference image
%%%
if strcmp(NewRef,'Yes')==1
    h=warndlg('Prepare to grab static reference.  Press OK to continue.');
    waitfor(h);
    Reasonable='No';
    while strcmp(Reasonable,'No')==1
        clear Atmp Aflat Zsurf
        Atmp=SerialGrab2;
        Aflat=mean(Atmp(:,2,:),3);
        figure(3)
        Zsurf=Zpoly(:,:,1)*0;
        for i=1:NumZern;
            Zsurf=Zsurf+Aflat(i)*Zpoly(:,:,i);
        end
        surf(x,y,Zsurf)
        shading flat
        myclmp=getmap;
        colormap(myclmp);
        colorbar southoutside
        %axis([-1 1 -1 1 -5 5])
        drawnow
        Reasonable=questdlg('Does the reference frame look reasonable?', ...
                 'Question','No');
    end
    close 3
end

if strcmp(NewRef,'Yes')==1
    h=warndlg('Prepare to grab dynamic frames.  Press OK to continue.');
    waitfor(h);
end

%%%%%%%%
% Grab moving frames
%%%
hh=figure(2);
A=SerialGrab2;
for j=1:Frames
    Zcoef(:,j)=A(:,2,j)-Aflat; % Zernike's from Wavescope
Zsurf(:,:,j)=Zpoly(:,:,1)*0;
for i=1:NumZern;
        Zsurf(:,:,j)=Zsurf(:,:,j)+Zcoef(i,j)*Zpoly(:,:,i);
```

```
    end
end

%%%%%%%%
% Display the moving frames and make the movie
%%%
for k=1:Frames
    surf(x,y,Zsurf(:,:,k))
    shading interp
    colormap bone
    colorbar southoutside
    axis([-1 1 -1 1 -2 2])
%     view(0,90);
drawnow
%     Movie(k)=getframe(hh);
end

close

Timer=42*Timer(length(Timer)-Frames*NumZern:length(Timer));
FRate=mean(Timer(2:Frames)-Timer(1:Frames-1));
FRateStd=std(Timer(2:Frames)-Timer(1:Frames-1));
disp(sprintf('\nMean Time Between Samples: %0.2g s',FRate))
disp(sprintf('Std Dev of Time Between Samples: %0.2g s',FRateStd))
disp(sprintf('Frame Rate: %0.2g Hz \n',1/FRate))

if strcmp(MakeMovie,'Yes')==1
    filename=inputdlg('Please enter a file name:','Question');
%     disp('Creating Movie...');
%     movie2avi(Movie,char(filename),'fps',5);
    disp('Saving Workspace Variables in Matlab v6 Format...');
    save(char(filename),'-v6');
end

disp('Script is done...END TRANSMISSION')
```

B.13 StaticBarGenerate

This code is used to process the static data in Section 5.5.4. It was used to create Figure 33.

```
%%%%%%%%%
%StaticBarGenerate.m
%%%
% This program plots a bar chart of the Zernike's.  For comparison
% any number of data sets can be called up for ploting in a group.
% Also plots a spiffy Zernike component breakdown.
%%%
% Author: Eric M. Trad
%%%

clc
clear all
close all
format short g

repeat='Yes';
ii=1;

while strcmp(repeat,'Yes')
%Load File
[File,Dir]=uigetfile('*.mat','Choose the MAT file you want to load');
load(strcat(Dir,File));
disp(File);

    Zc(:,ii)=Zcoef;
repeat=questdlg('Would you like to add another data set');
    ii=ii+1;
end

%%%%%%%%%
%PLOT the bar chart of the Zernike's
%%%
figure(1);
h=bar(Zc(1:42,:),'group');
colormap bone
axis([0,42,-.75,.75])
xlabel('Zernike Coeficient Number')
ylabel('Coefficient Value')

print -dbitmap

%%%%%%%%%
% Plot the Zernike Polynomial Components
%%%
figure(2)
NumZern=25; %Best if multiple of 5
for i=1:NumZern;
    subplot(5,ceil(NumZern/5),i);
    surf(x,y,Zpoly(:,:,i));
```

```
    shading interp
    view(0,90)
    colormap(getmap)
    grid off
    axis off
    text(-1,-1,sprintf('%i',i))
end
```

B.14 StaticPlotter

This code is used to process the static data in Section 5.5.4. It was used to create Figures 42 to 61.

```
%%%%%%%%
%StaticPlotter.m
%%%
% This program plots the surface deflection, radial cut pattern
% and standard deviation plots for the wavescope data.  Various
% max, min and other info is also calculated.
%%%
% Author: Eric M. Trad
%%%



%%%%%%%%
% Initialize
%%%
clc
clear all
close all
format short g

Flag=0; %0=Deflection Plot, 1=Radial Cut, 2=Std Plot

%%%%%%%%
%Load File
%%%
% [File,Dir]=uigetfile('*.mat','Choose the MAT file you want to load');
% load(strcat(Dir,File));
% disp(File);
load 7PatchB_Patch7_0Hz_100V_V6;

%%%%%%%%
%Average and STD the Surface
%%%
[tmp1, tmp2, tmp3]=size(Zsurf);
Zavg=mean(Zsurf(:,:,2:tmp3-1),3);
Zstd=std(Zsurf(:,:,2:tmp3-1),0,3);

%%%%%%%%
%Expand the data with zeros to fill the membrane
%%%
R=28-16;
P=48;
radius = linspace(1,2.5/1.5,R+1);
theta = [-pi:(2*pi)/P:pi];
for i = 1:R+1;
for j = 1:P+1;
        r = radius(i);
        t = theta(j);
x(17+i,j) = r*cos(t);
```

```
y(17+i,j) = r*sin(t);
Zavg(17+i,j) = 0;
Zstd(17+i,j) = 0;
end
end

%%%%%%%%
%Multiply by in2m() and 1.5 to fit to actual membrane size
%%%
x=in2m(x*1.5)*1e3; %Want the x axis in mm
y=in2m(y*1.5)*1e3; %Want the y axis in mm

%%%%%%%%
%Shift the data one or more points, rotate to align with control outline
%%%
S=1; %Shifter, clockwise, 0<S
Zavg_shift=zeros(size(Zavg));
for kkk=S+1:49
    Zavg_shift(:,kkk-S)=Zavg(:,kkk);
end
for kkkk=1:S
    Zavg_shift(:,49-(S-kkkk))=Zavg(:,kkkk+1);
end
Zavg=Zavg_shift;

%%%%%%%%
% Alter the filename for display in title
%%%
Fname=regexprep(File,'_',' ');
Fname=regexprep(Fname,'.mat','');

if Flag==0
%%%%%%%%
%PLOT the Surface Shape
%%%
figure(1)
surf(x,y,Zavg);
xlabel('X-dir (mm)');
ylabel('Y-dir (mm)');
axis([-in2m(2.6)*1e3 in2m(2.6)*1e3 -in2m(2.6)*1e3 in2m(2.6)*1e3 -2.7 2.7]);
caxis([-2.7 2.7]);
colorbar;
view(0,90);
myclmp=getmap;
colormap(myclmp);
shading interp;
grid off;

%%%%%%%%
% Draw the control pattern
%%%
hold on;
```

```
plot3(x(7,:),y(7,:),Zavg(7,:), 'k.') %Plot the center circle
plot3(x(:,37),y(:,37),Zavg(:,37),'k.') %Plot the center patch control lead
rad=[1:4,6:12,14:20,22:28,30:36,38:44,46:48];
rad2=[4,6,12,14,20,22,28,30,36,38,44,46];
plot3(x(10,rad),y(10,rad),Zavg(10,rad),'k.') %Draw r=0.75 inch lines
plot3(x(20,rad),y(20,rad),Zavg(20,rad),'k.') %Draw r=1.75 inch lines
plot3(x(10:20,rad2),y(10:20,rad2),Zavg(10:20,rad2), 'k.') %Draw lower radials
plot3(x(10:20,rad2),y(10:20,rad2),Zavg(10:20,rad2), 'k.') %Draw upper radials

%%%%%%%%
% Find the min and max of the surface
%%%
%Find the absolute minimum of the surface
[Bminmin, Ix]=min(min(Zavg,[],2));
[Bminmin, Iy]=min(min(Zavg,[],1));
%Find the interior minimum of the surface
[Iminmin, Ix]=min(min(Zavg(1:15,:),[],2));
[Iminmin, Iy]=min(min(Zavg(1:15,:),[],1));
%Find the absolute maximum of the surface
[Bmaxmax, Ix]=max(max(Zavg,[],2));
[Bmaxmax, Iy]=max(max(Zavg,[],1));
%Find the interior maximum of the surface
[Imaxmax, Ix]=max(max(Zavg(1:15,:),[],2));
[Imaxmax, Iy]=max(max(Zavg(1:15,:),[],1));

    disp(sprintf('Min Disp = %0.5g \nMax Disp = %0.5g \n',Bminmin,Bmaxmax));
disp(sprintf('Min Interior Disp = %0.5g \nMax Interior Disp = %0.5g',Iminmin,Imaxmax));

    %%%%%%%%
% Find the Peak-Valley Displacements
%%%
PV=abs(Bmaxmax)+abs(Bminmin);
disp(sprintf('\nPV = %0.5f microns (%0.5f wavelengths)',PV,PV/.633));
PV_interior=abs(Imaxmax)+abs(Iminmin);
disp(sprintf('PV_interior = %0.5f microns (%0.5f wavelengths)\n',PV_interior,PV/.633));

%Copy to the clipboard
%  print -dbitmap
    close 1
elseif Flag==1
%%%%%%%%
% PLOT the radial cut graphs
%%%
figure(2)
hold on;
RRR=linspace(0,in2m(2.5)*1e3,length(Zavg(:,1)));
for jjj=1:8:48
        errorbar(RRR,Zavg(:,jjj),Zstd(:,jjj),'k:')
end
hh=plot(RRR,Zavg(:,33)','k+',RRR,Zavg(:,25)','ko',RRR,Zavg(:,17)','kx',...
        RRR,Zavg(:,9)','ks',RRR,Zavg(:,1)','kd',RRR,Zavg(:,41)','k^');
legend(hh,'Patch 2','Patch 3', 'Patch 4', 'Patch 5', 'Patch 6', 'Patch 7',1)
```

```
set(hh,'MarkerEdgeColor','k','MarkerFaceColor','none','MarkerSize',6)
axis([0 in2m(2.5)*1e3 -3 3])
xlabel('Radius (mm)')
ylabel('Displacement (\mu m)')
hold off;

%Copy to the clipboard
print -dbitmap
else
    %%%%%%%%
%PLOT the Surface Standard Deviation
%%%
figure(3)
surf(x,y,Zstd);
xlabel('X-dir (mm)');
ylabel('Y-dir (mm)');
axis([-in2m(2.6)*1e3 in2m(2.6)*1e3 -in2m(2.6)*1e3 in2m(2.6)*1e3 0 .5]);
caxis([0 .5]);
% title(sprintf('%s',Fname))
colorbar;
view(0,90);
% colormap bone;
myclmp=getmap;
colormap(myclmp);
% colormap flag;
shading interp;
grid off;

%%%%%%%%
% Draw the control pattern
%%%
hold on;
plot3(x(7,:),y(7,:),Zstd(7,:), 'k.') %Plot the center circle
plot3(x(:,37),y(:,37),Zstd(:,37),'k.') %Plot the center patch control lead
rad=[1:4,6:12,14:20,22:28,30:36,38:44,46:48];
rad2=[4,6,12,14,20,22,28,30,36,38,44,46];
plot3(x(10,rad),y(10,rad),Zstd(10,rad),'k.') %Draw r=0.75 inch lines
plot3(x(20,rad),y(20,rad),Zstd(20,rad),'k.') %Draw r=1.75 inch lines
plot3(x(10:20,rad2),y(10:20,rad2),Zstd(10:20,rad2), 'k.') %Draw lower radials
plot3(x(10:20,rad2),y(10:20,rad2),Zstd(10:20,rad2), 'k.') %Draw upper radials

%%%%%%%%
% Find the min and max of the surface
%%%
%Find the absolute maximum of the surface
[Bmaxmax, Ix]=max(max(Zstd,[],2));
[Bmaxmax, Iy]=max(max(Zstd,[],1));
%Find the interior maximum of the surface
[Imaxmax, Ix]=max(max(Zstd(1:15,:),[],2));
[Imaxmax, Iy]=max(max(Zstd(1:15,:),[],1));

    disp(sprintf('Max Disp = %0.5g',Bmaxmax));
```

```
disp(sprintf('Max Interior Disp = %0.5g',Imaxmax));


%Copy to the clipboard
print -dbitmap
end
```

B.15 StaticFramePlot

This code is used to process the static data in Section 5.5.4. It was used to create Figure 41.

```
%%%%%%%%
%StaticFramePlot.m
%%%
% This program plots the mean surface deflection or standard
% deviation of the mean deflection for the static reference
% frame that is selected in a data file.
%%%
% Author: Eric M. Trad
%%%

%%%%%%%%
% Initialize
%%%
clc
clear all
close all
format short g

%%%%%%%%
%Load File
%%%
[File,Dir]=uigetfile('*.mat','Choose the MAT file you want to load');
load(strcat(Dir,File));

Flag=0; % 0=calculate mean, 1=calculate std

%%%%%%%%
% Average Reference frames
%%%
if Flag==0
    Amean=mean(A,3);
else
    Amean=std(A,0,3);
end
Amean=Amean(:,2);

%%%%%%%%
% Create the Surface Deformation
%   from coefficients and polynomials
%%%
ZZZ=0;
for i=1:NumZern;
    ZZZ=ZZZ+Amean(i)*Zpoly(:,:,i);
end

%%%%%%%%
%Expand the data with zeros to fill the membrane
%%%
R=28-16;
```

```
P=48;
radius = linspace(1,2.5/1.5,R+1);
theta = [-pi:(2*pi)/P:pi];
for i = 1:R+1;
for j = 1:P+1;
        r = radius(i);
        t = theta(j);
x(17+i,j) = r*cos(t);
y(17+i,j) = r*sin(t);
ZZZ(17+i,j) = 0;
Zstd(17+i,j) = 0;
end
end
x=in2m(x*1.5)*1e3; %Want the x axis in mm
y=in2m(y*1.5)*1e3; %Want the y axis in mm

%%%%%%%%
%Shift the data one or more points, rotate to align with control outline
%%%
S=1; %Shifter, clockwise, 0<S
Zavg_shift=zeros(size(ZZZ));
for kkk=S+1:49
    Zavg_shift(:,kkk-S)=ZZZ(:,kkk);
end
for kkkk=1:S
    Zavg_shift(:,49-(S-kkkk))=ZZZ(:,kkkk+1);
end
ZZZ=Zavg_shift;

%%%%%%%%
% Plot
%%%
surf(x,y,ZZZ)
shading flat
myclmp=getmap;
colormap(myclmp);
shading interp;
grid off;
xlabel('X-dir (mm)');
ylabel('Y-dir (mm)');
if Flag==0
    axis([-in2m(2.6)*1e3 in2m(2.6)*1e3 -in2m(2.6)*1e3 in2m(2.6)*1e3 -2.7 2.7]);
    caxis([-2.7 2.7]);
else
    axis([-in2m(2.6)*1e3 in2m(2.6)*1e3 -in2m(2.6)*1e3 in2m(2.6)*1e3 0 0.75]);
    caxis([0 .75]);
end
colorbar
view(0,90);

%%%%%%%%
% Draw the control pattern
```

```
%%%
hold on;
plot3(x(7,:),y(7,:),ZZZ(7,:), 'k.') %Plot the center circle
plot3(x(:,37),y(:,37),ZZZ(:,37),'k.') %Plot the center patch control lead
rad=[1:4,6:12,14:20,22:28,30:36,38:44,46:48];
rad2=[4,6,12,14,20,22,28,30,36,38,44,46];
plot3(x(10,rad),y(10,rad),ZZZ(10,rad),'k.') %Draw r=0.75 inch lines
plot3(x(20,rad),y(20,rad),ZZZ(20,rad),'k.') %Draw r=1.75 inch lines
plot3(x(10:20,rad2),y(10:20,rad2),ZZZ(10:20,rad2), 'k.') %Draw lower radials
plot3(x(10:20,rad2),y(10:20,rad2),ZZZ(10:20,rad2), 'k.') %Draw upper radials
hold off;

print -dbitmap
```

B.16 StaticVoltageDependence

This code is used to process the static data in Section 5.5.4. It was used to create Figure 62.

```
%%%%%%%%%
%StaticVoltageDependence.m
%%%
% This program plots the change of displacement with voltage.
% The data is gathered from other code outpus.
%%%
% Author: Eric M. Trad
%%%

clc
clear all
close all
format short g

%Enter Data from other calculations (low tech)

Min100=[ -0.82823
     -0.3501
     -0.36026
     -0.4821
     -0.55265
      -0.51593
     -0.43385];
Min200=[-1.5915
     -0.28348
     -0.61241
      -0.78587
      -1.1828
      -0.95211
     -0.60629];
Min300=[-1.0929
     -0.49212
      -1.0891
      -1.3505
      -1.3835
      -1.4651
      -0.77172];
Min400=[ -1.0121
       -0.70536
      -1.4521
      -1.6321
      -1.7879
      -2.0969
      -1.1939];
Min500=[-0.99005
      -1.0358
      -1.7944
       -1.8423
      -2.1288
```

```
      -2.5875
      -1.4155];
Min600=[-0.94603
       -1.1854
      -2.1269
      -1.7407
      -2.6766
      -2.6243
      -1.5429];

Volt=ones(6,7);
Volt(1,:)=100;
Volt(2,:)=200;
Volt(3,:)=300;
Volt(4,:)=400;
Volt(5,:)=500;
Volt(6,:)=600;

figure
plot(Volt,[mean(Min100);mean(Min200);mean(Min300);...
        mean(Min400);mean(Min500);mean(Min600)],'kx-',100:600,0,'k:')
xlabel('Charge (volts)')
ylabel('Average Surface Deformation (\mum)')

print -dbitmap
```

B.17 TensionCalc

This code is used to calculate the estimated tension in the membrane. It is related to Equation 34.

```
function T=TensionCalc(Freq,m,n,Radius,rho)

%%%%%%%%%
% TensionCalc.m
%%%
% This function will return the tension as calculated by circular
% membrane theory.  The material is assumed to be PVDF and the
% density is set accordingly
%%%
% VARIABLE DEFINITIONS AND UNITS
% Freq = frequency of the tension calculation [rad/s]
% m,n = describe the mode of freq
% Radius = radius of the circular membrane [meters]
% T = claculated tension [newtons]
%%%
% Author: Eric M. Trad
%%%

%%%%%%%%%
% Find the Zeros of the Bessel Fn
%%%
Mmax=m;
Nmax=n;
BesTable=BesZeros(Mmax,Nmax);
BesVal=BesTable(n,m+1);

%%%%%%%%%
% Calculate the tension
%%%
T=rho*(Freq*Radius/BesVal)^2; %Tension [kg/m^2][rad^2/s^2][m^2]=[kg/s^2]=[N/m]

disp(sprintf('\nThe tension is: %0.5e N/m for(%i,%i)\n',T,m,n))
```

B.18 WavefrontZernikes

This code generates the Zernike Polynomials for use with the acquisition code.

```
function[x,y,Zpoly] = Wavefront_Zernikes(R,P,radius_area);

%*********************************************************************
% PURPOSE: The Wavefront_Zernikes function generates a set of basis elements
% for plotting the Zernike polynomials from the Zernike Coefficients
% generated by the Wavefront sensor. The basis elements are consistent with
% only the Wavefront software, as the ordering of the Zernike polynomials
% by Wavefront is non-standard.
%
% Inputs:
% R : number of radial cuts
% P : number of angular cuts
% radius_area: radius of cicular area (Optional)
% The basis elements, Zpoly, may be plotted by using the surf command, i.e.
% surf(x,y,Zpoly(:,:,4) prints the fourth polynomial.
%
% **** OR *****
% single input R
% R : [n x 3] array of coordinates such that
% R(1,:) is the index
% R(2,:) is the radial coordinate
% R(3,:) is the theta coordinate
%
% The basis elements, Zpoly, may be plotted by using the plot3 command,
% i.e.
% plot3(x,y,Zpoly(:,:,4),'.') prints the fourth polynomial
%

%
%  WRITTEN  BY:  Maj Shepherd
%                Air Force Institute of Technology
%                Aeronautics and Astronautics Department
%                AFIT/ENY
%                2950 P Street
%                Wright-Patterson AFB, OH 45433-7765
%
%  CREATED:  18 Jan 05
%  REVISED:  n/a
%
%*********************************************************************

%*********************************************************************

if nargin > 1
if nargin == 2
radius_area = 1;
end;
radius = [0:radius_area/R:radius_area];
```

```
theta = [-pi:(2*pi)/P:pi];
for i = 1:R+1;
for j = 1:P+1;
    r = radius(i);
    t = theta(j);
x(i,j) = r*cos(t);
y(i,j) = r*sin(t);
Zpoly(i,j,1)  = r*cos(t); %(X Tilt)
Zpoly(i,j,2)  = r*sin(t); % (Y Tilt)
Zpoly(i,j,3)  = 2*r^2-1;  %(Focus)
Zpoly(i,j,4)  = r^2*cos(2*t); %(0 Astigmatism)
Zpoly(i,j,5)  = r^2*sin(2*t); %(45 Astigmatism)
Zpoly(i,j,6)  = (3*r^2-2)*r*cos(t); %(X Coma)
Zpoly(i,j,7)  = (3*r^2-2)*r*sin(t); %(Y Coma)
Zpoly(i,j,8)  = 6*r^4-6*r^2+1; %(Spherical)
Zpoly(i,j,9)  = r^3*cos(3*t);
Zpoly(i,j,10) = r^3*sin(3*t);
Zpoly(i,j,11) = (4*r^2-3)*r^2*cos(2*t);
Zpoly(i,j,12) = (4*r^2-3)*r^2*sin(2*t);
Zpoly(i,j,13) = (10*r^4-12*r^2+3)*r*cos(t);
Zpoly(i,j,14) = (10*r^4-12*r^2+3)*r*sin(t);
Zpoly(i,j,15) = 20*r^6-30*r^4+12*r^2-1;
Zpoly(i,j,16) = r^4*cos(4*t);
Zpoly(i,j,17) = r^4*sin(4*t);
Zpoly(i,j,18) = (5*r^2-4)*r^3*cos(3*t);
Zpoly(i,j,19) = (5*r^2-4)*r^3*sin(3*t);
Zpoly(i,j,20) = (15*r^4-20*r^2+6)*r^2*cos(2*t);
Zpoly(i,j,21) = (15*r^4-20*r^2+6)*r^2*sin(2*t);
Zpoly(i,j,22) = (35*r^6-60*r^4+30*r^2-4)*r*cos(t);
Zpoly(i,j,23) = (35*r^6-60*r^4+30*r^2-4)*r*sin(t);
Zpoly(i,j,24) = 70*r^8-140*r^6+90*r^4-20*r^2+1;
Zpoly(i,j,25) = r^5*cos(5*t);
Zpoly(i,j,26) = r^5*sin(5*t);
Zpoly(i,j,27) = (6*r^2-5)*r^4*cos(4*t);
Zpoly(i,j,28) = (6*r^2-5)*r^4*sin(4*t);
Zpoly(i,j,29) = (21*r^4-30*r^2+10)*r^3*cos(3*t);
Zpoly(i,j,30) = (21*r^4-30*r^2+10)*r^3*sin(3*t);
Zpoly(i,j,31) = (56*r^6-105*r^4+60*r^2-10)*r^2*cos(2*t);
Zpoly(i,j,32) = (56*r^6-105*r^4+60*r^2-10)*r^2*sin(2*t);
Zpoly(i,j,33) = (126*r^8-280*r^6+210*r^4-60*r^2+5)*r*cos(t);
Zpoly(i,j,34) = (126*r^8-280*r^6+210*r^4-60*r^2+5)*r*sin(t);
Zpoly(i,j,35) = 252*r^10-630*r^8+560*r^6-210*r^4+30*r^2-1;
Zpoly(i,j,36) = r^6*cos(6*t);
Zpoly(i,j,37) = r^6*sin(6*t);
Zpoly(i,j,38) = (7*r^2-6)*r^5*cos(5*t);
Zpoly(i,j,39) = (7*r^2-6)*r^5*sin(5*t);
Zpoly(i,j,40) = 924*r^12-2772*r^10+3150*r^8-1680*r^6+420*r^4-42*r^2+1;
Zpoly(i,j,41) = r^7*cos(7*t);
Zpoly(i,j,42) = r^7*sin(7*t);
end %i
end %j
else
```

```
%     R = 2 %test line
%     P = 8 %test line
% [X1X2,EL] = FEM_Membrane_cylindrical(R,P); %test line
X1X2 = R;
for i = 1:length(X1X2(:,1));
    r = X1X2(i,2);
    t = X1X2(i,3);
    x(i,1) = r*cos(t);
    y(i,1) = r*sin(t);
Zpoly(i,1,1)  = r*cos(t); %(X Tilt)
Zpoly(i,1,2)  = r*sin(t); % (Y Tilt)
Zpoly(i,1,3)  = 2*r^2-1;
Zpoly(i,1,4)  = r^2*cos(2*t); %(0 Astigmatism)
Zpoly(i,1,5)  = r^2*sin(2*t); %(45 Astigmatism)
Zpoly(i,1,6)  = (3*r^2-2)*r*cos(t); %(X Coma)
Zpoly(i,1,7)  = (3*r^2-2)*r*sin(t); %(Y Coma)
Zpoly(i,1,8)  = 6*r^4-6*r^2+1; %(Spherical)
Zpoly(i,1,9)  = r^3*cos(3*t);
Zpoly(i,1,10) = r^3*sin(3*t);
Zpoly(i,1,11) = (4*r^2-3)*r^2*cos(2*t);
Zpoly(i,1,12) = (4*r^2-3)*r^2*sin(2*t);
Zpoly(i,1,13) = (10*r^4-12*r^2+3)*r*cos(t);
Zpoly(i,1,14) = (10*r^4-12*r^2+3)*r*sin(t);
Zpoly(i,1,15) = 20*r^6-30*r^4+12*r^2-1;
Zpoly(i,1,16) = r^4*cos(4*t);
Zpoly(i,1,17) = r^4*sin(4*t);
Zpoly(i,1,18) = (5*r^2-4)*r^3*cos(3*t);
Zpoly(i,1,19) = (5*r^2-4)*r^3*sin(3*t);
Zpoly(i,1,20) = (15*r^4-20*r^2+6)*r^2*cos(2*t);
Zpoly(i,1,21) = (15*r^4-20*r^2+6)*r^2*sin(2*t);
Zpoly(i,1,22) = (35*r^6-60*r^4+30*r^2-4)*r*cos(t);
Zpoly(i,1,23) = (35*r^6-60*r^4+30*r^2-4)*r*sin(t);
Zpoly(i,1,24) = 70*r^8-140*r^6+90*r^4-20*r^2+1;
Zpoly(i,1,25) = r^5*cos(5*t);
Zpoly(i,1,26) = r^5*sin(5*t);
Zpoly(i,1,27) = (6*r^2-5)*r^4*cos(4*t);
Zpoly(i,1,28) = (6*r^2-5)*r^4*sin(4*t);
Zpoly(i,1,29) = (21*r^4-30*r^2+10)*r^3*cos(3*t);
Zpoly(i,1,30) = (21*r^4-30*r^2+10)*r^3*sin(3*t);
Zpoly(i,1,31) = (56*r^6-105*r^4+60*r^2-10)*r^2*cos(2*t);
Zpoly(i,1,32) = (56*r^6-105*r^4+60*r^2-10)*r^2*sin(2*t);
Zpoly(i,1,33) = (126*r^8-280*r^6+210*r^4-60*r^2+5)*r*cos(t);
Zpoly(i,1,34) = (126*r^8-280*r^6+210*r^4-60*r^2+5)*r*sin(t);
Zpoly(i,1,35) = 252*r^10-630*r^8+560*r^6-210*r^4+30*r^2-1;
Zpoly(i,1,36) = r^6*cos(6*t);
Zpoly(i,1,37) = r^6*sin(6*t);
Zpoly(i,1,38) = (7*r^2-6)*r^5*cos(5*t);
Zpoly(i,1,39) = (7*r^2-6)*r^5*sin(5*t);
Zpoly(i,1,40) = 924*r^12-2772*r^10+3150*r^8-1680*r^6+420*r^4-42*r^2+1;
Zpoly(i,1,41) = r^7*cos(7*t);
Zpoly(i,1,42) = r^7*sin(7*t);
end; % i loop
```

```
end; %nargin if then
```

Appendix C. Other Interesting Notes

C.1 Amplifier Characterization Data

Table 15: Test Parameters for ACX Amplifier Characterization

Parameter	Setting
Test Range	0 to 5 kHz
Input	Gaussian White Noise
Amplitude	10 mV
Window	Hanning
Lines	3200
Averages	10

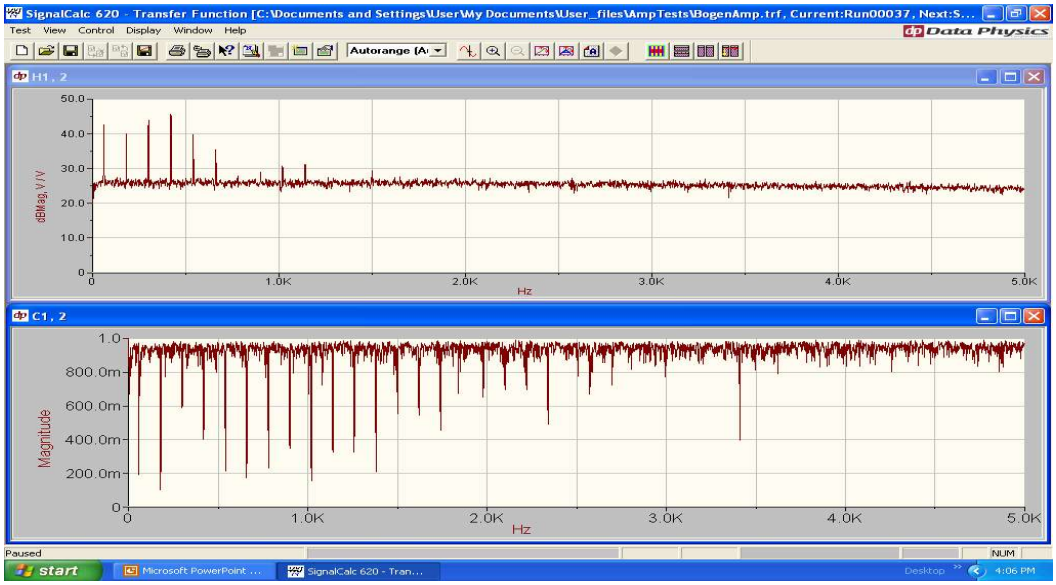

Figure 68: ACX Amplifier Characterization from 0 to 5 kHz (S/N: 8H263)

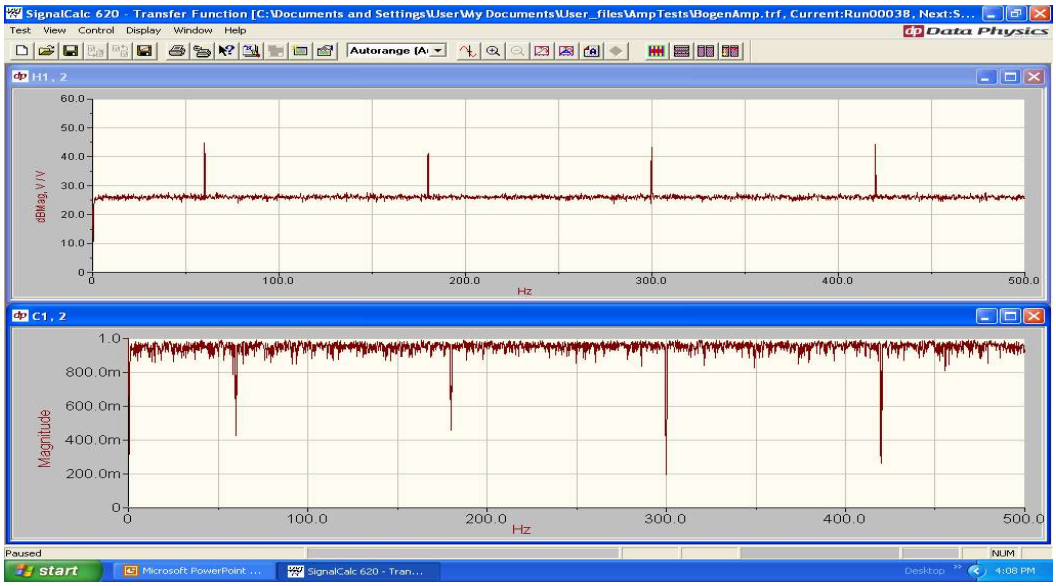

Figure 69: ACX Amplifier Characterization from 0 to 500 Hz (S/N: 8H263)

Table 16: Test Parameters for TREK Amplifier Characterization

Parameter	Setting
Test Range	0 to 100 Hz
Input	Gaussian White Noise
Amplitude	10 mV
Window	Hanning
Lines	3200
Averages	10

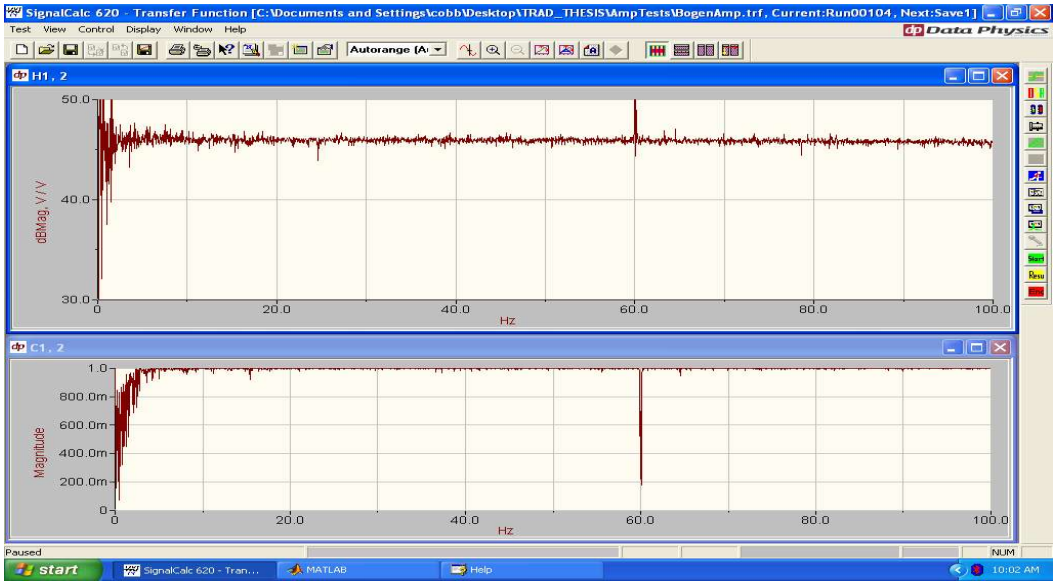

Figure 70: TREK Amplifier 1 Characterization from 0 to 100 Hz (S/N: 118A)

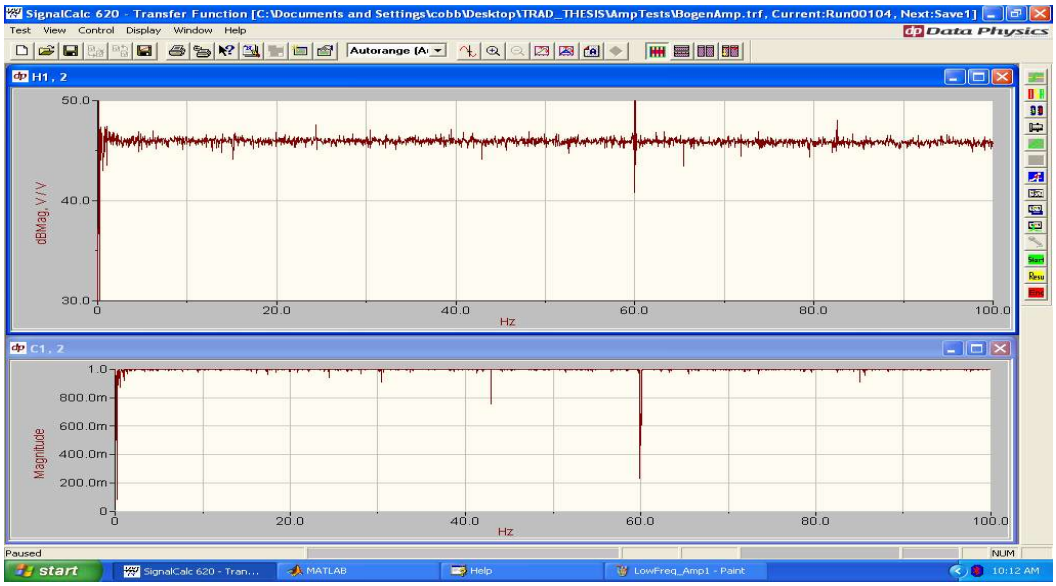

Figure 71: TREK Amplifier 2 Characterization from 0 to 100 Hz (S/N: 118B)

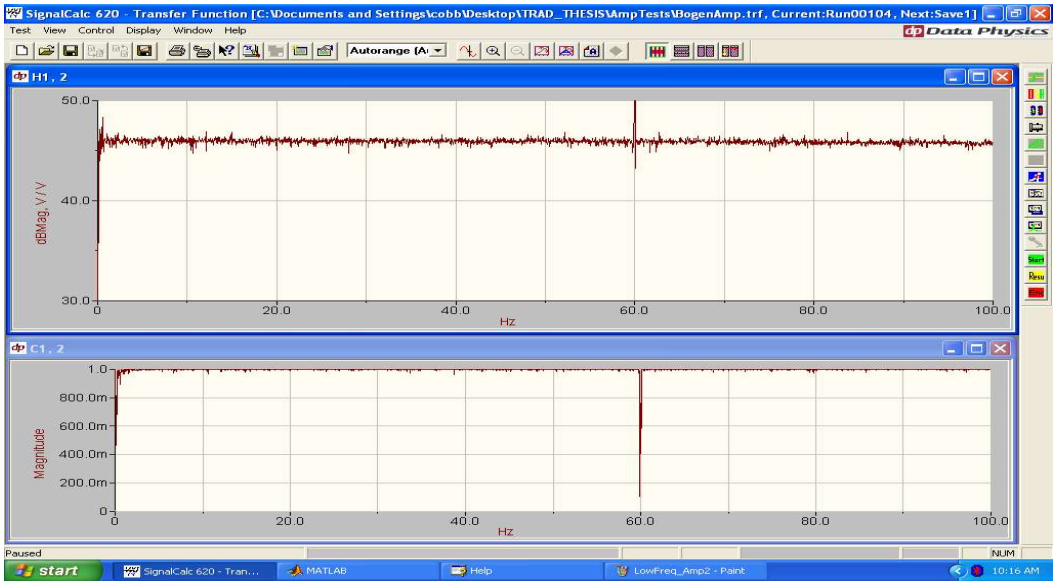

Figure 72: TREK Amplifier 3 Characterization from 0 to 100 Hz (S/N: 121A)

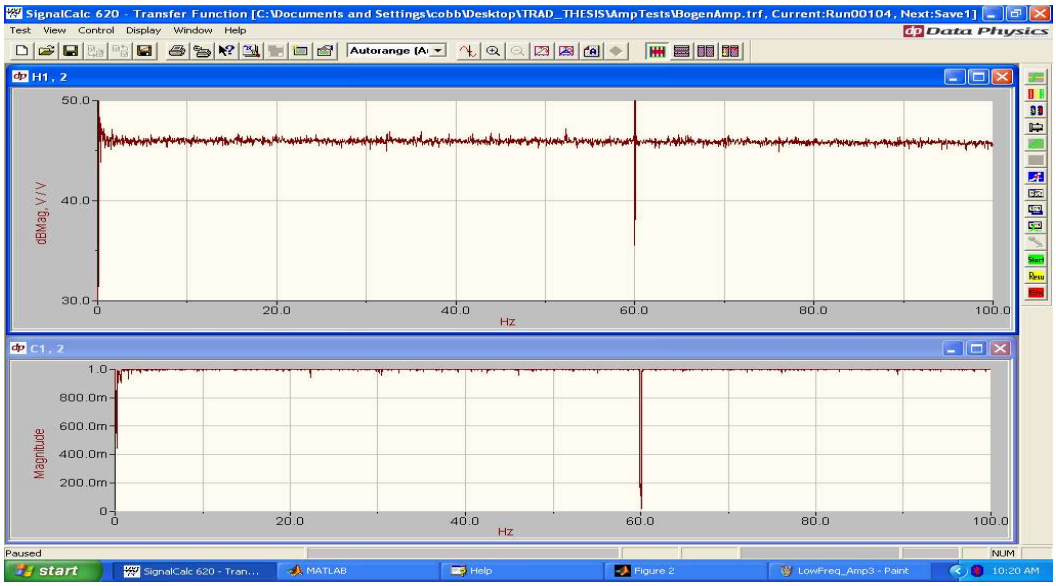

Figure 73: TREK Amplifier 4 Characterization from 0 to 100 Hz (S/N: 121B)

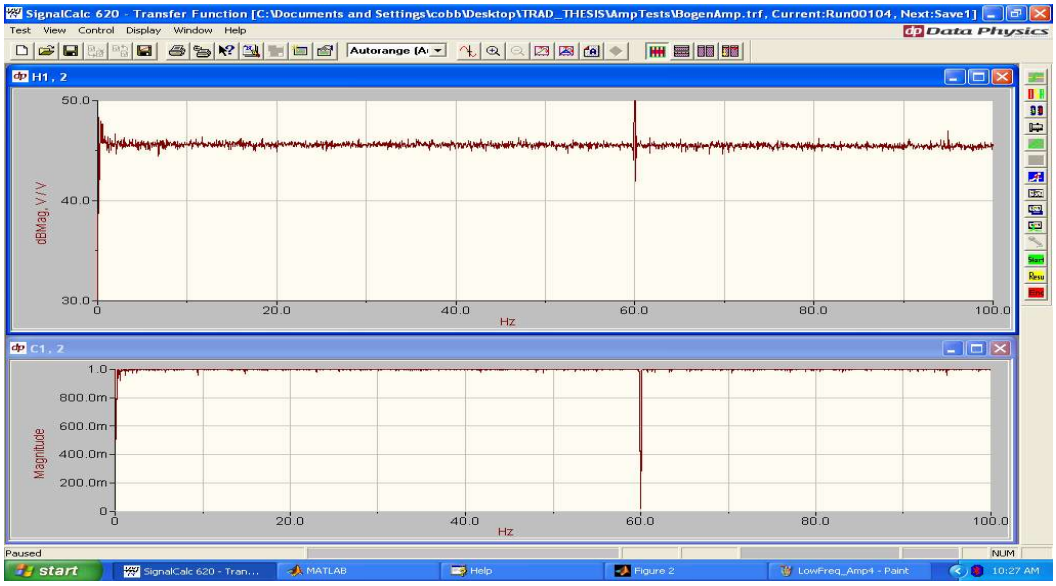

Figure 74: TREK Amplifier 5 Characterization from 0 to 100 Hz (S/N: 120A)

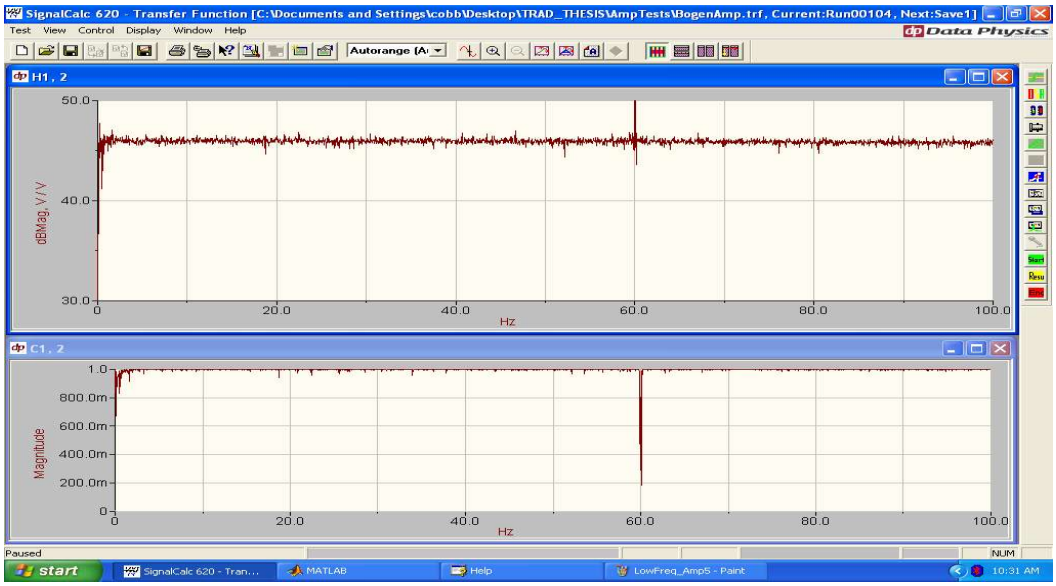

Figure 75: TREK Amplifier 6 Characterization from 0 to 100 Hz (S/N: 120B)

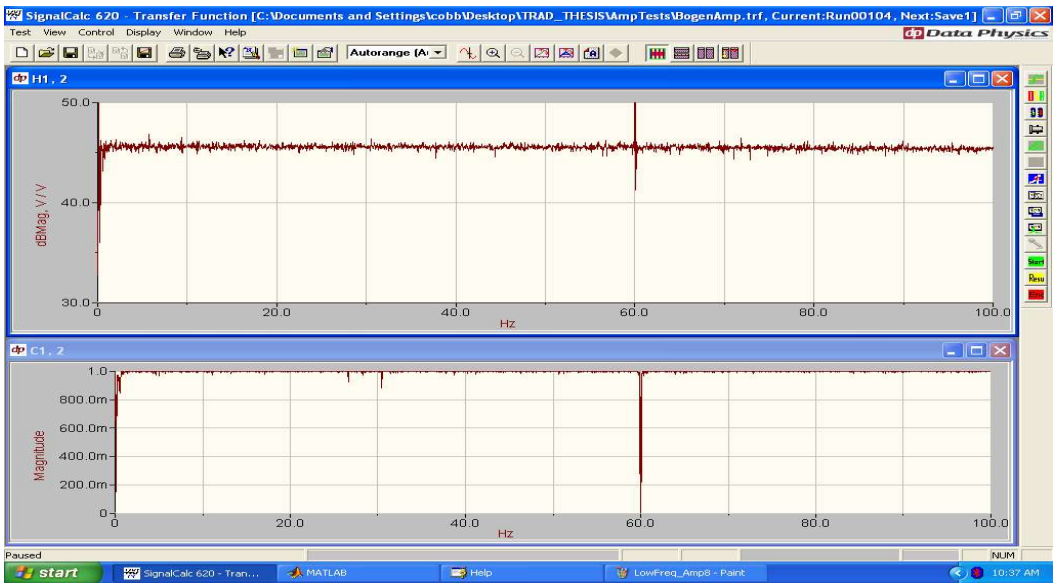

Figure 76: TREK Amplifier 7 Characterization from 0 to 100 Hz (S/N: 115A)

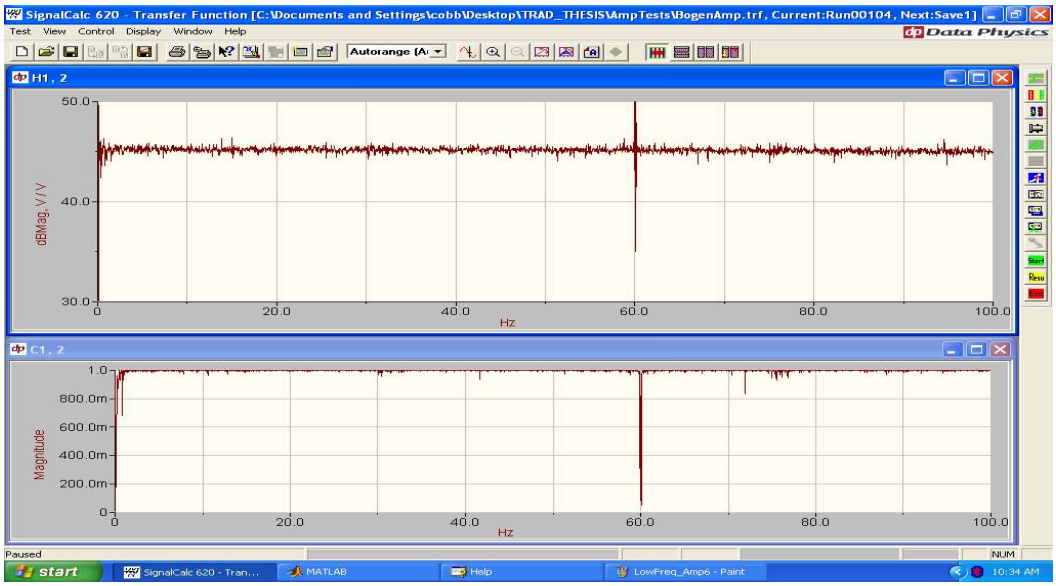

Figure 77: TREK Amplifier 8 Characterization from 0 to 100 Hz (S/N: 115B)

C.2 Relevant Telephone Numbers

Table 17: Phone Numbers

Name	Phone Number
Adaptive Optics Assoc. (AOA)	617-806-1400
Herb DeSilva (AOA software)	617-806-1816
Jay Anderson (AFIT/ENY Lab Supervisor)	937-255-3636 x4865
Dr. David Mollenhauer (ML contact)	937-255-9727 (office)
	937-255-9059 (lab)
	937-255-9070 (branch office)
Brian Langley (ML coop student)	937-255-9059 (lab)
Joel Johnson (ML contact)	937-255-4651

C.3 Zernike Polynomials

Given below are the first 42 Zernike Polynomials. Each term has a coefficient multiplier which scales the set. Upon combination, the surface deflection is given in terms of radius (r) and theta (θ). These coefficients are scaled so that the surface deflection is in terms of microns (μm).

$$Z_1 = rcos(\theta)$$

$$Z_2 = rsin(\theta)$$

$$Z_3 = 2r^2 - 1$$

$$Z_4 = r^2cos(2\theta)$$

$$Z_5 = r^2sin(2\theta)$$

$$Z_6 = (3r^2 - 2)rcos(\theta)$$

$$Z_7 = (3r^2 - 2)rsin(\theta)$$

$$Z_8 = 6r^4 - 6r^2 + 1$$

$$Z_9 = r^3cos(3\theta)$$

$$Z_{10} = r^3sin(3\theta)$$

$$Z_{11} = (4r^2 - 3)r^2cos(2\theta)$$

$$Z_{12} = (4r^2 - 3)r^2sin(2\theta)$$

$$Z_{13} = (10r^4 - 12r^2 + 3)rcos(\theta)$$

$$Z_{14} = (10r^4 - 12r^2 + 3)rsin(\theta)$$

$$Z_{15} = 20r^6 - 30r^4 + 12r^2 - 1$$

$$Z_{16} = r^4cos(4\theta)$$

$$Z_{17} = r^4sin(4\theta)$$

$$Z_{18} = (5r^2 - 4)r^3cos(3\theta)$$

$$Z_{19} = (5r^2 - 4)r^3sin(3\theta)$$

$$Z_{20} = (15r^4 - 20r^2 + 6)r^2cos(2\theta)$$

$$Z_{21} = (15r^4 - 20r^2 + 6)r^2 sin(2\theta)$$

$$Z_{22} = (35r^6 - 60r^4 + 30r^2 - 4)rcos(\theta)$$

$$Z_{23} = (35r^6 - 60r^4 + 30r^2 - 4)rsin(\theta)$$

$$Z_{24} = 70r^8 - 140r^6 + 90r^4 - 20r^2 + 1$$

$$Z_{25} = r^5 cos(5\theta)$$

$$Z_{26} = r^5 sin(5\theta)$$

$$Z_{27} = (6r^2 - 5)r^4 cos(4\theta)$$

$$Z_{28} = (6r^2 - 5)r^4 sin(4\theta)$$

$$Z_{29} = (21r^4 - 30r^2 + 10)r^3 cos(3\theta)$$

$$Z_{30} = (21r^4 - 30r^2 + 10)r^3 sin(3\theta)$$

$$Z_{31} = (56r^6 - 105r^4 + 60r^2 - 10)r^2 cos(2\theta)$$

$$Z_{32} = (56r^6 - 105r^4 + 60r^2 - 10)r^2 sin(2\theta)$$

$$Z_{33} = (126r^8 - 280r^6 + 210r^4 - 60r^2 + 5)rcos(\theta)$$

$$Z_{34} = (126r^8 - 280r^6 + 210r^4 - 60r^2 + 5)rsin(\theta)$$

$$Z_{35} = 252r^10 - 630r^8 + 560r^6 - 210r^4 + 30r^2 - 1$$

$$Z_{36} = r^6 cos(6\theta)$$

$$Z_{37} = r^6 sin(6\theta)$$

$$Z_{38} = (7r^2 - 6)r^5 cos(5\theta)$$

$$Z_{39} = (7r^2 - 6)r^5 sin(5\theta)$$

$$Z_{40} = 924r^12 - 2772r^10 + 3150r^8 - 1680r^6 + 420r^4 - 42r^2 + 1$$

$$Z_{41} = r^7 cos(7\theta)$$

$$Z_{42} = r^7 sin(7\theta)$$

Bibliography

1. Agnes, G. S. and others, . "Shaping of Parabolic Cylindrical Membrane Reflectors for the DART Precision Test Bed," *American Institute of Aeronautics and Astronautics*, *1661*:1–12 (2004).

2. Ares, J. and others, . "Position and displacement sensing with Shack-Hartmann wave-front sensors," *Applied Optics*, *Vol. 39(10)*:1511–1520 (April 2000).

3. Bao, X. and others, . "Numerical Modeling of Electroactive Polymer Mirrors for Space Applications," *SPIE Smart Structures and Materials Symposium, EAPAD Conference*, *Vol. 5051-45* (2003).

4. Carreras, R. A. and others, . "Deployable Near-Net Shape Membrane Optics," *SPIE Conference on High Resolution Wavefront Control*, *Vol. 3760*:232–238 (1999).

5. Denoyer, K. K. and others, . "Actively controlled thin-shell space optics," *SPIE Conference on Smart Structures and Materials*, *SPIE, 5054*:263–274 (2003).

6. Flint, E. M. and others, . "Boundary actuation shape control strategies for thin film single surface shells," *American Institute of Aeronautics and Astronautics*, *1825*:1–11 (2004).

7. GE Silicones. *Datasheet for RVT615*, 2005. Website: www.gesilicones.com.

8. L'Garde, , "L'Garde Website." Online at www.lgarde.com/programs/iae.html, February 2005.

9. M., G. R. and others, . "Modeling the dynamics of large diameter doubly curved shells made from thin-films," *American Institute of Aeronautics and Astronautics*, *1830*:1–9 (April 2003).

10. Maji, A. K. "Shape Measurement and Control of Deployable Membrane Structures," *Experimental Mechanics*, *Vol. 40(2)*:154–159 (June 2000).

11. Measurement Specialties, Inc. *Piezo Film Sensors: Technical Manual*, 1999.

12. Meilan, P. F. and others, . "Rayleigh Resolution Criterion for Light Sources of Different Spectral Composition," *Brazilian Journal of Physics*, *Vol. 27-4* (1997).

13. Meirovitch, L. *Principles and Techniques of Vibrations*. Prentice Hall Publishing, 1997.

14. Mollenhauer, D. and others, . "Multi-layered Polymer Mirror Experiment," *American Institute of Aeronautics and Astronautics*, *1341*:1–6 (2001).

15. Mollenhauer, D. and others, . "Advanced Materials and Processes for Large, Lightweight, Space-Based Mirrors," *Institute of Electrical and Electronics Engineering Publication*, *1137*:1–17 (2003).

16. Rogers, J. W. *Modeling axisymmetric optical precision piezoelectric membranes*. PhD dissertation, Air Force Institute of Technology, October 2001.

17. Rogers, J. W. and others, . "Modeling a piezothermoelastic laminated plate-membrane," *Journal of Intelligent Material Systems and Structures*, *13(5)*:303–316 (May 2002).

18. Rotge, J. R. and others, . "Large Optically Flat Membrane Mirrors," *SPIE Conference on High-Resolution Wavefront Control*, *3760*:207–212 (July 1999).

19. Shack, R. and others, . "History and principles of Shack-Hartmann wavefront sensing," *Journal of Refractive Surgery*, *17* (2001).

20. Silva, D. E. and others, . "Wave-front interpretation with Zernike polynomials," *Applied Optics*, *Vol. 19(9)*:1510–1518 (May 1980).

21. Sobers, D. M. *Smart Structures for Control of Optical Surfaces*. MS thesis, Air Force Institute of Technology, March 2002.

22. Sobers, D. M. and others, . "Smart structres for control of optical surfaces," *American Institute of Aeronautics and Astronautics*, 1–11 (2003).

23. Wagner, J. W. *Optical Metrology of Adaptive Membrane Mirrors*. MS thesis, Air Force Institute of Technology, March 2000.

24. Willians, R. B. and others, . "Limitations of using membrane theory for modeling PVDF patches on inflatable structures," *Journal of Intelligent Material Systems and Structures*, *12(1)*:11–19 (January 2001).

Vita

Eric M. Trad was raised in the suburbs of Chicago, IL. He graduated from Plainfield High School, Plainfield, IL, in 1999. Upon graduation he attended the distinguished University of Michigan, College of Engineering. In 2003 he graduated with a Bachelor of Science in Engineering, Aerospace Engineering.

Eric was commissioned a Second Lieutenant in the United States Air Force through the Michigan AFROTC program. He was accepted as a direct accession to the Air Force Institute of Technology for his first assignment, where he would pursue a Master of Science in Aeronautical Engineering. Upon graduation in 2005, he will be assigned to the Air Force Research Laboratory to work with the computational fluid dynamics group.

REPORT DOCUMENTATION PAGE

Form Approved
OMB No. 0704–0188

1. REPORT DATE *(DD–MM–YYYY)*	2. REPORT TYPE	3. DATES COVERED *(From — To)*
21–03–2005	Master's Thesis	Sep 2003 — Mar 2005

4. TITLE AND SUBTITLE

Dynamic Characterization of Thin Deformable PVDF Mirror

5a. CONTRACT NUMBER

5b. GRANT NUMBER

5c. PROGRAM ELEMENT NUMBER

6. AUTHOR(S)

Trad, Eric M., 2LT, USAF

5d. PROJECT NUMBER

05-165

5e. TASK NUMBER

5f. WORK UNIT NUMBER

7. PERFORMING ORGANIZATION NAME(S) AND ADDRESS(ES)

Air Force Institute of Technology
Graduate School of Engineering and Management
2950 Hobson Way
WPAFB OH 45433-7765

8. PERFORMING ORGANIZATION REPORT NUMBER

AFIT/GAE/ENY/05-M24

9. SPONSORING / MONITORING AGENCY NAME(S) AND ADDRESS(ES)

AFOSR
Lt. Col. Sharon Heise
4015 Wilson Blvd, Rm 713
Arlington VA, 22203-1954

10. SPONSOR/MONITOR'S ACRONYM(S)

11. SPONSOR/MONITOR'S REPORT NUMBER(S)

12. DISTRIBUTION / AVAILABILITY STATEMENT

Approval for public release; distribution is unlimited.

13. SUPPLEMENTARY NOTES

14. ABSTRACT

Methodology for the design and fabrication of 5 inch diameter membrane-like mirror structures is explored, resulting in test articles with areal densities as low as 1.57 kg/m^2 and a thickness of 1.5 mm. Each optical structure has 7 control patches etched into the PVDF layer, which can be used as actuators. These test articles are utilized to demonstrate the capabilities of an acquisition system to make measurements of static and dynamic actuation of the mirror surface. Static deformations are analyzed statistically and determined to yield maximum deformations in the actuated regions of -2.1 μm with a standard deviation of 0.33 μm when 400 volts are applied. The acquisition system was characterized for dynamic actuation of the surface and found to have a sample rate ranging from 4 to 14 Hz. This rate is found to be dependent upon the desired detail level of the surface description as calculated by the wavefront analysis software.

15. SUBJECT TERMS

Membrane-like Optical Structures, PVDF Surface Actuation, Adaptive Optics

16. SECURITY CLASSIFICATION OF:			17. LIMITATION OF ABSTRACT	18. NUMBER OF PAGES	19a. NAME OF RESPONSIBLE PERSON
a. REPORT	b. ABSTRACT	c. THIS PAGE			Richard G. Cobb, Professor, AFIT/ENY
U	U	U	UU	136	19b. TELEPHONE NUMBER *(include area code)* (937) 785–3636, ext 4559